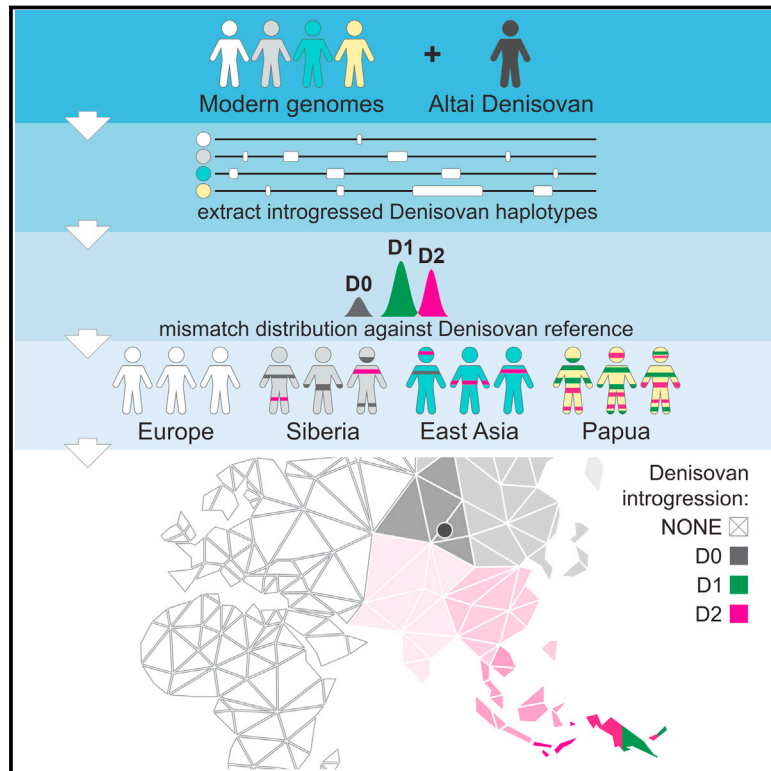# Cell

Multiple Deeply Divergent Denisovan Ancestries in Papuans

Graphical Abstract

Authors

Guy S. Jacobs, Georgi Hudjashov,
Lauri Saag, ..., Herawati Sudoyo,
J. Stephen Lansing, Murray P. Cox

Correspondence

g.hudjashov@massey.ac.nz (G.H.),
m.p.cox@massey.ac.nz (M.P.C.)

In Brief

Genome sequences from Island Southeast Asia suggest two independent Denisovan lineages, distinct from the Altai Denisovan, that have contributed to modern Papuan genomes, with one group potentially present east of the Wallace Line and thus capable of crossing geographical barriers.

Highlights

- A new dataset of 161 genomes covering the understudied Indonesia-New Guinea region

- Introgressing Denisovans comprise at least three genetically divergent groups

- Papuans carry haplotypes from two Denisovan groups, with one unique to Oceania

- Some Denisovan introgression was recent and likely occurred in New Guinea or Wallacea

CellPress

Multiple Deeply Divergent Denisovan Ancestries in Papuans

Guy S. Jacobs,[1,14] Georgi Hudjashov,[2,3,14,*] Lauri Saag,[3] Pradiptajati Kusuma,[1,4] Chelzie C. Darusallam,[4] Daniel J. Lawson,[5] Mayukh Mondal,[3] Luca Pagani,[3,6] François-Xavier Ricaut,[7] Mark Stoneking,[8] Mait Metspalu,[3] Herawati Sudoyo,[4,9,10] J. Stephen Lansing,[11,12,13] and Murray P. Cox[2,15,*]

[1]Complexity Institute, Nanyang Technological University, Singapore 637723, Singapore
[2]Statistics and Bioinformatics Group, School of Fundamental Sciences, Massey University, Palmerston North 4410, New Zealand
[3]Institute of Genomics, University of Tartu, Tartu, Tartumaa 51010, Estonia
[4]Genome Diversity and Diseases Laboratory, Eijkman Institute for Molecular Biology, Jakarta 10430, Indonesia
[5]Integrative Epidemiology Unit, Population Health Sciences, University of Bristol, Bristol BS8 2BN, UK
[6]APE Lab, Department of Biology, University of Padova, Padova 35131, Italy
[7]Department of Evolution and Biological Diversity (UMR 5174), Université de Toulouse Midi-Pyrénées, CNRS, IRD, UPS, 31062 Toulouse, France
[8]Department of Evolutionary Genetics, Max Planck Institute for Evolutionary Anthropology, Leipzig 04103, Germany
[9]Department of Medical Biology, Faculty of Medicine, University of Indonesia, Jakarta 10430, Indonesia
[10]Sydney Medical School, University of Sydney, Sydney, NSW 2006, Australia
[11]Asian School of the Environment, Nanyang Technological University, Singapore 637723, Singapore
[12]Santa Fe Institute, Santa Fe, NM 87501, USA
[13]Stockholm Resilience Center, Kräftriket, 10405 Stockholm, Sweden
[14]These authors contributed equally
[15]Lead Contact
*Correspondence: g.hudjashov@massey.ac.nz (G.H.), m.p.cox@massey.ac.nz (M.P.C.)
https://doi.org/10.1016/j.cell.2019.02.035

SUMMARY

Genome sequences are known for two archaic hominins—Neanderthals and Denisovans—which interbred with anatomically modern humans as they dispersed out of Africa. We identified high-confidence archaic haplotypes in 161 new genomes spanning 14 island groups in Island Southeast Asia and New Guinea and found large stretches of DNA that are inconsistent with a single introgressing Denisovan origin. Instead, modern Papuans carry hundreds of gene variants from two deeply divergent Denisovan lineages that separated over 350 thousand years ago. Spatial and temporal structure among these lineages suggest that introgression from one of these Denisovan groups predominantly took place east of the Wallace line and continued until near the end of the Pleistocene. A third Denisovan lineage occurs in modern East Asians. This regional mosaic suggests considerable complexity in archaic contact, with modern humans interbreeding with multiple Denisovan groups that were geographically isolated from each other over deep evolutionary time.

INTRODUCTION

Contact between modern humans and archaic hominins in the distant past has left a distinctive genetic signature in all human populations alive today. Modern humans interbred with multiple hominin species in different places around the world, including Neanderthals (Green et al., 2010), Denisovans (Reich et al., 2010), and possibly others (Hammer et al., 2011; Mondal et al., 2016). Examining genome sequences to identify regions that introgressed from these archaic species has revealed evolutionarily adaptive variants and extended deserts of introgression (Sankararaman et al., 2016; Vernot et al., 2016). Recently, analysis of Denisovan ancestry in populations across Eurasia uncovered introgression from an extra branch on the Denisovan hominin clade in East Asia (Browning et al., 2018). However, the center of gravity of Denisovan admixture today lies >8,000 km south of Denisova Cave in the Papuan populations of tropical eastern Indonesia and New Guinea, where the composition of Denisovan introgression remains poorly understood.

We therefore analyzed archaic introgression in a new dataset covering Island Southeast Asia (ISEA) and Papua, a maritime zone of densely inhabited archipelagos larger than Europe. This culturally and linguistically diverse region remains strikingly underrepresented in modern genetic surveys, despite its extraordinary human diversity and is a major missing link for medical and evolutionary studies (Horton, 2016). Notably, the area has some of the first traces of anatomically modern humans in Eurasia (Barker et al., 2007), archaic *H. floresiensis* likely coexisted with modern humans here (Sutikna et al., 2016), and eastern Indonesians, Papuans, and Philippine "negritos," together with Siberians and South and East Asians, are among the few living groups with substantial traces of archaic introgression from Denisovans (Jinam et al., 2017; Reich et al., 2011; Tucci et al., 2018).
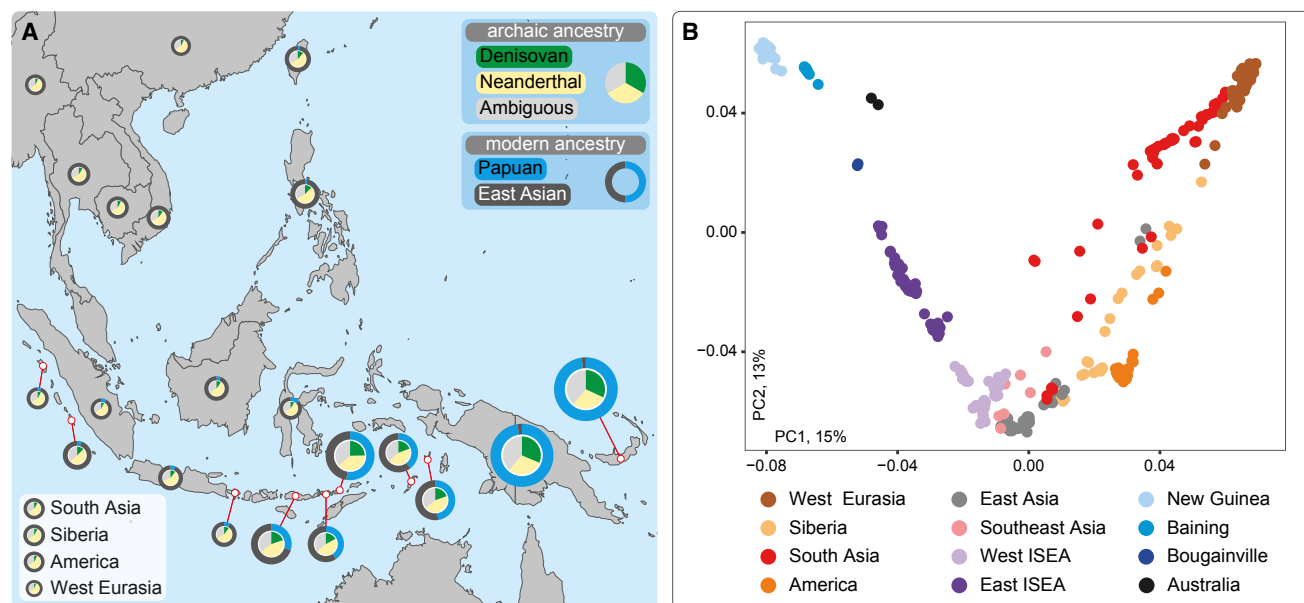
Figure 1. Modern and Archaic Ancestry

(A) Sampling locations of groups. Outer rims indicate modern ancestry components: blue, Papuan; dark gray, Asian (Table S2; STAR Methods S6). Inner pie charts indicate archaic introgression estimates: green, unambiguous Denisovan introgression; yellow, unambiguous Neanderthal introgression; light gray, introgression consistent with either Neanderthal or Denisovan ancestry (Table S3; STAR Methods S9); the total area of each pie chart corresponds to the total amount of unambiguous Denisovan introgression signal, with Papua 13.7-fold greater than West Eurasia.

(B) Principal-component analysis (PCA) of the new dataset including non-African reference samples, showing two major axes of variation—a "Papuan" axis stretching from New Guinea Papuans-New Britain Baining to West Eurasians, with ISEA intermediates, and an "Asian" axis stretching from Papuans-West Eurasians to East Asian samples (STAR Methods S2).

RESULTS AND DISCUSSION

The Indonesian Genome Diversity Project Fills a Gap in Regional Coverage

The Indonesian Genome Diversity Project (IGDP) has been run by the Eijkman Institute of Molecular Biology in Jakarta for over a decade, with the goal of capturing a representative sample of genomic diversity across this understudied region. Spanning a transect of communities across the Indonesian archipelago and neighboring regions of ISEA, populations chosen for whole-genome sequencing were selected to reflect the main axes of genomic variation observed in an earlier population genetic study (Hudjashov et al., 2017). We sequenced complete genomes to >30× coverage for 161 individuals, from Sumatra in the west to New Britain in the east (Figure 1). We combined this new dataset with 317 additional high-coverage human genomes sampled world-wide, including those few genomes previously available for ISEA and Oceania (Malaspinas et al., 2016; Mallick et al., 2016), and three complete archaic hominin sequences, the Altai and Vindija Neanderthals (Prüfer et al., 2014, 2017) and the Altai Denisovan (Meyer et al., 2012) (Figure S1; Table S1; STAR Methods S1–S5).

To confirm that the dataset captures expected genomic patterns, we calculated principal components and determined local ancestry along the genome (Dias-Alves et al., 2018) (Figure 1; Table S2; STAR Methods S2 and S6). We observed key features of population diversity in the region, notably a strong cline in Asian to Papuan ancestry across the archipelago with an abrupt

transition within the island zone of Wallacea (Cox et al., 2010; Hudjashov et al., 2017). These signals primarily reflect recent events of regional history, particularly the agricultural expansion of Austronesian-speaking populations from ca. 4500 ya. This cline serves, however, as an important backdrop to facilitate understanding of regional signals of genetic contact between anatomically modern humans and archaic hominins.

Combining Methods Identifies High-Confidence Denisovan Introgression

Because individuals in ISEA carry ancestry from both Neanderthals and Denisovans, these archaic signals must be disentangled. Assigning clear ancestry is a major challenge, especially for single variants or small ancestry blocks with few informative variants, because of extensive shared polymorphisms between the two archaic groups as well as incomplete lineage sorting due to the shared early history of Neanderthals and Denisovans. One way to overcome this problem is with haplotype methods to detect longer introgressing blocks, which have more easily assigned ancestry and are less likely to result from incomplete lineage sorting. Examining introgressing haplotypes of Denisovan ancestry offers further advantages over site-by-site methods such as D statistics (Patterson et al., 2012), because haplotypes provide additional information on introgression dates and better resolution of detailed relationships between introgressing and archaic genomes.

To obtain a set of high confidence blocks, rather than all possible stretches of Denisovan introgression, we developed
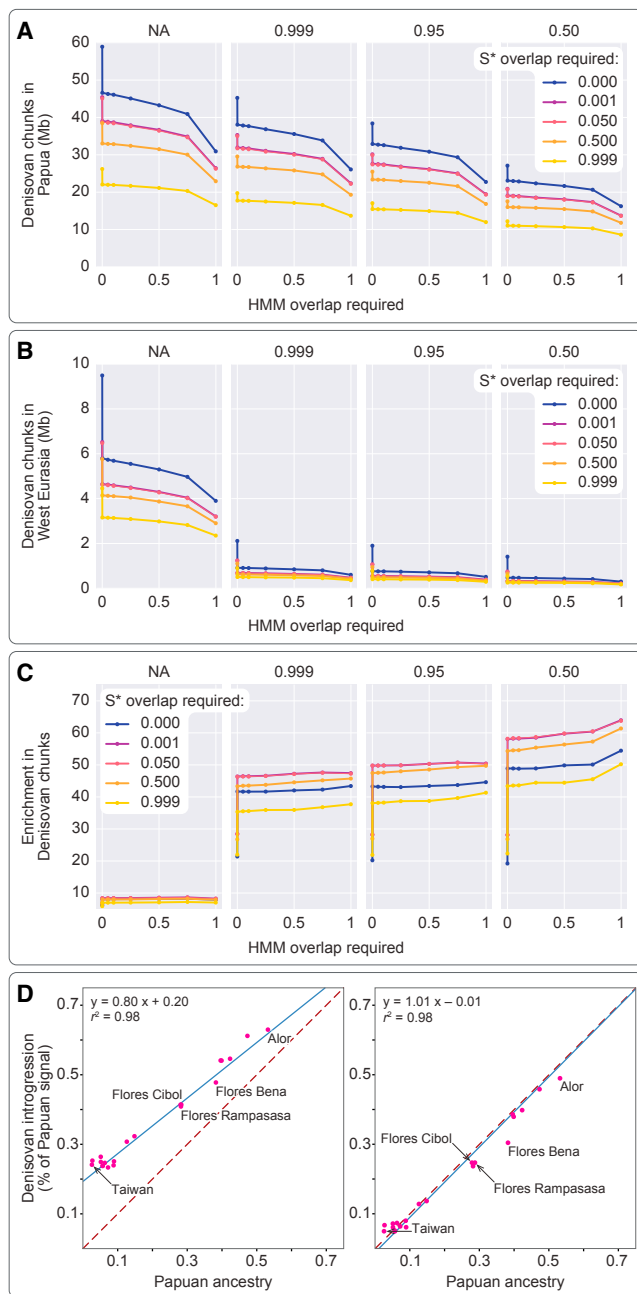
Figure 2. Effect of Block Filtering on the Denisovan Signal and the Correlation of the Denisovan Signal with Papuan Ancestry, Related to Tables S2 and S3 and STAR Methods

(A and B) Amount of Denisovan signal remaining in Papuans (A) and West Eurasians (B) following different filtering protocols. ChromoPainter (CP) Denisovan blocks are discarded if they lack a minimum overlap with HMM Denisovan blocks (x axis) and S* windows (line colors), or if they are covered more than a maximum amount by CP Neanderthal blocks (sub-plots; from left to right: not applied, 99.9%, 95% or 50%).

(C) Enrichment of Denisovan signal in Papuans versus West Eurasians based on the same filtering parameters as in (A) and (B).

(D) High correlation of Denisovan signal with Papuan ancestry in ISEA using CP Denisovan blocks only (left) or the final high-confidence Denisovan block set (right). The shift in the slope of the line when correlating the CP Denisovan

a protocol to extract archaic regions using the intersection of three different statistical methods (Table S3; STAR Methods S7 and S8). Denisovan blocks were classified based on the overlap of (1) ChromoPainter (CP) (Lawson et al., 2012), which was used to identify haplotypes that are more similar to the Denisovan genome than to a panel of sub-Saharan Africans; (2) an updated Hidden Markov Model (HMM) (Racimo et al., 2017; Seguin-Orlando et al., 2014) detecting the same signature; and (3) S* (Vernot et al., 2016), which identifies clusters of linked non-African variation. These haplotypes were then filtered, using a range of protocols (Figures 2A–2C; STAR Methods S9a), to remove blocks that were also similar to the Altai Neanderthal (Prüfer et al., 2014) and optionally the Vindija Neanderthal (Prüfer et al., 2017), as measured by CP, leaving a dataset of high-confidence introgressed Denisovan regions.

A clear correlation emerged between loci identified by the three methods. Most archaic introgression was detected in Papua and East ISEA, with the least in West Eurasia. Our multi-step filtering approach enriched detectable Denisovan introgression in Papuans relative to West Eurasians (Figures 2A–2C; STAR Methods S9c and S9d), who are thought to harbor little Denisovan introgression (Mallick et al., 2016). This enrichment rose from 6.4-fold when using CP alone to nearly 50-fold when combining CP, HMM, and S*. The result is approximately 32.3 Mb of high-confidence Denisovan introgressed blocks per genome copy for each Papuan individual. For comparison, just 688 kb of Denisovan blocks were identified in West Eurasians, which is consistent with earlier low estimates (Mallick et al., 2016).

As a further check, we compared the total amount of our high-confidence haplotypes with Denisovan ancestry proportions calculated with counting statistics as reported for the Simons Genome Diversity Project (SGDP) samples (Mallick et al., 2016) (STAR Methods S9b). The total introgression in West Eurasia estimated by CP alone did not correlate with genome-wide estimates of Denisovan introgression estimated by D statistics but instead correlated strongly with estimates of Neanderthal introgression (extracting 20% of the signal). Strikingly, however, this signal drops to 2% for our high-confidence Denisovan blocks, showing that Neanderthal spillover has been almost entirely removed from the high-confidence Denisovan block set by our multi-step filtering approach.

A strong correlation between Denisovan and Papuan ancestry ($r^2 = 0.98$, $p = 2.6 \times 10^{-20}$) confirms that these two components have interconnected histories (Figure 2D; STAR Methods S9d). In this correlation, a gradient close to 1 and a correspondingly low intercept of –0.01 is observed for the high-confidence Denisovan blocks, consistent with the inference that Denisovan introgression is largely confined to Papuans. Low levels of Papuan ancestry in West ISEA (<5%) match the limited Denisovan introgression observed in the region (Figure 1A).

blocks (left) is due to spillover signal from non-Denisovan archaic introgression (i.e., Neanderthal introgression incorrectly assigned as Denisovan). This is not observed in the high-confidence Denisovan block set (right).
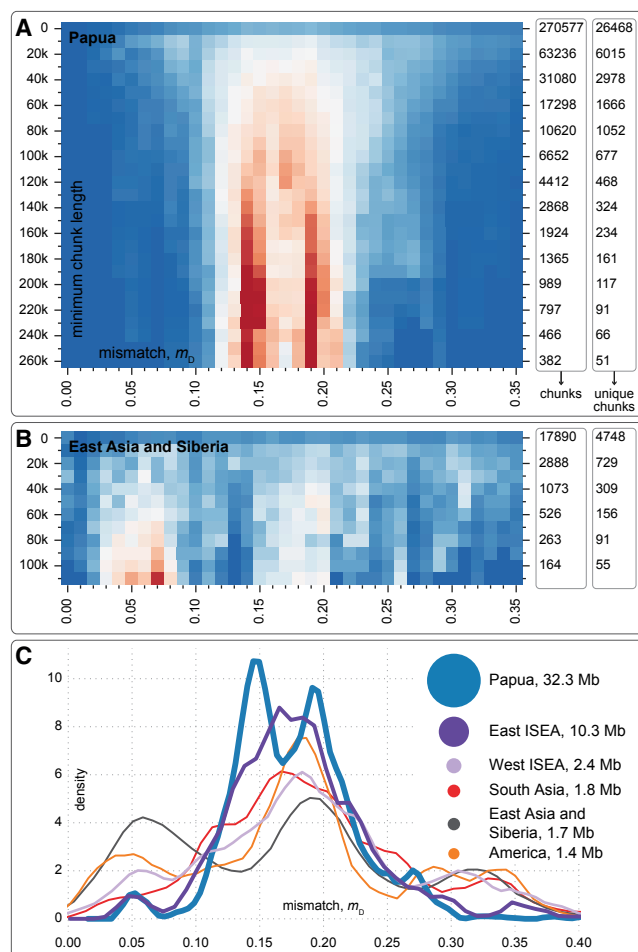
Figure 3. Mismatch Distributions by Block Size

(A) Heatmap showing the mismatch distribution of high-confidence Denisovan introgressed blocks against the Altai Denisovan (x axis; expressed as a percentage of the average genome-wide mismatch between the Denisovan genome and West Eurasians, m_D (STAR Methods S10a) given different minimum block lengths (y axis). The columns to the right indicate the total number of blocks and the number of entirely non-overlapping (i.e., unambiguously unique) blocks, respectively. As expected (see STAR Methods 10a for explanation), the two mismatch peaks are not visible for small block lengths (<50 kb), and only become clear for blocks of length around ≥ 130 kb. The two mismatch peaks are stable in their location after this point.

(B) Heatmap as in (A), this time showing the mismatch distribution when analyzing Siberian and East Asian samples together. Note the absence of the first peak observed in Papuans in (A) and the presence of the less diverged peak identified previously (Browning et al., 2018).

(C) Mismatch m_D of the 2000 longest high-confidence Denisovan blocks for different continental groups. Circle area corresponds to the average amount per individual (Mb) of high-confidence Denisovan sequence identified in each population.

See also Figures S2 and S3.

Denisovan Populations Introgressed into Papuans Twice

To determine whether there is structure within the Denisovan sequences, we calculated mismatch distributions between our high-confidence Denisovan blocks and the high-coverage Altai Denisovan genome (STAR Methods S10). Small ancestry blocks

can be a problem for mismatch analysis, because the mismatches of individual haplotypes have an imprecise correspondence to genetic divergence caused by the low resolution offered by a small number of stochastic, discrete polymorphisms (STAR Methods S10a) and because small blocks are more often affected by incomplete lineage sorting. We therefore profiled mismatches across a range of block lengths in Papuans, the population in our dataset with the highest Denisovan introgression. Intriguingly, we observe two clearly separate mismatch peaks in Papuans (Figure 3A; STAR Methods S10a). This suggests that Papuans carry lineages from two genetically different Denisovan populations that had been separated from each other for a very long time. These peaks are also observed when using just the CP blocks or just the HMM blocks alone (STAR Methods 10b). Resolution of the two peaks (here called D1 and D2) improves with block sizes greater than approximately 130 kb, with much less resolution for blocks <50 kb as expected for small block sizes (STAR Methods S10a).

We also confirm the signal previously reported in East Asians (Browning et al., 2018), but again only for longer block lengths (Figures 3B and 3C). The mismatch peak (here called D0) is additionally seen not just in East Asian populations, where it was originally detected, but also in Siberians, indigenous Americans and at very low frequency elsewhere across Asia (Figures 3B and 3C; STAR Methods S10a). The blocks in this predominantly East Asian mismatch peak have relatively low divergence to the Altai Denisovan, suggesting that modern humans in Asia mixed with a Denisovan population that was closely related to the Denisovan reference individual.

As longer blocks are better able to capture demographic complexity from mismatch distributions, we profiled mismatch patterns using the 2,000 longest blocks to maximize the signal in each population. Regional patterns are apparent: D1 is restricted to Papuans, while D2 has a wider geographical distribution spanning much of Asia and Oceania (Figure 3C; STAR Methods S10a; Figure S2).

Gaussian mixture model testing strongly supports the presence of two peaks in Papuans (Figure 4A, AIC = −5,809 versus unimodal −5,583, STAR Methods S10d). In Papuans, blocks of length >180 kb were assigned to one or the other peak based on >80% support from the mixture model. We confirmed that D1 (less divergent from Altai Denisovan) and D2 (more divergent) blocks do not differ in a wide range of molecular genetic and bioinformatic parameters, including GC content, genotype call quality of the archaic reference allele, alignability, recombination rate, sequencing batch effects, and levels of background selection (B values; McVicker et al., 2009) (STAR Methods 10e and 10f). We also checked whether variants within the D1 and D2 blocks have the same tree topologies. Both peaks show a strong signal of an origin within the Denisovan clade rather than branching from deeper points in the hominin tree (Table S4; STAR Methods S10g). We further verified that the observed bimodal mismatch distribution in our high-confidence Denisovan blocks is not due to misclassification of Neanderthal blocks. The polymorphic sites of both peaks predominantly show the Denisovan-specific topology, with the Neanderthal-specific topology observed only at low levels (STAR Methods S10g). Further, if one of the peaks
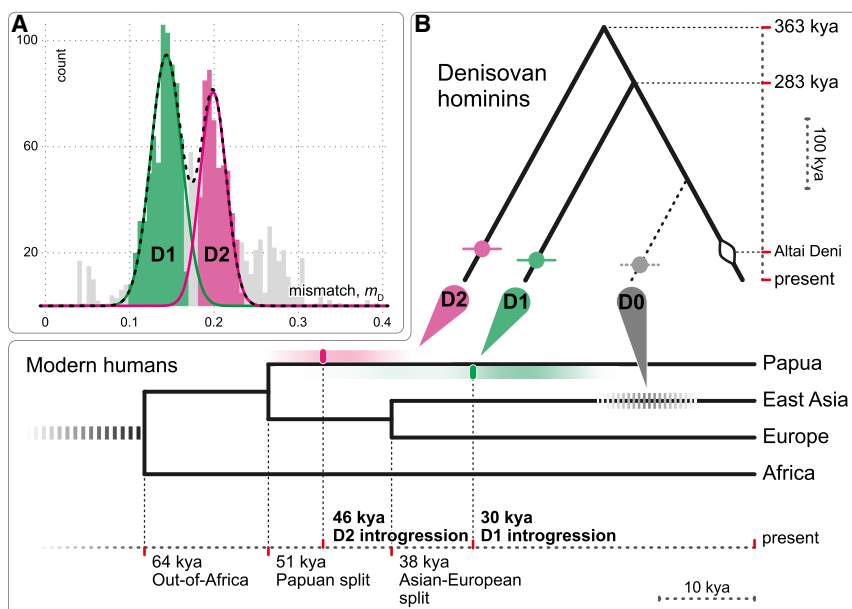
Figure 4. Multiple Denisovan Ancestries in Papuans

(A) Bimodal distribution and simulation fitting for long (>180 kb) high-confidence Denisovan blocks in Papuans (STAR Methods S10a and S10d).

(B) Schematic model of the relationships of archaic hominin and modern human groups. We detect introgression from three Denisovan-like populations: the previously reported D0 lineage (gray) into East Asians (Browning et al., 2018) and Siberians with a likely recent introgression date, and the D1 (green) and D2 (magenta) lineages into Papuans that are detected here. The tree topologies of D1 and D2 haplotypes indicate that they branch from the Denisovan clade, albeit deeply for D2, and their bimodal mismatch indicates that they are not sister clades. Note the different timescales of the two orthogonal trees. Shaded circles on archaic tree branches indicate introgression time estimates. The details of these estimates (STAR Methods S10h) are shown on the modern human tree; the 95% CIs of introgression dates are shaded with color proportional to probability density, with bootstrapped values showing the center of gravity lies toward younger dates. No time estimates were reported for D0 in the original publication and its divergence from the Altai Denisovan and introgression date are arbitrarily placed as indicated by dashed lines. The open diamond indicates the temporal sampling point of the Altai Denisovan genome sequence. See also Figures S3, S4, and S5 and Table S5.

were caused by Neanderthal introgression misclassified as Denisovan, that peak should be seen in West Eurasians, who have substantial Neanderthal but no Denisovan admixture. However, West Eurasians have neither of the two Denisovan mismatch peaks. To additionally check whether some portion of the Neanderthal introgression signal could have been missed by only using the Altai Neanderthal reference, we repeated several analyses using CP and the Vindija Neanderthal (Prüfer et al., 2017). This approach yields highly consistent results with the original analysis (Figure S3; STAR Methods S10c). Finally, we identified Neanderthal-specific blocks in Papuans using the same methodology as for the high-confidence Denisovan blocks. These do not show a bimodal mismatch distribution to the Altai Neanderthal (Figure S3; STAR Methods S10c), suggesting that the history of Denisovan introgression in Papua differed markedly from modern human interactions with Neanderthals.

Deep Divergence between Denisovan Populations

Next, we sought to retrieve dates of divergence between D1, D2, and the Altai Denisovan genome through coalescent modeling (Tables S5A and S5B; STAR Methods S10i). After extending an archaic demographic model (Malaspinas et al., 2016) to encompass two deeply divergent Denisovan-related components, our best fitting model indicates that D1 and D2 split from the Altai Denisovan approximately 283 kya (9,750 generations, 95% confidence interval [CI] 261–297 kya) and 363 kya (12,500 generations, 95% CI 334–377 kya), respectively (Figure 4B). While clearly branching off the Denisovan line, D2 diverged so closely to the Neanderthal-Denisovan split that it is perhaps better considered as a third sister group (STAR Methods S10i). For context, even the youngest of these divergence times is similar to the evolutionary age of anatomically modern humans (earliest

known fossils, with varied morphologies, date to 198 kya (McDougall et al., 2005) and 315 kya (Hublin et al., 2017)). Our model implies substantial reproductive separation of multiple Denisovan-like populations over a period of hundreds of thousands of years.

The Two Denisovan Lineages Introgressed at Different Times

The distribution of block lengths retains a signal of introgression time, with longer blocks expected from more recent introgression events. In general, block length is expected to decay over time approximately as an exponential distribution (Gravel, 2012). We confirmed the accuracy of introgression dating by exponential fitting of the block length distribution through extensive simulation, incorporating different introgression times over the time period of interest (0–2,000 generations), and considering the impact of using only long blocks rather than the entire distribution of block lengths, substantial block length estimation errors, and the consequences if introgression occurred as an extended process rather than a single pulse (Figure S4; STAR Methods S10h). We observed a slight tendency to infer overly recent dates under some of these conditions, but never by more than 10%–15%. Filtering to longer block lengths and fitting an exponential with a larger location parameter help to reduce even these biases in date estimates.

While the median block lengths of D1 and D2 are similar in Papuans (238 and 236 kb), their distributions are significantly different (Kolmogorov-Smirnov statistic = 0.15, p = 2.2 × 10^{-6}). Exponential fitting of D1 and D2 haplotype lengths yields introgression dates of 29.8 kya (95% CI 14.4–50.4) and 45.7 kya (95% CI 31.9–60.7), respectively, which are younger, though overlapping with, previously suggested estimates for Denisovan
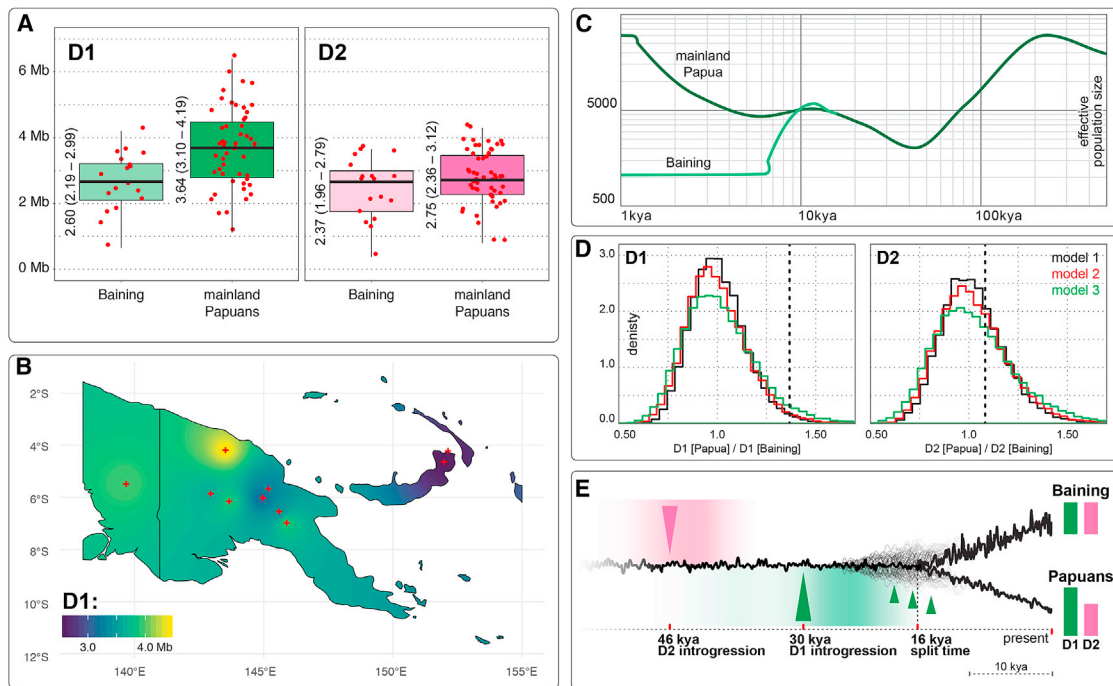
Figure 5. Geographic Patterns of D1 and D2 Ancestry

(A) Comparison of the total identified amounts of D1 and D2 sequence in Baining and mainland Papuan individuals. The difference in D1 between the groups is statistically significant, while the D2 difference is not. Average and 95% CIs obtained using resampling are shown next to each box (STAR Methods S10h).

(B) Interpolated map of D1 signal across sampled populations in mainland Papua and New Britain.

(C) SMC++ model of the (diploid) population sizes and split time of Baining and mainland Papua samples (STAR Methods 10j).

(D) Simulated distributions of the ratio of D1 in mainland Papua to D1 in Baining, and of D2 in mainland Papua to D2 in Baining, under three conservative demographic models simulating high levels of drift between the two populations (Figure S6; STAR Methods S10j). The observed ratios are indicated as vertical dashed lines. The observed D1 ratio is above the 95th percentile of the distribution (i.e., statistically significant) under all three models, while there is no difference for D2.

(E) Model for regional details of Denisovan introgression. D2 (magenta arrow) introgressed into the common ancestor of mainland Papuans and Baining about 46 kya. D1 (green arrow) introgression occurred later, closer to the separation of the two Papuan groups. The 95% CIs of introgression dates are shaded with color proportional to probability density (STAR Methods S10h). The split time between mainland Papuans and Baining (16 kya) estimated by SMC++ is an effective genetic parameter describing a divergence date without subsequent migration and hence is a lower bound with actual separation likely occurring somewhat earlier (indicated by alternative gray split paths). Our modeling shows that genetic drift alone (indicated by jittered branches) is insufficient to explain the observed higher D1 frequency in mainland New Guinea (bar charts on right) and instead requires additional D1 introgression into mainland Papuans after their separation from the Baining (small green arrows).

introgression (Figure 4B; STAR Methods S10h) (Malaspinas et al., 2016). The maximum likelihood introgression date for D2 introgression is 50% more ancient than the date for D1. Based on simulations, and given the greater statistical challenge of identifying shorter introgression blocks, we consider these dates to be probable lower bounds on introgression times, but with true dates no more than 15% more ancient.

Geographical Patterns of Denisovan Admixture in Papua

D1 and D2 introgression times that overlap the timescale of modern human arrival and their variable dispersal across Papua raise the possibility that Denisovan introgression occurred after local populations of modern humans had differentiated. We find geographic structure associated with the D1 variation between mainland New Guinea and the Baining, a population on the offshore island of New Britain. We observe slightly less high-confidence Denisovan introgression in the Baining than in mainland Papuans (31.5 Mb versus 33.1 Mb per haploid genome, Welch's

t test T = −3.4, p = 0.001), despite extremely similar population histories (Hudjashov et al., 2017), including similar levels of Asian ancestry (Figure 1A). However, there is less D1 sequence in the Baining than in mainland Papuans (1.33 Mb versus 1.82 Mb per haploid genome, Welch's t test T = −3.9, p < 0.01), although both carry similar levels of D2 sequence (1.28 Mb versus 1.37 Mb, T = −0.8, p = 0.41) (Figures 5A and 5B; STAR Methods S10h).

To determine whether this difference in D1 sequence could be due to random drift in the two populations or to different Denisovan introgression histories, we extended the simulation model (Malaspinas et al., 2016) to incorporate population structure representing both New Guinea mainlanders and Baining, in addition to the two introgressing Denisovan populations (D1 and D2) (Figure S5; STAR Methods S10j). To test a conservative model offering maximum opportunity for isolation and drift, we did not include any migration between Papuans and Baining after their population split. Archeological evidence suggests that New

Britain was settled by at least 35 kya (Pavlides and Gosden, 1994), and from the genomic data, SMC++ (Terhorst et al., 2017) infers a genetic split time between mainland Papuans and Baining of 15.7 kya (Figure 5C). We therefore implemented three alternative demographic models: using the SMC++ genetic split times and population sizes (M1); using the SMC++ split time and more conservative (smaller) population sizes, thus generating more drift (M2); and a model with a more conservative (older) genetic split time of 23.2 ky (800 generations), also generating more drift (M3) (Figure S6; STAR Methods S10j). As expected, the observed difference in rates of D2 introgression between Baining and mainland Papuans are within the distributions predicted by the simulations. However, in all three cases, the observed ratio of D1 in mainland Papuans to Baining lies outside simulated values (Figure 5D).

Together, these coalescent simulations suggest that the reduced frequency of D1 blocks among the Baining is unlikely to result from shared D1 introgression into a common ancestral Papuan population, followed by drift as each population subsequently diverged into the modern Baining and mainland groups. Instead, the difference in D1 levels more likely reflects different amounts of introgression from Denisovan populations into mainland New Guinea and the islands to the northeast, which occurred after the separation of the two Papuan populations (Figure 5E). The overall genetic similarity and relatively recent divergence of these Papuan groups (Figures 1 and 5C; STAR Methods S10h, S10j) have implications for the past distribution of D1 Denisovan populations and the process of archaic introgression.

First, our data suggest that the D1 Denisovans, in contrast to D2, contributed additional DNA to the mainland New Guinea population after the mainland and Baining populations diverged from their common Papuan ancestor (Figure 5E). This, together with the nearly complete absence of D1 in continental Asia, is most consistent with the scenario that D1 Denisovans were present in New Guinea or East ISEA (e.g., Wallacea). In turn, this would imply that at least some Denisovan populations had the ability to cross large bodies of water, such as the one represented by the Wallace Line. This idea does not seem implausible given archaeological evidence of archaic hominin dispersals—notably, the discovery of stone tools in the Philippines dating to 700 kya (Ingicco et al., 2018) and the related finding of *H. floresiensis* on the island of Flores (Brown et al., 2004), both across substantial water boundaries that persisted throughout the Pleistocene. Such geographical barriers would limit gene flow and might help to explain the extent of divergence between the D1 Denisovan population and other Denisovan groups.

Second, the late date for the D1 introgression and geographic structure in modern populations suggests that Denisovans survived until 30 kya, and perhaps as recently as 14.5 kya. This is longer than Neanderthals, who died out around 40 kya (Higham et al., 2014), or *H. floresiensis*, which recent dating suggests did not persist on Flores beyond 50–60 kya (Sutikna et al., 2016). The implication is that Denisovans living in ISEA may have been among the last of all the archaic hominins to survive. This provides an argument to screen for Denisovan remains possibly misclassified as other hominins in existing archaeological collections and encourages more archaeological research in the poorly accessible and hence incredibly understudied New Guinea region.

Third, the combined evidence of geographic structure and a recent D1 introgression date suggest that Denisovan introgression did not occur immediately following the first modern human settlement in the region (45–50 kya) (O'Connell et al., 2018). This implies that introgression with archaic hominins may not be an inevitable and immediate result of joint occupation of the same territory.

High-Frequency Denisovan Blocks Include Many Archaic Gene Variants

We also investigated whether the Denisovan DNA that entered modern Papuans could have included regions with adaptive benefits (Table S6; STAR Methods S11). We initially focused on genes introgressed from D1 and D2. As we could only assign long blocks to D1 or D2 ancestry, we can only partly describe diversity contributed by specific Denisovan groups. However, we did identify 412 unique genes in introgressed blocks assigned to D1 and D2, including high-frequency blocks. The haplotypes with highest frequency in either lineage included the linked genes *FAM178B/FAHD2B/ANKRD36* (65% frequency), *ZNF280D* (38%), and *FBXL20/MED1/CDK12* (28%) from D1, and *ANKRD28* (30%), a region 15 kb downstream of *CENPW* (29%) and *NFAT5/NQO1* (22%) from D2 (STAR Methods S11d).

To explore adaptive introgression from Denisovans more broadly, we profiled the frequency of all >20 kb introgressing haplotypes in East ISEA and Papua (Figure 6; STAR Methods S11a), an approach that considers the actual introgressing haplotypes rather than being window based and thus offers greater precision in identifying genes that may have contributed to adaptation. We first searched for evidence of ontology enrichment (Kuleshov et al., 2016) in genes found in the top 1% most frequent Denisovan haplotypes (STAR Methods S11c). Enrichment was observed in categories related to smooth muscle cell proliferation, immunity, and adipogenesis in both Papuans and East ISEA.

Focusing on the 10 highest-frequency introgressed haplotypes (STAR Methods S11a), we replicated several previously known signals—*WARS2* in East ISEA but not Papua (Racimo et al., 2017), introgression in *TNFAIP3* in both East ISEA and Papua (Gittelman et al., 2016), and *FAM178B* (Ilardo et al., 2018) but seen here more in Papuans than in East ISEA. We additionally observe two previously unknown high-frequency introgression signals in both regions, centered around the *TMPO*, *IKBIP*, and *APAF1* genes, as well as in a single gene, *WDFY2*. The latter has been identified as a focus of accelerated evolution in humans since the Neanderthal-Denisovan split (Racimo et al., 2014) and is involved in endocytosis (Hayakawa et al., 2006) and adipogenesis through regulation of *PPARG* (Fritzius and Moelling, 2008), which is also a high frequency Denisovan introgressed gene in Papua and East ISEA. Depletion of *WDFY2* in 3T3-L1 adipocytes is associated with reduced insulin-stimulated glucose uptake (Walz et al., 2010), indicating a role in both the differentiation and functioning of adipoctyes.

To determine whether Denisovan gene variants in modern humans may have experienced recent positive selection, we
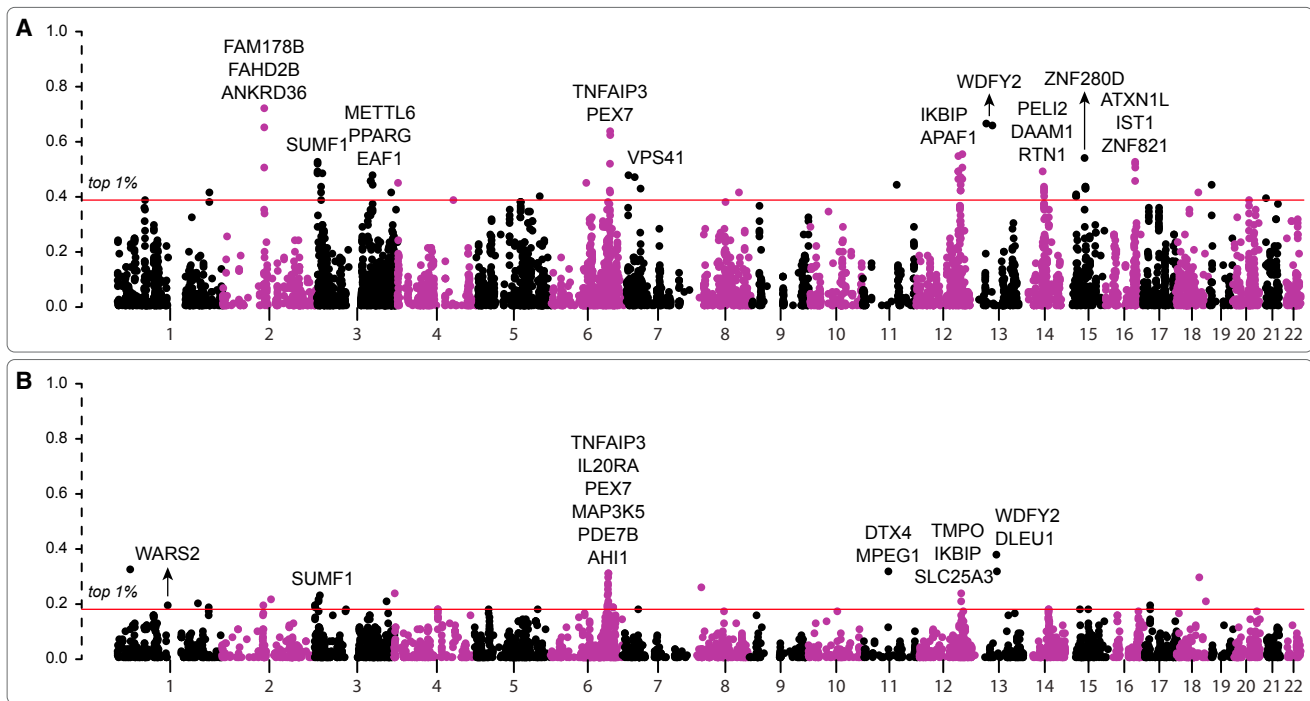
Figure 6. Manhattan Plot of High-Frequency High-Confidence Denisovan Blocks (>20 kb) across Chromosomes
(A and B) Manhattan plots of Denisovan block frequencies are shown for Papuans (A) and East ISEA (B). A selection of outlier genes are noted. See Table S6 and STAR Methods S11 for details.

calculated nSL (Ferrer-Admetlla et al., 2014) in 200 kb windows across the genome for mainland Papuan samples, the Baining, and East ISEA separately. Several top 1% high-frequency Denisovan introgressed genes were in the top 5% of nSL windows (STAR Methods S11b). Overlapping hits in the Baining included *TNFAIP3* (nSL window percentile 3.6%) and *WDFY2* (2.2%). The possibility of adaptive introgression at *TNFAIP3* has been raised previously in the context of selection on immunity (Gittelman et al., 2016). The function of *WDFY2* has been discussed above. We also note the top 1% nSL signals in genes with important roles in both lipid metabolism (*FASN* in Baining, mainland Papua, and East ISEA, and a window containing both *FADS1* and *FADS2* in Baining only) and carbohydrate metabolism (most notably *AGL* in both Baining and mainland Papua). Taken together, it appears that Denisovan introgression may have been an important source of diversity for recent adaptation, both in the context of immunity and, potentially, dietary adaptation.

Limited Evidence of Further Introgression Complexity in East ISEA and Papua
Given the recent presence of *Homo floresiensis* in our study area (Brown et al., 2004; Sutikna et al., 2016), and the possibility that late *Homo erectus* was contemporary with the earliest anatomically modern humans in ISEA (Yokoyama et al., 2008), we investigated whether there might be any hints of archaic hominin ancestry, other than Denisovan or Neanderthal, in the dataset. We attempted to detect such signals by analyzing S* windows that exhibit minimal overlap with Denisovan or Neanderthal

blocks as identified by CP and HMM (residual S*, STAR Methods S12).

We first note a pronounced excess in total S* signal in our Papuan samples (97.2 Mb) compared to East Asians (50.9 Mb), South Asians (48.3 Mb), and West Eurasians (40.8 Mb). After confirming that this excess was primarily driven by introgressing Denisovan ancestry, we estimate that any additional introgression from outside the Human-Neanderthal-Denisovan clade was limited with an upper bound of about 1% (STAR Methods S12a). Next, by profiling residual S* among different continental groups, we detect a slight excess of unique variation that is not shared with other humans, the Altai Denisovan or the Altai Neanderthal in East ISEA and Papua (Figure S7; STAR Methods S12b). The signal is not strong, and the difference in total residual S* between different global populations is small, suggesting at most little introgression from outside the Human-Neanderthal-Denisovan lineage in these two populations. This could hint at a more complex introgression history involving unknown archaic hominins in ISEA and Papua, such as *H. erectus*, as has been recently suggested for other Asian populations (Mondal et al., 2016). For instance, the Altai Denisovan is also thought to have some *H. erectus* ancestry (Lipson and Reich, 2017; Mallick et al., 2016; McColl et al., 2018; Prüfer et al., 2017; Skoglund et al., 2016), although it is not yet clear whether this is also true for introgressing Denisovan populations. Equally, however, these genomic signals could arise without further introgression events, notably through balancing selection or incomplete lineage sorting, and so warrant careful further study.
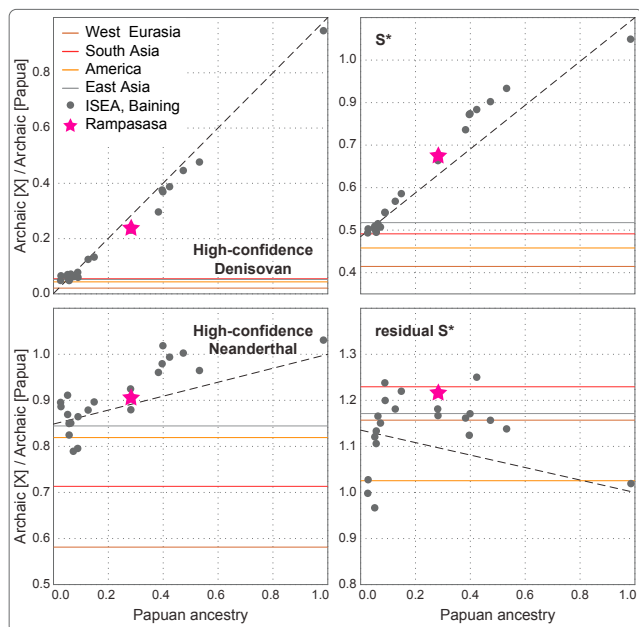
Figure 7. Correlations of Papuan Ancestry with Archaic and S* Components

High Correlation of Papuan Ancestry with High-Confidence Denisovan (upper left), High-Confidence Neanderthal (bottom left), S* (top right), and residual S* (bottom right) in ISEA. Reference continental values are shown as horizontal colored lines. Note that Rampasasa (star) does not differ greatly from other regional populations.

Finally, our dataset includes Rampasasa, a village on Flores that is close to the cave site where the *H. floresiensis* bones were found (Sutikna et al., 2016), and whose inhabitants were the subject of a recent genetic study (Tucci et al., 2018) The proportion of Neanderthal and Denisovan introgression, and the amount of residual S* in this village is comparable to neighboring populations (Figure 7; STAR Methods S13), suggesting the absence of unusual archaic admixture in Rampasasa villagers relative to other people in East ISEA.

Conclusions

The discovery and characterization of archaic hominins has typically begun with the analysis of fossil remains (Meyer et al., 2012; Prüfer et al., 2014, 2017; Slon et al., 2018). However, as Denisovan admixture has its center of gravity in ISEA and Papua where DNA rarely survives more than a few thousand years in the humid tropical environment (Lipson et al., 2018; McColl et al., 2018), studying the genetic record from modern humans remains the sole way to shed light on the substructure and phylogeography of archaic hominins in this important but understudied region.

Here, we use a statistical approach on new genomes from ISEA and Papua to identify two new Denisovan groups (D1 and D2) and describe the relationships between these archaic hominins long before they first interacted with anatomically modern humans. Both groups branched off early from the Altai Denisovan clade at 283 and 363 kya and were reproductively isolated from the individuals at Denisova cave in Siberia

and from each other. Yet both groups bred with modern humans, contributing around 4% of the genomes of Papuans, including over 400 gene variants enriched for traits involving immunity and diet. Some of this introgression is restricted to modern New Guinea and its surrounding islands and may have occurred as late as the very end of the Pleistocene, making the admixing D1 Denisovan population among the last surviving archaic hominins in the world.

The genetic diversity within the Denisovan clade is consistent with their deep divergence and separation into at least three geographically disparate branches, with one contributing an introgression signal in Oceania and to a lesser extent across Asia (D2), another apparently restricted to New Guinea and nearby islands (D1), and a third in East Asia and Siberia (D0). This suggests that Denisovans were capable of crossing major geographical barriers, including the persistent sea lanes that separated Asia from Wallacea and New Guinea. They therefore spanned an incredible diversity of environments, from temperate continental steppes to tropical equatorial islands. The emerging picture suggests that far from moving into sparsely inhabited country, modern humans experienced repeated and persistent interactions as they expanded out of Africa into this highly structured archaic landscape across Eurasia. This genetic contact yielded a rich legacy, including hundreds of gene variants that continue to contribute to the adaptive success of anatomically modern humans today.

STAR★METHODS

Detailed methods are provided in the online version of this paper and include the following:

- KEY RESOURCES TABLE
- CONTACT FOR REAGENT AND RESOURCE SHARING
- EXPERIMENTAL MODEL AND SUBJECT DETAILS
  - Human subjects
  - Ethical approvals and dataset description
- METHOD DETAILS
  - S1 - Sequencing and SNP calling
  - S2 - Kinship and outlier analysis
  - S3 - Adding archaic data and ancestral information
  - S4 - Phasing and phasing assessment
- QUANTIFICATION AND STATISTICAL ANALYSIS
  - S5 - Dataset genetic diversity and SNP novelty
  - S6 - Estimating Asian-Papuan admixture proportions
  - S7 - Archaic block identification
  - S8 - Introgression results from the three methods
  - S9 - Refining archaic block sets
  - S10 - Archaic mismatch analysis
  - S11 - Frequency distribution of archaic blocks
  - S12 - Residual S* signal
  - S13 – Rampasasa is not an introgression outlier
- DATA AND SOFTWARE AVAILABILITY

AUTHOR CONTRIBUTIONS

G.S.J. and G.H. performed the primary analyses; L.S. performed SNP calling and validation; P.K. analyzed the genes; C.C.D. provided laboratory support; M. Mondal, D.J.L., and L.P. advised on ancestry detection; F.-X.R., M.S., and M. Metspalu advised on analyses and interpretation; G.S.J., G.H., H.S., J.S.L., and M.P.C. designed the project; G.S.J., G.H., and M.P.C. wrote the manuscript based on input from all the other authors. The sequence data are available from the European Genome-phenome Archive (accession EGAS00001003054). Variant files are available from the Estonian Biocenter data archive (http://evolbio.ut.ee).

DECLARATION OF INTERESTS

The authors declare no competing interests.

REFERENCES

1000 Genomes Project Consortium, Auton, A., Brooks, L.D., Durbin, R.M., Garrison, E.P., Kang, H.M., Korbel, J.O., Marchini, J.L., McCarthy, S., McVean, G.A., and Abecasis, G.R. (2015). A global reference for human genetic variation. Nature 526, 68–74.

Abi-Rached, L., Jobin, M.J., Kulkarni, S., McWhinnie, A., Dalva, K., Gragert, L., Babrzadeh, F., Gharizadeh, B., Luo, M., Plummer, F.A., et al. (2011). The shaping of modern human immune systems by multiregional admixture with archaic humans. Science 334, 89–94.

Barker, G., Barton, H., Bird, M., Daly, P., Datan, I., Dykes, A., Farr, L., Gilbertson, D., Harrisson, B., Hunt, C., et al. (2007). The 'human revolution' in lowland tropical Southeast Asia: the antiquity and behavior of anatomically modern humans at Niah Cave (Sarawak, Borneo). J. Hum. Evol. 52, 243–261.

Bergström, A., Oppenheimer, S.J., Mentzer, A.J., Auckland, K., Robson, K., Attenborough, R., Alpers, M.P., Koki, G., Pomat, W., Siba, P., et al. (2017). A Neolithic expansion, but strong genetic structure, in the independent history of New Guinea. Science 357, 1160–1163.

Bolger, A.M., Lohse, M., and Usadel, B. (2014). Trimmomatic: a flexible trimmer for Illumina sequence data. Bioinformatics 30, 2114–2120.

Brown, P., Sutikna, T., Morwood, M.J., Soejono, R.P., Jatmiko, Saptomo, E.W., and Due, R.A. (2004). A new small-bodied hominin from the Late Pleistocene of Flores, Indonesia. Nature 431, 1055–1061.

Browning, S.R., Browning, B.L., Zhou, Y., Tucci, S., and Akey, J.M. (2018). Analysis of human sequence data reveals two pulses of archaic Denisovan admixture. Cell 173, 53–61.

Chang, C.C., Chow, C.C., Tellier, L.C., Vattikuti, S., Purcell, S.M., and Lee, J.J. (2015). Second-generation PLINK: rising to the challenge of larger and richer datasets. Gigascience 4, 7.

Cox, M.P., Karafet, T.M., Lansing, J.S., Sudoyo, H., and Hammer, M.F. (2010). Autosomal and X-linked single nucleotide polymorphisms reveal a steep Asian-Melanesian ancestry cline in eastern Indonesia and a sex bias in admixture rates. Proc. Biol. Sci. 277, 1589–1596.

Delaneau, O., Howie, B., Cox, A.J., Zagury, J.F., and Marchini, J. (2013). Haplotype estimation using sequencing reads. Am. J. Hum. Genet. 93, 687–696.

Dias-Alves, T., Mairal, J., and Blum, M.G.B. (2018). Loter: a software package to infer local ancestry for a wide range of species. Mol. Biol. Evol. 35, 2318–2326.

Ferrer-Admetlla, A., Liang, M., Korneliussen, T., and Nielsen, R. (2014). On detecting incomplete soft or hard selective sweeps using haplotype structure. Mol. Biol. Evol. 31, 1275–1291.

Frazer, K.A., Ballinger, D.G., Cox, D.R., Hinds, D.A., Stuve, L.L., Gibbs, R.A., Belmont, J.W., Boudreau, A., Hardenbol, P., Leal, S.M., et al.; International HapMap Consortium (2007). A second generation human haplotype map of over 3.1 million SNPs. Nature 449, 851–861.

Friedlaender, J.S., Friedlaender, F.R., Reed, F.A., Kidd, K.K., Kidd, J.R., Chambers, G.K., Lea, R.A., Loo, J.-H., Koki, G., Hodgson, J.A., et al. (2008). The genetic structure of Pacific Islanders. PLoS Genet. 4, e19.

Fritzius, T., and Moelling, K. (2008). Akt- and Foxo1-interacting WD-repeat-FYVE protein promotes adipogenesis. EMBO J. 27, 1399–1410.

Gittelman, R.M., Schraiber, J.G., Vernot, B., Mikacenic, C., Wurfel, M.M., and Akey, J.M. (2016). Archaic hominin admixture facilitated adaptation to Out-of-Africa environments. Curr. Biol. 26, 3375–3382.

Gravel, S. (2012). Population genetics models of local ancestry. Genetics 191, 607–619.

Green, R.E., Krause, J., Briggs, A.W., Maricic, T., Stenzel, U., Kircher, M., Patterson, N., Li, H., Zhai, W., Fritz, M.H., et al. (2010). A draft sequence of the Neanderthal genome. Science 328, 710–722.

Hammer, M.F., Woerner, A.E., Mendez, F.L., Watkins, J.C., and Wall, J.D. (2011). Genetic evidence for archaic admixture in Africa. Proc. Natl. Acad. Sci. USA 108, 15123–15128.

Hayakawa, A., Leonard, D., Murphy, S., Hayes, S., Soto, M., Fogarty, K., Standley, C., Bellve, K., Lambright, D., Mello, C., and Corvera, S. (2006). The WD40 and FYVE domain containing protein 2 defines a class of early endosomes necessary for endocytosis. Proc. Natl. Acad. Sci. USA 103, 11928–11933.

Henn, B.M., Botigué, L.R., Bustamante, C.D., Clark, A.G., and Gravel, S. (2015). Estimating the mutation load in human genomes. Nat. Rev. Genet. 16, 333–343.

Henningsson, S., Hovey, D., Vass, K., Walum, H., Sandnabba, K., Santtila, P., Jern, P., and Westberg, L. (2017). A missense polymorphism in the putative pheromone receptor gene VN1R1 is associated with sociosexual behavior. Transl. Psychiatry 7, e1102.

Higham, T., Douka, K., Wood, R., Ramsey, C.B., Brock, F., Basell, L., Camps, M., Arrizabalaga, A., Baena, J., Barroso-Ruíz, C., et al. (2014). The timing and spatiotemporal patterning of Neanderthal disappearance. Nature 512, 306–309.

Hofreiter, M., Jaenicke, V., Serre, D., von Haeseler, A., and Pääbo, S. (2001). DNA sequences from multiple amplifications reveal artifacts induced by cytosine deamination in ancient DNA. Nucleic Acids Res. 29, 4793–4799.

Horton, R. (2016). Indonesia – unravelling the mystery of a nation. Lancet 387, 830.

Hublin, J.-J., Ben-Ncer, A., Bailey, S.E., Freidline, S.E., Neubauer, S., Skinner, M.M., Bergmann, I., Le Cabec, A., Benazzi, S., Harvati, K., and Gunz, P. (2017).

New fossils from Jebel Irhoud, Morocco and the pan-African origin of *Homo sapiens*. Nature *546*, 289–292.

Hudjashov, G., Karafet, T.M., Lawson, D.J., Downey, S., Savina, O., Sudoyo, H., Lansing, J.S., Hammer, M.F., and Cox, M.P. (2017). Complex patterns of admixture across the Indonesian archipelago. Mol. Biol. Evol. *34*, 2439–2452.

Hudson, R.R. (2002). Generating samples under a Wright-Fisher neutral model of genetic variation. Bioinformatics *18*, 337–338.

Ilardo, M.A., Moltke, I., Korneliussen, T.S., Cheng, J., Stern, A.J., Racimo, F., de Barros Damgaard, P., Sikora, M., Seguin-Orlando, A., Rasmussen, S., et al. (2018). Physiological and genetic adaptations to diving in sea nomads. Cell *173*, 569–580.e15.

Ingicco, T., van den Bergh, G.D., Jago-On, C., Bahain, J.J., Chacón, M.G., Amano, N., Forestier, H., King, C., Manalo, K., Nomade, S., et al. (2018). Earliest known hominin activity in the Philippines by 709 thousand years ago. Nature *557*, 233–237.

Jinam, T.A., Phipps, M.E., Aghakhanian, F., Majumder, P.P., Datar, F., Stoneking, M., Sawai, H., Nishida, N., Tokunaga, K., Kawamura, S., et al. (2017). Discerning the origins of the Negritos, First Sundaland Peoples: deep divergence and archaic admixture. Genome Biol. Evol. *9*, 2013–2022.

Kelleher, J., Barton, N.H., and Etheridge, A.M. (2013). Coalescent simulation in continuous space. Bioinformatics *29*, 955–956.

Kuleshov, M.V., Jones, M.R., Rouillard, A.D., Fernandez, N.F., Duan, Q., Wang, Z., Koplev, S., Jenkins, S.L., Jagodnik, K.M., Lachmann, A., et al. (2016). Enrichr: a comprehensive gene set enrichment analysis web server 2016 update. Nucleic Acids Res. *44* (W1), W90-7.

Lawson, D.J., Hellenthal, G., Myers, S., and Falush, D. (2012). Inference of population structure using dense haplotype data. PLoS Genet. *8*, e1002453.

Lek, M., Karczewski, K.J., Minikel, E.V., Samocha, K.E., Banks, E., Fennell, T., O'Donnell-Luria, A.H., Ware, J.S., Hill, A.J., Cummings, B.B., et al.; Exome Aggregation Consortium (2016). Analysis of protein-coding genetic variation in 60,706 humans. Nature *536*, 285–291.

Li, H. (2011). A statistical framework for SNP calling, mutation discovery, association mapping and population genetical parameter estimation from sequencing data. Bioinformatics *27*, 2987–2993.

Li, H. (2013). Aligning sequence reads, clone sequences and assembly contigs with BWA-MEM. arXiv:1303.3997 https://arxiv.org/abs/1303.3997.

Liang, M., and Nielsen, R. (2014). The lengths of admixture tracts. Genetics *197*, 953–967.

Lipson, M., and Reich, D. (2017). A working model of the deep relationships of diverse modern human genetic lineages outside of Africa. Mol. Biol. Evol. *34*, 889–902.

Lipson, M., Cheronet, O., Mallick, S., Rohland, N., Oxenham, M., Pietrusewsky, M., Pryce, T.O., Willis, A., Matsumura, H., Buckley, H., et al. (2018). Ancient genomes document multiple waves of migration in Southeast Asian prehistory. Science *361*, 92–95.

Lu, D., Lou, H., Yuan, K., Wang, X., Wang, Y., Zhang, C., Lu, Y., Yang, X., Deng, L., Zhou, Y., et al. (2016). Ancestral origins and genetic history of Tibetan highlanders. Am. J. Hum. Genet. *99*, 580–594.

Malaspinas, A.S., Westaway, M.C., Muller, C., Sousa, V.C., Lao, O., Alves, I., Bergström, A., Athanasiadis, G., Cheng, J.Y., Crawford, J.E., et al. (2016). A genomic history of Aboriginal Australia. Nature *538*, 207–214.

Mallick, S., Li, H., Lipson, M., Mathieson, I., Gymrek, M., Racimo, F., Zhao, M., Chennagiri, N., Nordenfelt, S., Tandon, A., et al. (2016). The Simons Genome Diversity Project: 300 genomes from 142 diverse populations. Nature *538*, 201–206.

Manichaikul, A., Mychaleckyj, J.C., Rich, S.S., Daly, K., Sale, M., and Chen, W.-M. (2010). Robust relationship inference in genome-wide association studies. Bioinformatics *26*, 2867–2873.

Maples, B.K., Gravel, S., Kenny, E.E., and Bustamante, C.D. (2013). RFMix: a discriminative modeling approach for rapid and robust local-ancestry inference. Am. J. Hum. Genet. *93*, 278–288.

McColl, H., Racimo, F., Vinner, L., Demeter, F., Gakuhari, T., Moreno-Mayar, J.V., van Driem, G., Gram Wilken, U., Seguin-Orlando, A., de la Fuente Castro, C., et al. (2018). The prehistoric peopling of Southeast Asia. Science *361*, 88–92.

McDougall, I., Brown, F.H., and Fleagle, J.G. (2005). Stratigraphic placement and age of modern humans from Kibish, Ethiopia. Nature *433*, 733–736.

McVicker, G., Gordon, D., Davis, C., and Green, P. (2009). Widespread genomic signatures of natural selection in hominid evolution. PLoS Genet. *5*, e1000471.

Meyer, M., Kircher, M., Gansauge, M.-T., Li, H., Racimo, F., Mallick, S., Schraiber, J.G., Jay, F., Prüfer, K., de Filippo, C., et al. (2012). A high-coverage genome sequence from an archaic Denisovan individual. Science *338*, 222–226.

Mondal, M., Casals, F., Xu, T., Dall'Olio, G.M., Pybus, M., Netea, M.G., Comas, D., Laayouni, H., Li, Q., Majumder, P.P., and Bertranpetit, J. (2016). Genomic analysis of Andamanese provides insights into ancient human migration into Asia and adaptation. Nat. Genet. *48*, 1066–1070.

Narasimhan, V.M., Rahbari, R., Scally, A., Wuster, A., Mason, D., Xue, Y., Wright, J., Trembath, R.C., Maher, E.R., van Heel, D.A., et al. (2017). Estimating the human mutation rate from autozygous segments reveals population differences in human mutational processes. Nat. Commun. *8*, 303.

O'Connell, J.F., Allen, J., Williams, M.A.J., Williams, A.N., Turney, C.S.M., Spooner, N.A., Kamminga, J., Brown, G., and Cooper, A. (2018). When did *Homo sapiens* first reach Southeast Asia and Sahul? Proc. Natl. Acad. Sci. USA *115*, 8482–8490.

O'Connor, S. (2010). Pleistocene migration and colonization in the Indo-Pacific region. In The Global Origins and Development of Seafaring, A. Anderson, J.H. Barrett, and K.V. Boyle, eds. (McDonald Institute for Archaeological Research), pp. 41–55.

Pagani, L., Lawson, D.J., Jagoda, E., Mörseburg, A., Eriksson, A., Mitt, M., Clemente, F., Hudjashov, G., DeGiorgio, M., Saag, L., et al. (2016). Genomic analyses inform on migration events during the peopling of Eurasia. Nature *538*, 238–242.

Patterson, N., Price, A.L., and Reich, D. (2006). Population structure and eigenanalysis. PLoS Genet. *2*, e190.

Patterson, N., Moorjani, P., Luo, Y., Mallick, S., Rohland, N., Zhan, Y., Genschoreck, T., Webster, T., and Reich, D. (2012). Ancient admixture in human history. Genetics *192*, 1065–1093.

Pavlides, C., and Gosden, C. (1994). 35,000 year old sites in the rainforests of west New Britain, Papua New Guinea. Antiquity *68*, 604–610.

Pedregosa, F., Varoquaux, G., Gramfort, A., Michel, V., Thirion, B., Grisel, O., Blondel, M., Prettenhofer, P., Weiss, R., Dubourg, V., et al. (2011). Scikit-learn: Machine Learning in Python. J. Mach. Learn. Res. *12*, 2825–2830.

Plagnol, V., and Wall, J.D. (2006). Possible ancestral structure in human populations. PLoS Genet. *2*, e105.

Poplin, R., Ruano-Rubio, V., DePristo, M.A., Fennell, T.J., Carneiro, M.O., Van der Auwera, G.A., Kling, D.E., Gauthier, L.D., Levy-Moonshine, A., Roazen, D., et al. (2017). Scaling accurate genetic variant discovery to tens of thousands of samples. bioRxiv. https://doi.org/10.1101/201178.

Price, A.L., Patterson, N.J., Plenge, R.M., Weinblatt, M.E., Shadick, N.A., and Reich, D. (2006). Principal components analysis corrects for stratification in genome-wide association studies. Nat. Genet. *38*, 904–909.

Price, A.L., Tandon, A., Patterson, N., Barnes, K.C., Rafaels, N., Ruczinski, I., Beaty, T.H., Mathias, R., Reich, D., and Myers, S. (2009). Sensitive detection of chromosomal segments of distinct ancestry in admixed populations. PLoS Genet. *5*, e1000519.

Prüfer, K., Racimo, F., Patterson, N., Jay, F., Sankararaman, S., Sawyer, S., Heinze, A., Renaud, G., Sudmant, P.H., de Filippo, C., et al. (2014). The complete genome sequence of a Neanderthal from the Altai Mountains. Nature *505*, 43–49.

Prüfer, K., de Filippo, C., Grote, S., Mafessoni, F., Korlević, P., Hajdinjak, M., Vernot, B., Skov, L., Hsieh, P., Peyrégne, S., et al. (2017). A high-coverage Neandertal genome from Vindija Cave in Croatia. Science *358*, 655–658.

Quinlan, A.R., and Hall, I.M. (2010). BEDTools: a flexible suite of utilities for comparing genomic features. Bioinformatics 26, 841–842.

Racimo, F., Kuhlwilm, M., and Slatkin, M. (2014). A test for ancient selective sweeps and an application to candidate sites in modern humans. Mol. Biol. Evol. 31, 3344–3358.

Racimo, F., Gokhman, D., Fumagalli, M., Ko, A., Hansen, T., Moltke, I., Albrechtsen, A., Carmel, L., Huerta-Sánchez, E., and Nielsen, R. (2017). Archaic adaptive introgression in TBX15/WARS2. Mol. Biol. Evol. 34, 509–524.

Reich, D., Green, R.E., Kircher, M., Krause, J., Patterson, N., Durand, E.Y., Viola, B., Briggs, A.W., Stenzel, U., Johnson, P.L.F., et al. (2010). Genetic history of an archaic hominin group from Denisova Cave in Siberia. Nature 468, 1053–1060.

Reich, D., Patterson, N., Kircher, M., Delfin, F., Nandineni, M.R., Pugach, I., Ko, A.M.-S., Ko, Y.-C., Jinam, T.A., Phipps, M.E., et al. (2011). Denisova admixture and the first modern human dispersals into Southeast Asia and Oceania. Am. J. Hum. Genet. 89, 516–528.

Rodriguez, I., and Mombaerts, P. (2002). Novel human vomeronasal receptor-like genes reveal species-specific families. Curr. Biol. 12, R409–R411.

Sankararaman, S., Mallick, S., Patterson, N., and Reich, D. (2016). The combined landscape of Denisovan and Neanderthal ancestry in present-day humans. Curr. Biol. 26, 1241–1247.

Seabold, S., and Perktold, J. (2010). Statsmodels: econometric and statistical modeling with Python. In Proceedings of the 9th Python in Science Conference, S. van der Walt and J. Millman, eds., pp. 57–61.

Seguin-Orlando, A., Korneliussen, T.S., Sikora, M., Malaspinas, A.-S., Manica, A., Moltke, I., Albrechtsen, A., Ko, A., Margaryan, A., Moiseyev, V., et al. (2014). Paleogenomics. Genomic structure in Europeans dating back at least 36,200 years. Science 346, 1113–1118.

Skoglund, P., Posth, C., Sirak, K., Spriggs, M., Valentin, F., Bedford, S., Clark, G.R., Reepmeyer, C., Petchey, F., Fernandes, D., et al. (2016). Genomic insights into the peopling of the Southwest Pacific. Nature 538, 510–513.

Skoglund, P., Mallick, S., Patterson, N., and Reich, D. (2018). No evidence for unknown archaic ancestry in South Asia. Nat. Genet. 50, 632–633.

Skov, L., Hui, R., Shchur, V., Hobolth, A., Scally, A., Schierup, M.H., and Durbin, R. (2018). Detecting archaic introgression using an unadmixed outgroup. PLoS Genet. 14, e1007641.

Slon, V., Mafessoni, F., Vernot, B., de Filippo, C., Grote, S., Viola, B., Hajdinjak, M., Peyrégne, S., Nagel, S., Brown, S., et al. (2018). The genome of the offspring of a Neanderthal mother and a Denisovan father. Nature 561, 113–116.

Stoneking, M., Jorde, L.B., Bhatia, K., and Wilson, A.C. (1990). Geographic variation in human mitochondrial DNA from Papua New Guinea. Genetics 124, 717–733.

Sutikna, T., Tocheri, M.W., Morwood, M.J., Saptomo, E.W., Jatmiko, Awe, R.D., Wasisto, S., Westaway, K.E., Aubert, M., Li, B., et al. (2016). Revised stratigraphy and chronology for Homo floresiensis at Liang Bua in Indonesia. Nature 532, 366–369.

Swadling, P., and Hide, R. (2005). Changing landscape and social interaction: looking at agricultural history from a Sepik-Ramu perspective. In Papuan Pasts: Cultural, Linguistic and Biological Histories of Papuan-Speaking Peoples, A. Pawley, R. Attenborough, J. Golson, and R. Hide, eds. (Pacific Linguistics), pp. 289–327.

Tennessen, J.A., Bigham, A.W., O'Connor, T.D., Fu, W., Kenny, E.E., Gravel, S., McGee, S., Do, R., Liu, X., Jun, G., et al.; Broad GO; Seattle GO; NHLBI Exome Sequencing Project (2012). Evolution and functional impact of rare coding variation from deep sequencing of human exomes. Science 337, 64–69.

Terhorst, J., Kamm, J.A., and Song, Y.S. (2017). Robust and scalable inference of population history from hundreds of unphased whole genomes. Nat. Genet. 49, 303–309.

Tucci, S., Vohr, S.H., McCoy, R.C., Vernot, B., Robinson, M.R., Barbieri, C., Nelson, B.J., Fu, W., Purnomo, G.A., Sudoyo, H., et al. (2018). Evolutionary history and adaptation of a human pygmy population of Flores Island, Indonesia. Science 361, 511–516.

Vernot, B., Tucci, S., Kelso, J., Schraiber, J.G., Wolf, A.B., Gittelman, R.M., Dannemann, M., Grote, S., McCoy, R.C., Norton, H., et al. (2016). Excavating Neandertal and Denisovan DNA from the genomes of Melanesian individuals. Science 352, 235–239.

Wall, J.D. (2017). Inferring human demographic histories of non-African populations from patterns of allele sharing. Am. J. Hum. Genet. 100, 766–772.

Wall, J.D., Lohmueller, K.E., and Plagnol, V. (2009). Detecting ancient admixture and estimating demographic parameters in multiple human populations. Mol. Biol. Evol. 26, 1823–1827.

Wall, J.D., Yang, M.A., Jay, F., Kim, S.K., Durand, E.Y., Stevison, L.S., Gignoux, C., Woerner, A., Hammer, M.F., and Slatkin, M. (2013). Higher levels of neanderthal ancestry in East Asians than in Europeans. Genetics 194, 199–209.

Walz, H.A., Shi, X., Chouinard, M., Bue, C.A., Navaroli, D.M., Hayakawa, A., Zhou, Q.L., Nadler, J., Leonard, D.M., and Corvera, S. (2010). Isoform-specific regulation of Akt signaling by the endosomal protein WDFY2. J. Biol. Chem. 285, 14101–14108.

Weir, B.S., and Cockerham, C.C. (1984). Estimating F-statistics for the analysis of population structure. Evolution 38, 1358–1370.

Yasukochi, Y., and Ohashi, J. (2017). Elucidating the origin of HLA-B*73 allelic lineage: Did modern humans benefit by archaic introgression? Immunogenetics 69, 63–67.

Yokoyama, Y., Falguères, C., Sémah, F., Jacob, T., and Grün, R. (2008). Gamma-ray spectrometric dating of late Homo erectus skulls from Ngandong and Sambungmacan, Central Java, Indonesia. J. Hum. Evol. 55, 274–277.

STAR★METHODS

KEY RESOURCES TABLE

REAGENT or RESOURCE	SOURCE	IDENTIFIER
Biological Samples		
161 human samples from Island Southeast Asia	Eijkman Institute for Molecular Biology, Jakarta, Indonesia	Table S1
Deposited Data		
FASTQ sequence files	European Genome-phenome Archive (EGA; https://www.ebi.ac.uk/ega/home)	Accession number: EGAS00001003054
Variant files	The Estonian Biocenter data archive (http://evolbio.ut.ee)	N/A
Software and Algorithms		
The new HMM model	This study	https://github.com/guysjacobs/archHMM
Topology counting code	This study	https://github.com/guysjacobs/archTopoCount
Code to combine BED-format introgressed windows	This study	https://github.com/guysjacobs/archBedCombine
BCFtools 1.4	Li (2011)	https://samtools.github.io/bcftools/
BEDtools 27	Quinlan and Hall (2010)	https://github.com/arq5x/bedtools2
bwa 0.7.16a	Li (2013)	https://github.com/lh3/bwa/releases
ChromoPainter 2	Lawson et al. (2012)	https://people.maths.bris.ac.uk/~madjl/finestructure/index.html
EIGENSOFT 7.2.0	Patterson et al. (2006); Price et al. (2006)	https://github.com/DReichLab/EIG
GATK 3.5	Poplin et al. (2017)	https://software.broadinstitute.org/gatk/
KING 2.1	Manichaikul et al. (2010)	http://people.virginia.edu/~wc9c/KING/manual.html
LOTER	Dias-Alves et al. (2018)	https://github.com/bcm-uga/Loter
ms	Hudson (2002)	http://home.uchicago.edu/rhudson1/source/mksamples.html
msprime 0.6.1	Kelleher et al. (2013)	https://github.com/tskit-dev/msprime/releases
nSL	Ferrer-Admetlla et al. (2014)	http://www.nielsenlab.org/wp-content/uploads/2011/05/nSL1.zip
picard-tools 2.12.0	Broad Institute	http://broadinstitute.github.io/picard
PLINK 1.9	Chang et al. (2015)	https://www.cog-genomics.org/plink2
SHAPEIT 2.r837	Delaneau et al. (2013)	https://mathgen.stats.ox.ac.uk/genetics_software/shapeit/shapeit.html
SMC++ 1.9.3	Terhorst et al. (2017)	https://github.com/popgenmethods/smcpp

CONTACT FOR REAGENT AND RESOURCE SHARING

Further information and requests for resources and reagents should be directed to and will be fulfilled by the Lead Contact, Murray Cox (m.p.cox@massey.ac.nz).

For consistency of process, all requests to access the sequences presented in this work are managed through the Data Access Committee of the official data repository (accession EGAS00001003054) at the European Genome-phenome Archive (EGA; https://www.ebi.ac.uk/ega/home).

EXPERIMENTAL MODEL AND SUBJECT DETAILS

Human subjects
All samples were obtained from adult human subjects. For full information about the new and published samples used in this study, refer to Table S1 – Sample and combined dataset list.

Ethical approvals and dataset description

Here we report a new genomic dataset, the Indonesian Genome Diversity Project (IGDP), which includes 161 high coverage genomes from 14 islands and a wide variety of ethnic groups from Island Southeast Asia (ISEA), spanning the Indonesian archipelago and stretching into Island Melanesia (Table S1). The samples used in this study were collected by J. Stephen Lansing, Herawati Sudoyo and an Indonesian team from the Eijkman Institute for Molecular Biology, with the assistance of Indonesian Public Health clinic staff, and also by Mark Stoneking (see Stoneking et al., 1990) and Jonathan Friedlander (see Friedlaender et al., 2008), in collaboration with the Institute for Medical Research of Papua New Guinea. A subset of the samples have also been incorporated into the Genome Asia 100K Project (http://www.genomeasia100k.com).

All collections followed protocols for the protection of human subjects established by institutional review boards at the Eijkman Institute, Nanyang Technological University and the University of Arizona. All individuals gave their informed consent for participation in the study. The study as a whole, including the generation of whole genome sequencing data for the samples, was approved by the institutional review board at the Eijkman Institute (EIREC#90). Full ethical approval and oversight of consenting processes was also granted by the Nanyang Technological University institutional review board (IRB-2014-12-011).

Permission to conduct research in Indonesia was granted by the State Ministry of Research and Technology (RISTEK).

METHOD DETAILS

A schematic overview of the analytical pipeline presented here is shown in Figure S1A (STAR Methods S1–5) and Figure S1B (STAR Methods S6–13). Datasets used are shaded in green; analyses and inferences in yellow; and key steps are outlined in bold.

S1 - Sequencing and SNP calling

Sequencing libraries were prepared using TruSeq DNA PCR-Free and TruSeq Nano DNA HT kits depending on DNA quantity. 150 bp paired-end sequencing was performed on the Illumina HiSeq X sequencer.

Individuals were sequenced to expected mean depth of 30x, with an achieved median depth of raw reads across samples of 43x. These newly generated whole genome sequences were combined with the following published genomes (raw reads):

  a) 292 genomes from the Simons Genome Diversity Project (SGDP) (Mallick et al., 2016)
  b) 25 Papuan genomes from the Malaspinas et al. (2016) study

SNP calling was performed on the combined dataset, with published genomes analyzed from raw reads exactly as for the new sequence data.

Trimmomatic v. 0.38 (Bolger et al., 2014) was used to cut adapters and low-quality sequences from the reads. After trimming, the vast majority of reads were longer than 145 bp; those below 60 bp were excluded. We aligned the reads to the 'decoy' version of the GRCh37 human reference sequence (hs37d5) using BWA MEM (Li, 2013). We removed duplicate reads with picard-tools v. 2.12.0 (http://broadinstitute.github.io/picard) and performed local realignment around indels with GATK v. 3.5 (Poplin et al., 2017).

After alignment, and keeping only properly paired reads that mapped to the same chromosome, the sequencing depth across the samples used in downstream analyses was as follows: min = 18x, Q1 = 35x, median = 38x, Q3 = 43x, max = 48x. Only three samples had median coverage rates below 30x: CBL34, RAM005 and RAM067.

Base calling was undertaken with GATK v. 3.5 following GATK best practices. Per-sample gVCF files were generated using GATK HaplotypeCaller (using only reads with mapping quality $\geq$ 20). Single sample gVCFs were combined into multisample files using CombineGVCFs, and joint genotyping was performed using GATK GenotypeGVCFs, outputting all sites to a multisample VCF. Exactly the same base calling steps were applied to new and published samples, and the joint genotyping included all samples in this study.

Using BCFtools v. 1.4 (Li, 2011), the following filters were applied to each genotype call: base depth (DP) $\geq$ 8x and $\leq$ 400x, and genotype quality (GQ) $\geq$ 30. We then kept only biallelic SNPs and invariable reference sites. For the majority of our analyses, we kept only sites that had high quality variant calls in at least 99% of samples. (Specifically, all analyses in STAR Methods S5-S9 and S11, and all analyses in S10, apart from two result robustness checks that assessed phasing and archaic haplotype topologies. Additionally, we did not apply the call rate filter in the motif-counting analysis in STAR Methods S12). Applying this 99% call-rate filter yielded a total of 36,462,963 SNPs in the combined dataset. We removed sites within segmental duplications, repeats and low complexity regions. These masks were downloaded from the UCSC and Broad Institute genome resources:

  http://hgdownload.soe.ucsc.edu/goldenPath/hg19/database/genomicSuperDups.txt.gz
  http://software.broadinstitute.org/software/genomestrip/node_ReferenceMetadata.html

In the filtered and masked VCF files, we examined several statistics across the samples: the percentages of no-calls and singletons; the average depth; transition/transversion ratio; the number of variants; and heterozygosity. One highly heterozygous sample from the SGDP (LP6005441-DNA_A09, Naxi-2) was excluded based on these metrics, as well as on the basis that the original authors determined that this sample had been contaminated (Mallick et al., 2016).

S2 - Kinship and outlier analysis

We performed sample kinship analysis using KING v. 2.1 (Manichaikul et al., 2010). Of the 161 new genomes, 6 were excluded due to the presence of a first-degree relative in the dataset, leaving a total of 155 genomes for downstream analysis. This relatedness is a consequence of the village-scale sampling strategy employed in this study. In addition, 7 sample pairs display second-degree relatedness (BNA05 / BNA12-F, BNA21-F / BNA26-F, CBL018 / CBL019, RAM045-F / RAM067, RAM022 / RAM039-F, NIAS08 / NIAS12, NIAS01 / NIAS10). These samples were kept for further analyses, and the final dataset comprised 471 genomes: 155 newly generated complete genomes, 25 genomes from the Malaspinas et al. (2016) study and 291 genomes from SGDP.

Principal component analysis (PC) was used to detect sample outliers and characterize regional diversity. First, we applied LD pruning of our SNP set using PLINK v. 1.9 (Chang et al., 2015). Pruning was performed in 1 Kb sliding windows with a step size of 100 bp, and SNPs with $R^2 > 0.1$ were removed. Next, PCA was performed in EIGENSOFT v. 7.2.0 (Patterson et al., 2006; Price et al., 2006) without the outlier removal step. The results of a PCA without African samples (N = 429) is shown in Main Text Figure 1B.

S3 - Adding archaic data and ancestral information

The combined primary dataset of 471 modern human genomes was merged with two high-coverage archaic hominin genomes:

a) Denisovan (Meyer et al., 2012). Downloaded from
http://cdna.eva.mpg.de/denisova/VCF/hg19_1000g/
b) Neanderthal (Prüfer et al., 2014). Downloaded from http://cdna.eva.mpg.de/neandertal/altai/AltaiNeandertal/VCF/

Positions with missing or low-quality calls (marked as 'LowQual' in the original VCF files) in one of the archaic samples were excluded during the merging procedure. In addition, heterozygous archaic SNPs were also removed to improve phasing quality (but see later analyses). Both types of SNPs were masked for both archaic and modern individuals. These additional filters resulted in a dataset comprising 35,395,615 SNPs.

A second merged dataset was produced by excluding missing and low-quality archaic calls but retaining SNPs that were heterozygous in archaic individuals. This dataset was used to cross validate our results and assess potential bias (if any) introduced by trimming archaic heterozygous positions.

A third dataset was produced by merging the primary dataset containing 471 modern and 2 archaic genomes without heterozygous archaic SNPs with the Vindija Neanderthal genome data (Vindija33.19, downloaded from http://cdna.eva.mpg.de/neandertal/Vindija/VCF/Vindija33.19/). As with the main dataset, positions that were missing, low-quality or heterozygous in the Vindija individual were masked for all archaic and modern individuals.

We added ancestral allele information to our dataset using the Ensembl Compara 71 database (ensembl_compara_71@ens-staging2:3306, MethodLinkSpeciesSet: 6 primates EPO (548)).

S4 - Phasing and phasing assessment

The combined dataset comprising both modern and archaic samples was phased using read aware phasing with SHAPEIT v. 2.r837 (Delaneau et al., 2013). Phase informative reads (PIRs) were extracted using software guidelines from both modern and archaic BAM files. The HapMap phase II b37 recombination map (Frazer et al., 2007) was used and the phasing was performed using the following arguments: *–states 400 –window 0.5 –states-random 200*.

We assessed the performance of our phasing approach, which incorporated phase informative reads, by comparing our phased haplotypes to two experimentally phased individuals (Prüfer et al., 2014) that overlap with the Simons Genome Diversity Project genomes included in our dataset – WON,M (corresponding to sample B_Australian-4 in the Simons dataset, Illumina ID SS6004477) and BUR,E (corresponding to sample B_Australian-3 in the Simons dataset, Illumina ID SS6004478). These two samples come from Aboriginal Australians with unknown geographic origin, but containing no genetic signals of recent admixture with Papuan or European populations.

For each of the two individuals, we applied the following procedure:

- Divide the genome into 8 Kb windows that are non-overlapping and at least 50 bp from any chunk masked by the alignability mask
- Retrieve the corresponding SNPs from the experimentally phased FASTA files and our computationally phased VCFs. The BWA algorithm (v0.7.16a) (Li, 2013) was used to confirm that the windows aligned correctly.
- Mask sites that disagree or are missing in the 8 Kb chunks (due to different SNP calling procedures)
- Discard chunks that contain ≤ 1 heterozygote site.
- Count the number of heterozygous sites and the number of switch errors in the remaining chunks, and divide the totals to obtain a switch error rate.

This approach accounts for the impact of solitary heterozygote sites and the alignability mask, which can hide switch errors (if an even number of switch errors occur within a masked region).

Based on 11164 8 Kb windows for WON,M and 11245 windows for BUR,E, we calculated switch error rates of 3.7% and 4% respectively. These are expected rates (see supplementary text S9 in the Mallick et al. (2016) study). Note that singletons

are randomly placed in our phasing procedure, unless they are part of a phase informative read, and will also act to disrupt haplotypes.

QUANTIFICATION AND STATISTICAL ANALYSIS

S5 - Dataset genetic diversity and SNP novelty
As an exploratory analysis of our phased dataset, we retrieved lists of SNPs in the 1000 Genomes Project (Phase 3) (1000 Genomes Project Consortium et al., 2015), dbSNP (Build 150), ESP (ESP6500SI-V2-SSA137) (Tennessen et al., 2012) and ExAc (ExAcRelease 1.0) (Lek et al., 2016). We counted the number of SNPs defined when considering each population group separately, and determined how many were observed in one or more of these datasets, and how many were not observed. Across all of our newly reported samples, we observed 11,859,578 SNPs, of which 21% (2,525,213) were novel. Existing datasets are better able to capture variation in West ISEA (9.3% SNPs novel) than East ISEA (14.3%) or Papua (21.1%), likely because previously published datasets incorporate a large number of mainland Asian samples.

S6 - Estimating Asian-Papuan admixture proportions
To estimate Asian-Papuan admixture proportions in ISEA and Papua, we used local ancestry inference implemented in LOTER (Dias-Alves et al., 2018). LOTER has been shown to outperform similar methods, such as HAPMIX (Price et al., 2009) and RFMix (Maples et al., 2013), and its accuracy is greatest when admixture is more ancient than 150 generations. This time frame (ca 4500 ya) is directly relevant for Indonesian prehistory – linguistic, archaeological and genetic evidence all point to the spread of Austronesian speakers beginning 4000–4500 ya from Taiwan, reaching eastern Indonesia 3500–3000 ya (Hudjashov et al., 2017).

We specified two reference datasets: Papuans from the current study (N = 72; see Table S1) and East Asians (N = 293). The East Asian reference dataset included 293 geographically diverse samples, specifically 43 samples from the Simons Genome Diversity Project, and 50 random samples from each of the five East Asian populations in the 1000 Genomes Project (CDX – Chinese Dai, CHS – Southern Chinese Han, CHB – Northern Chinese Han, KHV – Vietnamese Kihn and JPT – Japan).

Samples from ISEA were analyzed separately using the Papuan and East Asian reference datasets. To infer local ancestry tracts in Papuan samples, we created an individual Papuan reference dataset for every single target genome by excluding the individual sample from the full Papuan reference set to avoid self-copying. Results are reported in Main Text Figure 1A and Table S2.

S7 - Archaic block identification
a. ChromoPainter
We used ChromoPainter v.2 (CP) (Lawson et al., 2012) to detect archaic ancestry in the genomes of our present-day individuals. This method relies on phased haplotype data and describes each individual recipient chromosome as a mixture of genetic blocks from the set of predefined donor individuals. This process, known as chromosome 'painting', generates a matrix of copying vectors, which can be analyzed further. For each recipient haplotype, CP also outputs the expected probability of copying from each donor population at each SNP. CP uses an Expectation-Maximization (EM) algorithm to re-estimate the proportion of genetic material copied from each donor by using the previous estimates as a new prior under the model, and then iterating.

We painted each of our modern non-African human genomes individually using a set of 35 sub-Saharan African genomes from SGDP, which represents modern non-Eurasian human ancestry, and each of the archaic samples separately. We used a two-step approach:

1. The initial run was performed with 10 EM steps to estimate prior copying probabilities for each individual and chromosome separately using the following command line arguments: *-i 10 -in -iM.*
2. Next, estimated prior copying probabilities were averaged across the genome for each individual. The main run was performed with a recombination scaling constant, global mutation (emission) probability and genome-wide average prior copying probability from the first step using the following command line arguments: *-n Ne -M mu -p prior_copying_probability.*

Either archaic or modern ancestry was then assigned to individual SNPs using a probability threshold of 0.85. Unknown ancestry was assigned to SNPs with intermediate copying probability.

b. Hidden Markov Model
To explore the behavior of the CP approach, we additionally implemented a hidden Markov model (HMM, https://github.com/guysjacobs/archHMM). Our approach is inspired by that of Racimo and colleagues (Racimo et al., 2017; Seguin-Orlando et al., 2014), and we follow their notation where possible.

The problem is to partition the genome into blocks of DNA that have introgressed from an archaic hominin and non-introgressed DNA. To do this, we consider a test haplotype vector of SNPs $h = (h_1, \ldots, h_k) \in {0, 1}$ of length k, with each SNP indicated by either a

0 (if ancestral) or 1 (if derived). The SNPs have an associated genetic map vector $R = (r_1, ..., r_k)$ where $r_j \geq r_i$ if $j > i$. We assume that each SNP has one of two hidden states (human, 0, or archaic, 1), which form the ancestry vector $z = (z_1, ..., z_k) \in 0, 1$. We also define an observation vector $y = (y_1, ..., y_k) \in 0, 1$ with

1. $y_i = 1$ if $h_i = 1$ and $f_i^{archaic} > 0$ and $f_i^{afr} \leq \eta$
2. $y_i = 0$ otherwise

where f_i^{afr} denotes the frequency of the derived state in a panel of comparative African populations and $f_i^{archaic}$ is the frequency of the derived state in a panel of archaic hominins. In our case, the panel of archaic hominins is the single Altai Denisovan individual and our condition $f_i^{archaic} > 0$ simply requires that the derived state is observed, whether in the homozygous or heterozygous state. We apply a non-0 η of $1/2n_{afr}$ such that the observed state 1 may still be assigned if a single African individual is heterozygous at a site. This guards against sequencing errors given the moderately large panel of sub-Saharan Africans ($n_{afr} = 35$), and importantly, also provides some robustness against low levels of recent back migration into Africa from populations with archaic introgression.

We only consider the subset of SNPs that have known ancestral state and are not missing in the test haplotype or archaic panel. We also chose to exclude SNPs that are variable only in the African panel as these are prone to bias the density of observations depending on local African diversity patterns. Local African diversity may be impacted by complex molecular (e.g., mutation rate variation) and evolutionary processes (e.g., purifying selection).

We want to identify blocks of the test haplotype that have elevated observed state $y_i = 1$ corresponding to derived alleles that are shared with the archaic hominin and are rare in Africa. To do this, we define a two-state, time-homogeneous HMM, with four parameters – the emission probability of the two observed states for each hidden state: $p_{10} = P(y = 1 | z = 0)$ and $p_{11} = P(y = 1 | z = 1)$, which also define $p_{00} = 1 - p_{10}$ and $p_{01} = 1 - p_{11}$; and asymmetric transition rates between the two hidden states $p_{0 \rightarrow 1}^i = P(z_i = 1 | z_{i-1} = 0)$ and $p_{1 \rightarrow 0}^i = P(z_i = 0 | z_{i-1} = 1)$, which define $p_{0 \rightarrow 0}^i$ and $p_{1 \rightarrow 1}^i$ in a similar manner. We seek to estimate these parameters and retrieve a most likely ancestry vector z given them, and use a Viterbi algorithm and expectation maximization procedure to do so (see also Lu et al. (2016)).

We first assume transition probabilities that are linear with genetic distance with a maximum cut-off,

$$p_{0 \rightarrow 1}^i = min(k_1 r_{i,i-1}, 0.5)$$

and

$$p_{1 \rightarrow 0}^i = min(k_2 r_{i,i-1}, 0.5),$$

where $r_{i,i-1} = r_i - r_{i-1}$ and k_1 and k_2 are rates to be fitted. The maximum cut-off is to ensure realistic behavior when $r_{i,i-1}$ is large, although SNPs are rarely sufficiently separated for this to be required. Note that we do not constrain k_2 to be a function of k_1 as in the Racimo approach, which can be used to include an assumption of a simple introgression model. Our intention is to identify the most plausible archaic blocks, but we purposely make no assumptions about the introgression history where possible.

Our block estimation and parameter estimation algorithm is as follows:

1. Initialize parameters $[p_{10}(t = 0), p_{11}(t = 0), k_1(t = 0), k_2(t = 0)]$ to $[0.1, 0.25, 100.0, 100.0]$. The probability of $z_1 = 1$ must also be initialised and is set to 0.01.
2. Apply the Viterbi algorithm to estimate z, given y and the model parameters at iteration t.
3. Re-estimate the model parameters based on the estimated ancestry vector z. $p_{10}(t + 1) = \sum_1^k y_i (1 - z_i)/k$, $p_{11}(t + 1) = x$, $k_1(t + 1) = \sum_2^k (1 - z_{i-1}) z_i r_{i,i-1} / \sum_2^k (1 - z_{i-1}) r_{i,i-1}$ and $k_2(t + 1) = \sum_2^k z_{i-1}(1 - z_i) r_{i,i-1} / \sum_2^k z_{i-1} r_{i,i-1}$.
4. Repeat steps 2 and 3 until either the ancestry vectors at t and $t - 1$ are identical or $t = 50$, and output the ancestry vector and parameter estimates.

Note that parameter p_{11} is fixed during the estimation procedure. This is to ensure that the model is inferring archaic blocks with similar properties when the model is run on different chromosomes and different individuals, while still offering flexibility in the timing of introgression (by re-estimating transition parameters) and human diversity patterns (by re-estimating p_{10}). We fixed parameter p_{11} by running a free estimation, where p_{11} is re-estimated in a manner analogous to p_{10}, for a set of 10 Papuans, who have a well-established history of Denisovan introgression, and 10 West Eurasians, who do not. We found that setting $p_{11} = 0.25$ was successful in detecting Denisovan blocks in Papuans, while limiting the false positive rate in West Eurasians.

Our approach differs from the Racimo method in its parameter estimation procedure and the transition probabilities. It also purposely ignores African-specific diversity. However, the principle of applying an HMM to detect tracts enriched for non-African derived alleles shared with an archaic hominin has been widely applied in several slight variations (e.g., Lu et al., 2016; Prüfer et al., 2014; Racimo et al., 2017; Seguin-Orlando et al., 2014 and others) and as such is a standard approach in archaic introgression block estimation.

c. S*

We used the S* method (Plagnol and Wall, 2006; Vernot et al., 2016; Wall et al., 2009), which seeks to detect introgressed haplotypes from archaic hominins without using an archaic reference genome, following the implementation of Vernot et al. (2016). S* is sensitive

toward highly diverged sequences with high LD, and thus is adequate to detect hominin introgressed haplotypes without having a reference sequence of the hominin in question.

To calculate empirical S* in our non-African samples, we used 35 sub-Saharan Africans as a reference population and analyzed one non-African sample at a time. We removed any non-segregating sites from our data. We used the HapMap phase II b37 recombination map (Frazer et al., 2007), and ancestral information from the Ensembl Compara 6 primates EPO (548) database. Empirical S* values were estimated in 50 Kb genomic windows.

After calculating the S* value from the real dataset, we used simulations to assign statistical significance to our empirical estimates. We performed simulations using different combinations of the number of segregating sites and recombination rates from the previous step. We simulated a previously described demographic model (Henn et al., 2015) with the simulator ms (Hudson, 2002). For non-West Eurasians samples, we performed simulations with the East Asian demographic model as presented in the Vernot et al. (2016) study. We obtained a neutral distribution of S* without hominin introgression for 50 Kb regions using 60000 simulations for every combination of the number of segregating sites and recombination rate. The following ms command line was used:

```
ms <Total_N> 60000 -I 3 <Africa_N> <WEurasia_N> <EAsia_N> -s <SegSites> -r 38.7* <recombination_rate> 50001 -n 1 2.20 -n
2 4.47 -n 3 6.53 -g 2 101.69 -g 3 146.31 -m 1 2 1.49 -m 2 1 1.49 -m 1 3 0.46 -m 3 1 0.46 -m 2 3 1.85 -m 2 3 1.85 -ej 0.029 3 2 -
en 0.029 2 0.29 -em 0.029 1 2 8.93 -em 0.029 2 1 8.93 -ej 0.087 2 1 -en 0.23 1 1 -p 5
```

We then used the computationally efficient strategy employed to estimate the S* value for every region as in Vernot et al. (2016). Finally, we assigned a p value for each 50 Kb genomic window in every individual sample in our non-African dataset using the neutral distribution of S* from the simulations without archaic introgression. Genomic windows with a recombination rate less than 0.005 or more than 20.01 and/or a number of segregating sites less than 20 or more than 511 were excluded. To assess the overall fit of the neutral demographic simulations to the data, we built General Additive Models (GAM) of the 95th and 99th percentiles of simulated neutral S* as a function of the number of segregating sites and recombination rate.

We established two thresholds of significance:

1. To estimate the overlap between CP, HMM and S*, and define high confidence Denisovan blocks, we identified regions as introgressed if the S* in the real data is more than the 95th percentile of the simulated data distribution.
2. In addition, for the residual S* analysis, we identified a region as introgressed if the S* in the real data is more than the 99th percentile of the simulated data distribution. This yields a more conservative, high confidence S* set, which allows for more robust inferences of residual S* signal (see below).

S8 - Introgression results from the three methods

Details of the amount of introgression based on the different methods, and profiling of the methods, are shown in Table S3.

The total amount of introgression detected by the three methods, per phased haploid genome, is shown in Table S3A. There is a clear correlation between the methods, with most archaic introgression detected by all three methods in Papua and East ISEA, and with least in West Eurasia. The total amount of archaic introgression detected by CP was slightly less than that detected by the HMM, which was in turn considerably less than that detected by S* with 95% confidence. We note that different methods are expected to extract different amounts of introgression signal (see e.g., Skov et al., 2018 Table 1 for a recent comparison). The relative enrichment of Denisovan signal in Papua over West Eurasia was greater for CP (6.4-fold) than the HMM (5.0-fold), based on all pairwise Papuan/West Eurasian comparisons (paired t test, T = 280.5, p ≈ 0.0; Cohen's D = 1.49). As Denisovan introgression is not expected in West Eurasia, the clear excess in enrichment seen in CP over the widely applied HMM approach strongly supports CP – when used in the manner described above – as an effective method for detecting archaic hominin introgression. Nevertheless, as Table S3A shows, a substantial amount of Denisovan introgression was detected by both methods in West Eurasia, suggesting that the three methods are individually detecting a number of false positive introgressed blocks.

We hypothesize that this phenomenon is driven by 'spillover' signal from Neanderthal introgression. Indeed, incomplete lineage sorting could lead Neanderthal-introgressed blocks to have greater genetic similarity to the Altai Denisovan than Altai Neanderthal; and even blocks that coalesce with the Altai Neanderthal before the Denisovan/Neanderthal common ancestor will often show greater similarity to the Altai Denisovan than humans due to Denisovan/Neanderthal common ancestry. As an initial check on this hypothesis, we categorized the genome into regions that *only* had evidence for Denisovan or Neanderthal introgression (from one or both of the HMM and CP methods); regions that had conflicting evidence for both Denisovan and Neanderthal introgression from the two methods; and regions with an unknown signal arising from S* (> 95% confidence), thus identifying a region as introgressed but with no support from the HMM and CP methods (Table S3B). As predicted, discounting ambiguous signal, there is now 12.5 times as much Denisovan introgression in Papua compared to West Eurasia.

We used these observations – that higher confidence Denisovan blocks are supported by multiple methods, and that unexpected signal can be driven by spillover from Neanderthal introgressed blocks – to refine our Denisovan block set (STAR Methods S9 below).

S9 - Refining archaic block sets
a. Iterated filtering improves specificity

Both CP and the HMM were run using the Denisovan and Neanderthal genomes independently. However, Neanderthals and Denisovans are believed to share common ancestry more recently than the human/Neanderthal/Denisovan common ancestor (e.g., 495 versus 657 kya in Malaspinas et al. (2016)), increasing the probability of introgressing archaic blocks showing greater similarity to both Neanderthals and Denisovans than modern humans. Table S3B profiles the degree to which the archaic portion of genomes overlaps in different continental groups. Importantly, we note that while only very little of the West Eurasian genome is assessed as unambiguously Denisovan (that is, identified by at least one of the CP or HMM methods as Denisovan, but as Neanderthal by neither), a considerable amount is ambiguous – that is, identified by different methods as both Neanderthal and Denisovan.

This suggests that looking at the overlap of methods, and actively removing ambiguous blocks, may be a promising way to obtain a high confidence set of Denisovan blocks. A logical approach to this is to iteratively discard Denisovan CP blocks that are either i) not supported by the other methods (Denisovan HMM and S*) or ii) also identified as Neanderthal by CP. We can do this by requiring more than a minimum overlap between each Denisovan CP block and the supporting methods, or less than a maximum overlap with a Neanderthal CP block. However, it is not clear how much overlap is appropriate to ensure that ambiguous or weakly supported Denisovan introgression blocks are removed, but that sufficient signal remains for further analysis.

We therefore sought parameters for an incremental filtering procedure that maximizes the excess Denisovan signal in Papuans against West Eurasians, the two samples expected to have highest and lowest Denisovan introgression, respectively (Main Text Figures 2A–2C). For each Denisovan CP block on a chromosome copy of an individual, the procedure progresses in three steps:

1. Discard the block if the proportion of its length that is overlapped by Denisovan HMM blocks on that chromosome copy of the individual is under $I_{HMM}^{Deni} \in [1.0, 0.75, 0.5, 0.25, 0.1, 0.05, 0.001]$.
2. If the block survived (1), discard it if the proportion of its length overlapped by S* windows for the individual is under $I_{S*} \in [0.999, 0.75, 0.5, 0.25, 0.1, 0.05, 0.001, 0.0]$.
3. If the block survived (1) and (2), discard it if the proportion of its length overlapped by Neanderthal CP blocks on the chromosome copy of the individual is over $I_{CP}^{Nean} \in [0.999, 0.95, 0.75, 0.5, 0.25, 0.1]$.

Here, $I_{HMM}^{Deni} = 1.0$ indicates a requirement that the entire CP Denisovan block is entirely covered by a single HMM Denisovan block, or by the union of multiple HMM Denisovan blocks, while $I_{HMM}^{Deni} = 0.001$ indicates that only 0.1% of the block needs to be covered. We specifically chose to use CP Neanderthal blocks to exclude ambiguous signal, rather than HMM Neanderthal blocks, in order to additionally exclude any regions that might be readily, and perhaps falsely, identified as non-human specifically by the CP method; for instance, due to local patterns of African variation. We used the bedtools suite v.2.27.0 (Quinlan and Hall, 2010) with the *subtract* command and *-N* flag and *-f* flags to perform this procedure.

We sought to retrieve high confidence Denisovan blocks while still retaining enough Denisovan signal for further analysis. Noting that the total genome inferred as Denisovan in Papua relative to West Eurasia (Main Text Figure 2C) increases greatly even with minimal overlap requirements ($I_{HMM}^{Deni} = 0.001$, $I_{S*} = 0.001$ and $I_{CP}^{Nean} = 0.999$), we chose these to define our high confidence Denisovan block set. Thus, the refinement procedure is:

1. Starting with the Denisovan CP output, remove any block that is less than 0.1% overlapped by Denisovan HMM output. For example, for a 100 Kb Denisovan block identified by CP to be kept, we require at least 100 bp to be covered by Denisovan HMM output in the same chromosome copy of the individual as well.
2. Of the remaining blocks, remove any block that is less than 0.1% overlapped by S* output.
3. Of the remaining blocks, remove any block that is over 99.9% overlapped by Neanderthal CP output.

After applying these filters, we are left with approximately 32.3 Mb of high-confidence Denisovan introgressed blocks per genome copy for a Papuan individual, from our original set of 59.2 Mb. For a West Eurasian, we are left with just 688 Kb, down from 9.5 Mb. There is now nearly 50 times as much Denisovan signal in Papuans, a profound enrichment from the 6 times in the original method output. Some genuinely Denisovan-like blocks may be found in West Eurasians due to a) introgressing blocks from a Neanderthal population that randomly coalesce with the sampled Denisovan before the sampled Neanderthal, b) incomplete lineage sorting dating to the common ancestor of modern humans and Denisovans, and c) limited migration between populations with known Denisovan ancestry (e.g., East and South Asians) and West Eurasians since introgression occurred.

b. Filtering supported by SGDP introgression values

The substantial increase in the enrichment of Denisovan signal in Papuans over West Eurasians following our iterated filtering approach is a strong indication that we are successful in removing spillover signal from Neanderthal introgression. This increased accuracy comes at the cost of decreased power to detect true Denisovan introgression. While the filtering method reduces the Denisovan signal in West Eurasia from 9.5 to 0.7 Mb (93%), the signal halves in Papua from 59.2 to 32.3 Mb, which is a greater signal depletion in absolute terms despite broadly similar proposed levels of Neanderthal introgression in both regions (Mallick et al., 2016).

To profile this behavior in real data, we turn to genome-wide estimates of Denisovan and Neanderthal introgression reported for the SGDP samples in our dataset, calculated using counting statistics (Mallick et al., 2016). Genome-wide estimates of introgression have a benefit over haplotype inference in that they measure the average signal of introgression over the entire genome rather

than pulling out small chunks; as a result, they are better able to estimate the overall level of introgression, and necessarily yield genome-wide proportions that are greater than the sum of excavated archaic sequence haplotypes. The SGDP samples represent global populations, including groups thought to harbor just Neanderthal introgression (West Eurasian), but also Asian and Oceanian groups with both Neanderthal and Denisovan ancestry, and so are ideally suited for a comparison of methods.

We performed multiple linear regression using the Python statsmodels v.0.8.0 package (Seabold and Perktold, 2010) on the SGDP genome-wide estimates of Denisovan (SGDP$_{Deni}$) and Neanderthal (SGDP$_{Nean}$) introgression (Table S1 in Mallick et al., 2016) as independent variables, and either the total Denisovan sequence identified for each sample by CP alone or our high confidence Denisovan introgressed sequence as the dependent variable.

In this analysis, our introgression estimates are expressed as a proportion of introgressed sequence per individual genome, such that the units are the same in the two datasets. Given the high correlation coefficients, the factors in Table S3C provide an indication of the amount of spillover signal (significant correlations of our Denisovan introgression estimates with SGDP$_{Nean}$, or of our Neanderthal estimates with SGDP$_{Deni}$) and the relative power of our methods to detect overall levels of introgression. We assume that the published introgression estimates from the SGDP data are accurate, which is supported by the strong consistency of their results with other published findings (e.g., the Denisovan introgression peak in Papua; more Neanderthal introgression in East Asians than West Eurasians as in Wall et al. (2013)).

We find evidence of considerable 'spillover' signal in the raw CP results. On a worldwide scale, SGDP$_{Nean}$ significantly predicts CP Denisovan signal (factor 0.15), while SGDP$_{Deni}$ predicts CP Neanderthal signal (factor 0.19). In West Eurasia, where SGDP$_{Deni}$ is minimal (highest 0.2%, in populations with some Asian ancestry like the Saami), levels of SGDP$_{Nean}$ alone are sufficient to predict our CP Denisovan signal with high accuracy (factor 0.21, $r^2 = 0.99$); the spillover effect accounts for the entire signal.

Studying the Denisovan CP signal in Papuans only – a population with high levels of both Denisovan and Neanderthal ancestry – is especially informative about the amount of spillover signal, with a SGDP$_{Nean}$ factor of 0.28 only marginally smaller than the SGDP$_{Deni}$ factor of 0.36. Note, however, that the substantially greater amount of Denisovan than Neanderthal introgression in Papuans (4%–6% compared to ~2%) means that the CP Denisovan signal is still largely composed of Denisovan introgression. The high spillover rate in the CP Denisovan signal and generally lower power to detect Denisovan than Neanderthal introgression reflect the more distant relationship between the Alai Denisovan and the introgressing Denisovan population, compared to the Altai Neanderthal and introgressing Neanderthal population.

Spillover largely disappears when using the high confidence blocks. Worldwide, while SGDP$_{Nean}$ and SGDP$_{Deni}$ remain significant predictors of our high confidence Denisovan and Neanderthal introgression signals, their factors drop from 0.15 to −0.01 and 0.19 to 0.04, respectively. There is minimal spillover when estimating our high confidence Denisovan signal in West Eurasia (SGDP$_{Nean}$ factor falls from 0.21 to 0.03), and both SGDP$_{Nean}$ and SGDP$_{Deni}$ are now only significant predictors of the high confidence signal for their corresponding archaic species.

Our high confidence intersection method thus substantially reduces the false positive rate as reflected in the spillover signal when estimating genome-wide levels of introgression. There is also a substantial decrease in relative power – at a worldwide scale, from about 41% to 28% when searching for Denisovan introgression, and 56% to 39% when searching for Neanderthal introgression. The low overall power of methods that detect introgression blocks compared to genome-wide statistics is expected, as is the higher power to detect Neanderthal introgression due to the more recent ancestry between the Altai and introgressing Neanderthal than the Altai and introgressing Denisovan. The reduction in power when using the more conservative high-confidence signal is also expected – it reflects the cost of higher specificity. We note that in cases where Denisovan introgression is essentially absent (West Eurasia), a reduction in relative power is still observed for our high confidence Neanderthal signal due to spillover of Neanderthal introgression signal into the CP Denisovan block set. Thus, when there is strong evidence of only one introgression source, it may be better to avoid stringent block filtering.

c. Distribution of high confidence introgression

Table S3D shows the amount of remaining Denisovan signal after removing Neanderthal spillover per haploid phased genome. The results are particularly interesting because our trimming method leads to substantial depletion of the signal in Asian populations, as well as in West Eurasia. Previous work has suggested approximately 0.5% Denisovan introgression into South and East Asians, as compared to a 4%–6% contribution to Papuans (Browning et al., 2018; Mallick et al., 2016; Reich et al., 2010). The relatively small amount of Denisovan signal in non-Papuans strongly implies either that previous work has overestimated the Denisovan contribution outside of Papua, likely due to ambiguous Neanderthal spillover, or that the amount of Denisovan introgression into Papua is higher than previously thought. If the former is the case, a rough calculation based on a linear additional contribution from the introgression percentage, and assuming West Eurasia has 0% introgression and Papua 4%–6%, implies continent average Denisovan introgression levels of 0.17%–0.33% in mainland Asia.

Performing a similar trimming procedure using Neanderthal, rather than Denisovan, blocks similarly yields estimates of Neanderthal introgression levels (Table S3E). We are also able to clearly detect the known excess Neanderthal signal in East Asians over West Eurasians, with East Asians, Siberians, Americans and Southeast Asians having about 45% more Neanderthal introgressed sequence than West Eurasians. This is highly consistent with previous estimates of a 40% increase (Wall et al., 2013), as is the placement of South Asians as intermediate between the groups.

The standard deviation of the amount of archaic introgression within continental groups reflects variation in introgression levels both within and between continental subpopulations, which in turn reflect patterns of introgression into ancestral populations and

more recent demography. We note that the variation in Neanderthal ancestry is greatest, and that the coefficient of variation is greatest, among West Eurasians compared to other groups. There is a higher coefficient of variation for Denisovan ancestry among East Asians and Siberians compared to Papuans. The highest coefficient of variation is in West ISEA, where it is driven by the inclusion of the Sulawesi population, which has relatively higher Papuan ancestry (13.4%, Table S2) and greater high-confidence Denisovan introgression (∼4.2 Mb) than more westerly groups.

d. Denisovan signal follows Papuan ancestry

We assessed the correlation between Papuan ancestry and Denisovan introgression in southeast Asia using the LOTER output and various measures of archaic introgression. Models were fit using Ordinary Least-squares and the Python package statsmodels v.0.8.0. We fitted the gradient of a linear model with point [1,1] fixed to ensure that a 100% Papuan individual has 100% the Denisovan introgression observed in Papua. We fitted both the raw CP Denisovan output (Main Text Figure 2D, left pane) and the high-confidence Denisovan blocks (Main Text Figure 2D, right pane). In each case, the correlation was strong ($r^2 = 0.98$) and the linear fitting highly significant ($p < 1 \times 10^{-30}$). The linear fitting of the raw CP Denisovan blocks against Papuan ancestry had a gradient of 0.8 [0.79-0.81] implying an intercept of 0.20 [0.19-0.21]. A gradient close to 1, 1.01 [1.0-1.03], and a correspondingly low intercept of −0.01 [0.03-0.0] is observed for the high-confidence Denisovan blocks, consistent with the signal of Denisovan introgression being primarily related to Papuan ancestry in ISEA. Note that LOTER tends to predict a small proportion (< 5%) of Papuan ancestry in West ISEA, which matches the limited Denisovan introgression in the region (Table S2). This may imply that a considerable portion of Denisovan signal in East Asia more broadly is due to very low levels of Papuan ancestry, despite some additional introgression known to be specific to the region (see Browning et al., 2018 and our Main Text Figure 3).

Comparing the linear regressions in Main Text Figure 2D, the predicted amount of Denisovan ancestry for a fully Asian population falls when using the high-confidence blocks in which the Neanderthal spillover signal has been removed. This emphasizes that Neanderthal introgression needs to be carefully controlled for when asking questions about Denisovan-specific ancestry. The village of Rampasasa, near the Liang Bua cave site at which *Homo floresiensis* (Brown et al., 2004) remains were found, and the island of Flores on which the site is located, do not emerge as regional anomalies; the Denisovan signal observed is closely predicted by their level of Papuan ancestry. This suggests that any introgression specific to this part of East ISEA would not be contributed by an archaic hominin on the Denisovan clade; we study the possibility of other local introgression signals from alternative hominin species below (e.g., S*, STAR Methods S12 and S13, and Main Text Figure 7).

S10 - Archaic mismatch analysis

a. Mismatch against the Altai Denisovan genome

An informative way of assessing the relationship of our high confidence Denisovan blocks to the Altai Denisovan genome, which was used to extract them, is by mismatch analysis. As longer blocks are better able to resolve a mismatch distribution (explored in Figure S2 and below), we extracted the 2000 longest blocks from each continental population. For each block with > 50 Kb of total unmasked sequence data (counts in Table S3F), we calculated the number of differences compared to the Denisovan reference (with Denisovan and Neanderthal heterozygous positions masked; see STAR Methods S3). We then calculated the effective block length by subtracting the portion of each block covered by the alignability mask from the total block length, and converted these values into a mismatch (difference/bp). As the number of differences per bp will be impacted by our masking of low quality and heterozygous archaic sites, quality control decisions (e.g., call rate > 99% filter) and the SNP calling protocol, it is not possible to directly translate mismatch distance into times based on a standard human genome mutation rate. We therefore chose to scale the observed mismatches by dividing the mismatches of each block by the average genome-wide mismatch rate between the Altai Denisovan and West Eurasian samples, m_D. We chose West Eurasians as our baseline mismatch rate because that population has the lowest amount of Denisovan introgression. Note that the average genome-wide mismatch rate between Altai Denisovans and West Eurasians, assuming 0% Denisovan ancestry in West Eurasians, reflects both the divergence time of humans and the Neanderthal/Denisovan clade, and the ancestral population size of the common ancestor of humans, Neanderthals and Denisovans. We calculated the scale factor by summing the total number of mismatches between each of the 75 samples × 2 = 150 West Eurasian haploid genomes and the Altai Denisovan, and dividing this by 150 times the total length of unmasked sequence in the dataset.

Plotting these mismatches by continent yields the distribution pictured in Main Text Figure 3C. The variation in the number of blocks > 50 Kb between continental groups reflects varying sample size, as well as the total amount of Denisovan introgression and the time since Denisovan introgression in different groups.

Two primary patterns emerge. First, we replicate the results of Browning et al. (2018) in identifying a mainland Asian-specific peak with relatively low divergence to the Altai Denisovan. This peak is not limited to East Asian populations (in whom it was originally detected), but also extends into Siberia and the Americas. Interestingly, our American populations show some reduction in the extent of this peak, potentially suggesting that introgression was ongoing more recently than the divergence of American and East Asian populations.

Second, there is a clear dual mismatch peak in the Papuan population that is not apparent in other groups, which instead show a single divergent mismatch peak with some fluctuation in its exact placement. Given these fluctuations, we sought to confirm that the twin Papuan peaks were not a result of a very small number of common blocks being overrepresented due to high frequency in the

sample, which could emphasize stochasticity in the coalescent and mutation processes. For example, in an extreme case, if a set of 2000 blocks consists of just 14 blocks near fixation then only a few independent coalescent histories might be represented in the mismatch distribution.

Focusing on the full set of 2000 largest Papuan blocks, we instead observed 226 entirely disjoint regions using the bedtools 'merge' function. Of these, 151 were > 0.5 Mb from any other region. Although the top ten most introgressed regions contributed 515 blocks, this leaves 216 disjoint regions with an average frequency of 4.8% in Papuans. The two highest frequency blocks, at 94/144 and 57/144 in the 72 (diploid) Papuan samples, lie outside both of the Papuan-specific mismatch peaks, the former having an intermediate mismatch and the latter an unusually large mismatch versus the Altai Denisovan.

To assess the impact of using a different minimum block length cut-off, we determined the mismatch using thresholds from 0 to 260 Kb (Main Text Figure 3A). To ensure mismatch accuracy is not being impacted by the alignability mask, we additionally required that blocks contained total called sequence over the minimum cut-off. We did not calculate the mismatch when less than 50 entirely non-overlapping blocks are involved in the analysis. The twin peaks obtain resolution at approximately 130 Kb (based on 3556 blocks). As expected for small block sizes, the overall resolution is poor below 50 Kb. We also explored the role of the minimum block length cut-off for our combined Siberia and East Asia sample (Main Text Figure 3B) and East ISEA continental groups (Figure S2). Again, the East Asian and Siberian specific peak only resolves when a minimum block length cut off $\geq$ 50 Kb is applied. The two peaks observed in Papua do not clearly resolve for East ISEA, due to the reduced sample size and small Papuan ancestry leading to fewer observed blocks in this region.

We hypothesize that the challenge in resolving mismatch peaks using short blocks is related to two factors. First, mutations are discrete. In our analysis, it might be typical to observe 0 or 1 mismatching base pairs in a small 1 Kb block, corresponding, respectively, to extremely low and extremely high mismatch compared to the average mismatch of larger, 'higher resolution' blocks. Equivalently, it is not possible to observe a theoretically expected mismatch of, for example, 0.0005 in a 1 Kb block as 1/1000 = 0.001 and 0/1000 = 0.0; a better approximation of the expected value is possible with larger blocks. Second, the ratio of stochasticity in the mutation process along the branches of a coalescent tree versus the difference in coalescent times driving two mismatch peaks is also an important variable.

To explore these phenomena, we performed a simple simulation of expected mismatch for two populations diverging from a source population at two fixed times, t_1 and t_2. The distribution of mismatches corresponds to a Poisson with mean $2\mu l c$ where $\mu = 1.45 \times 10^{-8}$ and is the mutation rate per base pair per generation, l is the block length and c is a coalescent time. The values of c are repeatedly drawn from the distribution of coalescence times – either an exponential distribution with location parameter t_1 and mean $t_1 + 2N_e$, or with location parameter t_2 and mean $t_2 + 2N_e$. In this way, we are able to incorporate random coalescence and mutation. Using the values of $t_1 = 9750$, $t_2 = 12500$ and $N_e = 100$ from our simulation fitting (see below) for the two Denisovan-like populations contributing to Papua, and $t_1 = 5000$, $t_2 = 12500$ and $N_e = 100$ for the two Denisovan-like populations contributing to East Asia, we confirm that longer blocks are required to detect two signals of divergence (Figure S2C). This is particularly true when the divergence times are less widely separated, as is the case for Papua. The value used here for the divergence time of $t_1 = 5000$ generations for the Asian-specific Denisovan introgression signal is an approximation based on the location of that mismatch peak and not based on explicit modeling.

This phenomenon also explains why we are able to detect the multiple peaks in East Asia and Siberia, despite having considerably shorter blocks in these populations. For example, the 2000 longest blocks in these populations have an average length of just 43 Kb and 35 Kb respectively, yet we are still able to detect two Denisovan mismatch peaks due to the probable difference in population divergence driving these of 7500 generations (5000 versus 12500). In contrast, the longest 2000 blocks have an average length of 263 Kb in Papuans, and such long blocks appear necessary to capture two populations diverging from the Altai Denisovan in a narrower time frame, approximately 2750 generations apart (9750 versus 12500). Among East ISEA, the longest 2000 blocks have an average length of 152 Kb; Figure S2C implies that this lack of resolution may be hiding the two peaks that we detect in Papua.

We further assessed the hypothesis that the lack of a clearly bimodal East ISEA mismatch distribution could be related to our power to resolve the true mismatch distribution. To address this, we re-sampled Papuan blocks to mimic the distribution of block lengths in East ISEA based on rejection sampling (with replacement). We sampled 1000 sets of 2000 blocks, and generated mismatches against the Altai Denisovan. Plotting these mismatch distributions against the observed Papuan and East ISEA mismatch distributions (Figure S2B) demonstrates that the signal of a dual mismatch peak would be expected to be weak in our East ISEA sample based on the smaller number of long blocks available.

b. Confirming the dual Denisovan mismatch signal

Before proceeding to analyze possible causes of the dual Denisovan mismatch signal in Papuans, we sought to confirm that it is observed in block sets retrieved using a variety of methods. We first confirmed that the signal is apparent both in the raw CP Denisovan and HMM Denisovan output (Figures S3A and S3B) to verify that our iterative trimming approach is not causing the signal. The HMM tends to detect longer archaic blocks than CP, which incorporates sequence with greater divergence from the Altai Denisovan, consistent with its lower specificity (higher West Eurasian Denisovan signal in Table S3A). The signal remains (Figure S3B) when performing a similar trimming procedure to that described above on our HMM block set (see STAR Methods S9a), this time removing blocks that were i) less than 50% overlapped by CP Denisovan blocks, ii) less than 0.1% overlapped by S* windows, or iii) over 99.9% covered by Neanderthal HMM output. These criteria were chosen to obtain a high level of enrichment of Papuan Denisovan signal over West Eurasian Denisovan signal.

We next considered the possibility that our masking of heterozygous sites in the archaic genomes to simplify phasing was causing the double peak. Briefly, in a tree of a single introgressing haplotype X and two haplotypes of the Altai Denisovan, D_a and D_b, there are two possible coalescent topologies – either the first coalescent event is between two Altai Denisovan haplotypes, $(X,(D_a,D_b))$, or between an Altai Denisovan haplotype and the introgressing haplotype, $(D_a,(D_b,X))$ or $(D_b,(D_a,X))$. As more homozygote mismatches are expected in the former case, our masking of sites that are heterozygous in one of the archaic genomes could generate a complex mismatch signal. To confirm that the masking of heterozygotes was not causing the multiple peaks, we re-phased the data retaining loci with archaic heterozygotes, and performed the CP and mismatch analysis on this data. This time, we trimmed the CP Denisovan set by simply removing blocks that were more than 99.9% overlapped by CP Neanderthal blocks. As before, the twin peaks are clearly visible (Figure S3A).

c. No dual mismatch signal in Neanderthal blocks

To better understand the potential demographic implications of the dual mismatch peaks observed in introgressed Denisovan blocks among Papuans, we generated similar mismatch distributions based on our 2000 longest high-confidence Neanderthal-specific introgressed blocks for each continental group. These were generated using the same trimming protocol described above (STAR Methods S9a), but starting with CP Neanderthal blocks and requiring overlap with both the Neanderthal HMM output and S*, and only allowing limited overlap with CP Denisovan blocks (see Table S3E for continental distributions of these blocks). As before, we only used blocks with > 50 Kb of unmasked sequence data. A large number of blocks remained for all continental groups (1978–1999 blocks), and the average block length ranged from 168 Kb (America, with 27 samples) to 287 Kb (Papua, with 72 samples). As with the Denisovan introgressed chunks, the average length of the 2000 longest blocks reflects both sample size and introgression history; the higher levels of Neanderthal introgression in the continental groups translates to longer chunks being successfully extracted. The mismatch for each continental group is shown in Figure S3D. For ease of comparison, the curves are again scaled to the genome-wide average mismatch between West Eurasians and the Altai Denisovan.

Interestingly, despite slight fluctuations, a single dominant Neanderthal peak is observed for all populations. This strongly suggests a) that any demographic cause of the dual mismatch peak relates to events occurring in the Denisovan population, rather than among Neanderthals or the Denisovan/Neanderthal common ancestor, and b) that the dual peak is not caused by a bioinformatic error or property of our methods (see further discussion below) that might give rise to a bimodal mismatch distribution against any archaic hominin.

We confirmed the single mismatch peak using the HMM Neanderthal block set, removing blocks that were i) less than 50% overlapped by CP Neanderthal blocks, ii) less than 0.1% overlapped by S* windows, or iii) over 99.9% covered by Denisovan HMM output. This confirmed the unimodal mismatch distribution of Neanderthal introgressing blocks against the Altai Neanderthal (Figure S3E).

As a final consistency check, we sought to make use of a second ancient Neanderthal genome, the Vindija Neanderthal (Prüfer et al., 2017). This sequence is known to be more closely related to the Neanderthal that introgressed into modern humans than the Altai Neanderthal, and thus may be better suited for extracting introgressed Neanderthal blocks (a 10%–20% increase is reported by Prüfer et al. (2017)). We used CP to extract introgressing blocks from Papuan and East ISEA individuals, this time with either the Vindija Neanderthal genome or both Neanderthal genomes as our Neanderthal group. The mismatch of these blocks against the Altai Neanderthal again shows a unimodal distribution (Figure S3F). We additionally repeated our trimming procedure of the CP Denisovan blocks to create high-confidence block sets, now with CP Vindija blocks or blocks identified by CP as affiliated with either Vindija or the Altai Neanderthal removed. Again, the bimodal mismatch distribution is observed (Figure S3C). If the more divergent peak were Neanderthal spillover signal, then we would expect it to be reduced by removing more Neanderthal introgressed sequence; such behavior is not apparent.

d. Assigning blocks to Denisovan ancestries

To statistically confirm the bimodal distribution, we fitted a Gaussian and Gaussian mixture to the mismatch distribution of long (> 180 Kb; Main Text Figure 3A) Denisovan introgressed blocks identified in Papuans for $0.1 < M_D < 0.23$ using the Python package sklearn v. 0.19.1 (function sklearn.mixture.GaussianMixture; Pedregosa et al., 2011). We used blocks > 180 Kb because i) large blocks are needed to resolve a complex mismatch distribution (Figure S2C); ii) the mismatch distribution is relatively stable with a minimum block length of 180 Kb or more (Figure 3A); and iii) sufficient Papuan blocks (n = 1683) remain for downstream analysis using this minimum block length. The bimodal distribution was strongly supported (AIC = −5808.85, versus unimodal −5582.72). Note that the negative AIC values occur due to the high probability density in the range of mismatch values observed, with the probability density function of the Gaussian mixture model concentrated over a mismatch range less than 1; and that the difference between AIC scores rather than their values are relevant here. The Gaussians are distributed according to $N(0.146, 0.018)$ and $N(0.199, 0.015)$, and are weighted [58%, 42%] respectively, where $N(\mu,s)$ indicates a Normal distribution with mean μ and standard deviation s (Main Text Figure 4A).

We additionally statistically confirmed that a bimodal mismatch distribution was supported for unique chunks > 180kb in Papuans. Here, we recorded the mismatch of sets of exactly overlapping chunks as their average mismatch, to limit the impact of high frequency chunks on the distribution. The bimodal distribution remains strongly supported (AIC = −2158.53, versus unimodal −2076.80). This confirms that the bimodal mismatch distribution is unlikely to be an artifact due to selection (i.e., a small number of introgressed regions with high frequency) or sampling effects.

We used the Gaussian mixture model to assign blocks to either the less-divergent Denisovan component (D1) or the more divergent Denisovan component (D2), classifying as ambiguous any block with less than 80% support for one model over the other (i.e., $0.2 < p(D1) < 0.8$). We were able to classify 1538 of 1683 blocks in this manner, 718 to D1 and 508 to D2; we did not classify blocks outside the $0.1 < m_D < 0.23$ bounds. These block sets were used in most subsequent analyses. When studying the demographic implications of the bimodal mismatch distribution, we studied either the full mismatch distribution (when retrieving split dates of Denisovan populations), or the entire set of high-confidence Denisovan blocks, classifying blocks with $m_D < 0.1$ to D1 and blocks $m_D > 0.23$ to D2. This allows us to maximize the information in those analyses. Spillover from D0 or Neanderthal – into D1 or D2 respectively – will be minimal as those introgression sources are extremely limited in our high confidence Denisovan block set.

In total, only 6 blocks were assigned to both D1 and D2 in 6 different genomic regions. We suspected that these cases reflect occasional misclassification due to the stochasticity of the mutation process; most blocks in a region are consistent with the D1 or D2 classification, but some spill over to the other peak. We expect a negative correlation between block frequencies in this case. Calculating the frequency as in described in STAR Methods S12, we compared the correlation between D1 and D2 frequencies in our small sample of 6 overlapping blocks with 1000 randomly selected sets of 6 non-overlapping block pairs. We observed a weak negative correlation trend in the set of overlapping blocks (gradient = −1.15, lower than 92% of resampled sets), consistent with the probability of occasional block misclassification.

A simple way to achieve a bimodality in a mismatch distribution is through a demographic model involving multiple sources of archaic introgression. Browning et al. (2018) recently inferred that two Denisovan-like ancestries introgressed into East Asians on the basis of a bimodal mismatch distribution. Before proceeding to analyze the mismatch distribution of Denisovan introgressed blocks in Papuans in this context, we sought to exclude other factors, including bioinformatic bias, and to confirm that the driving signal is consistent with introgression from two source populations on the Denisovan clade and not potential confounders.

e. D1/D2 signal is not a bioinformatic bias

The set of Papuan samples that we study come from three different sources – 30 newly generated sequences, 25 samples from Malaspinas et al. (2016) and 17 samples from Mallick et al. (2016). We used exactly the same pipeline for mapping and base calling on all three datasets, and while we did not observe any obvious differences between data from the three sources during our quality control steps, we thought it possible that the bimodal distribution could conceivably be caused by this batch effect. However, blocks assigned to D1 and D2 were common over all three sample sources, and the number of blocks assigned to D1 and D2 in sequences from the three sources showed no significant deviation from random expectations ($\chi^2 = 0.0997$; p = 0.95).

While the high coverage of the Altai Denisovan genome argues for high confidence in SNP calls, a bimodal distribution of mismatch distances could be generated by certain quality biases. To rule this out, we performed two checks. First, a well-documented form of ancient DNA damage is cytosine deamination leading to C-to-T substitution (Hofreiter et al., 2001). If there were a strong bias in GC content in the genomic regions of the two block sets, with higher GC content in the D2 regions, then deamination of the ancient Altai Denisovan genome could increase the D2 mismatch between the modern (introgressing blocks) and ancient sequences. We therefore assessed GC content in the two Denisovan block sets using the UCSC Table Browser (GRCh37/hg19, Mapping and Sequencing, GC percent, gc5Base). The average GC content is very similar in both sets (39.75% for D1 and 38.75% for D2) and the distributions clearly overlap.

Second, we confirmed that the number of Denisovan low-quality alleles does not differ greatly between the D1 and D2 blocks sets (D1: 0.122%, D2: 0.124%; of the 23.1 Mb and 19.2 Mb of D1 and D2 sequence identified, respectively). While low-quality SNP calls were masked in the dataset used to identify the two block sets (see STAR Methods S3), a strong bias in the amount of low-quality calls in the genomic regions covered by one block set could imply relevant biases in region quality. We did not observe this.

These checks, along with the lack of a bimodal mismatch distribution when comparing introgressing blocks retrieved using the Altai Neanderthal genome against the Altai Neanderthal (Figures S3C–S3E) and the fact that our filtering process to retrieve high confidence Denisovan blocks requires that blocks overlap S* output (which does not use a reference archaic genome), suggest that genetic properties of the Altai Denisovan genome do not substantially contribute to the mismatch difference between D1 and D2 blocks.

We then sought to determine whether the mismatch seen in the two block sets might reflect challenges related to alignability. The overall proportion of coverage by the alignability mask was extremely similar in the genomic regions covered by the two block sets (median: D1 = 6.55%, D2 = 6.52%), indicating that alignability challenges are unlikely to be leading to biases in sequence diversity.

We then considered whether phasing errors might be higher in one block set than the other. For example, if a considerable amount of human sequence were erroneously incorporated into D2 blocks but not D1 blocks, this could drive up the D2 mismatch versus the Altai Denisovan. A simple calculation based on the Malaspinas et al. (2016) model of hominin evolution, with a split between a single introgressing Denisovan clade and the Altai Denisovan $t_{D,DI} = 11998$ generations ago ($N_D = 13249$) and the Denisovan/Human split $t_{H,D} = 20225$ generations ago ($N_{HA} = 32671$), suggests a considerable human input would be required for D2 blocks to be approximately 30% more divergent from the Altai Denisovan than D1 blocks. The approximate human component required is h where:

$$\frac{(1-h)(2(t_{D,DI} + 2N_D)) + h(2(t_{H,D} + 2N_{HA}))}{2(t_{D,DI} + 2N_D)} = 1.3$$

such that $h \approx 0.25$. This can be considered a conservative lower bound, in that many introgressed Denisovan haplotypes will survive into the larger N_e regime and hence have greater mismatch versus the Altai Denisovan.

Such a pronounced phasing error is unexpected, and would be easily observed. As a check, we asked whether the average recombination rate differs between D1 and D2 genomic regions. A higher recombination rate in one set of blocks would be expected to lead to faster recombination between human and introgressing haplotypes and could complicate phasing. Additionally, recombination rate is expected to generally impact local genetic variation as it determines the linkage of neutral regions to any nearby selected variation. We compressed the sets of blocks in the two components to their respective overlapping subsets using the bedtools function 'merge', leaving 86 D1 regions and 68 D2 regions. For each region we calculated the average recombination rate using the same combined HapMap phase II b37 genetic map as used for phasing (Frazer et al., 2007); the distribution of recombination rate between the two chunk sets was not significantly different (standardized 2-sample Anderson-Darling test statistic –0.60, asymptotic p = 0.71).

Ideally, we would directly profile switch point errors by comparing our Denisovan introgressed blocks to those retrieved using experimentally phased haplotypes. However, experimentally phased data are only available for two Australian samples in our dataset, and given the low Australian sample size, we only called D1 and D2 blocks in Papuans. We therefore searched for local variation in the mismatch within D1 and D2 blocks. For CP to call a block as Denisovan that has human sequence data incorporated into it, we expect that the human sequence data would need to be closely surrounded by real introgressing Denisovan sequence. If this were not the case, then CP is expected to simply bisect the Denisovan block. A Denisovan block containing human sequence is therefore expected to have a sharp increase in the mismatch against the Altai Denisovan and a sharp dip in the mismatch against a human genome toward the center of the block. We assessed this signal by dividing D1 and D2 blocks into thirds, and calculating the mismatch of each third against the Altai Denisovan and a West Eurasian sample. For this analysis, we used a minimally masked version of the dataset where the main phased data was combined with unphased data in which archaic heterozygous/low quality sites were not masked, and the call rate filter was not applied; heterozygote/homozygote mismatches in unphased regions were half-weighted to reflect the average 50% probability of applying to the block, and heterozygote-heterozygote mismatches were not counted. The West Eurasian was chosen to be sample LP6005441-DNA_G10, a Russian with approximately average high confidence Denisovan-specific introgression as compared to other West Eurasian samples.

We second counted the number of blocks showing a pattern indicative of potential incorporation of human sequence – lower mismatch against the human sample and higher mismatch against the Altai Denisovan in the middle third. 3.2% of blocks were consistent with this pattern in D1, compared to 5.0% of blocks in D2 (non-significant Chi square statistic 1.87, p = 0.17). The patterns of mismatches over individual blocks suggest that incorporation of human sequence due to phasing errors is rare, and similarly rare in D1 and D2.

We additionally confirmed that the tendency for Denisovan blocks to be called on both chromosome copies of an individual – the Denisovan haplotype homozygosity within that individual – was similar between D1 and D2 blocks (10.9% and 10.2%, corrected χ^2 = 0.066, p = 0.80).

Based on these consistency checks, we do not interpret the mismatch difference between D1 and D2 as being bioinformatic in origin.

f. D1/D2 signal is not caused by selection

We second considered the possibility that the two peaks represented differential selection. Under this explanation, we might expect D1 blocks to be under strong purifying selection, reducing variation and mismatch, with D2 blocks evolving under neutrality.

Purifying selection is expected to be focused on genic regions. We therefore assessed whether D1 blocks have more overlap with genes than D2 blocks. As when assessing recombination rate differences, we compressed the sets of blocks in the two components to their respective overlapping subsets using the bedtools function 'merge', leaving 86 D1 regions and 68 D2 regions. 79 and 60 regions overlapped genes (Ensemble 91 GRCh37) respectively (non-significant χ^2, p = 0.63).

As an additional test for differing levels of purifying selection, we asked whether D1 and D2 genomic regions differed in their B values. B values are measures of background selection over the genome based on observed diversity in an alignment of human, chimp, gorilla, orangutan and macaque (McVicker et al., 2009). After converting original B values to GRCh37/hg19 genome coordinates, we calculated the average B value over each D1 and D2 region. The distributions of average B values in D1 and D2 regions were not significantly different (standardized 2-sample Anderson-Darling test statistic −0.87, asymptotic p = 0.91). The total average and standard deviation for all D1 and D2 regions were 0.48 ± 0.24 and 0.50 ± 0.23, respectively, and hence statistically overlapping.

As D1 bocks have lower mismatch estimates compared to D2, they could have been under strong purifying selection since the time of introgression and might show a more pronounced skew toward rare blocks. We therefore performed a Mann-Whitney U test to assess whether the frequency distribution of blocks in D1 and D2 are different in our Papuan samples. There was a significant statistical difference in the frequency distributions (U = 3304, two-tailed p = 0.031), but summary statistics describing the distributions were similar (mean D1: 0.048, D2: 0.049; median D1: 0.028, D2: 0.021; standard deviation D1: 0.062, D2: 0.069). Importantly, the proportion of rare blocks with frequency < 5% was in fact lower in D1 (70%) than D2 (76%), which is consistent with neutrality.

Based on the lack of a clear genic/non-genic division between D1 and D2 blocks, their similar B values, and no pronounced frequency skew toward rarer D1 blocks, we do not interpret the mismatch difference between D1 and D2 as being driven by selection.

g. The topology of D1/D2 blocks

The network of interacting hominin populations in the Middle Pleistocene is becoming increasingly complex. One phenomenon that is included in some models (Lipson and Reich, 2017; Mallick et al., 2016; McColl et al., 2018; Prüfer et al., 2014; Skoglund et al., 2016), but not others (such as the main model in the Malaspinas et al. (2016) study) is a usually small *Homo erectus* component in the Altai Denisovan. Our approach does not allow us to identify genomic regions derived from *H. erectus* that may have introgressed

into modern humans only, but not into the Altai Denisovan (but see STAR Methods S12). However, if the genetic contact between *H. erectus* and Denisovans occurred before the divergence of the Altai Denisovan and the Denisovan population that introgressed into humans, our D1 and/or D2 blocks could include regions with *H. erectus* ancestry, which were introduced into modern humans by a Denisovan population that was already pre-admixed with *H. erectus.* If so, there would be two categories of blocks identified as introgressed in the modern human – those derived from the Denisovan clade and those with an *H. erectus* origin – which could have different mismatch distributions and create a bimodal signal. While this phenomenon is likely to be rare if the proportion of *H. erectus* in Altai Denisovan is small (2–14%), some models incorporate a surprisingly large contribution (e.g., 66% in Figure 3 of Skoglund et al. (2016)).

We therefore attempted to assign D1 and D2 blocks to specific coalescent topologies by counting mutation sharing patterns and assessing consistency with the fifteen possible topologies implied by the four leaves of the tree (the block, Altai Denisovan, Altai Neanderthal, and human). For this analysis, we followed the phasing assessment (see STAR Methods S10e above) in using the Russian LP6005441-DNA_G10 to represent humans and a minimally masked dataset. We counted the number of mutations in the 16 possible sharing categories. For example, with notation 0 indicating the ancestral allele and 1 indicating the derived allele and in order [Human, Neanderthal, Denisovan, Block], a derived mutation that is unique to the block would contribute to mutation motif 0001, a derived mutation shared between the block and the Altai Denisovan would contribute to motif 0011, and a fixed derived mutation would contribute to mutation motif 1111. When counting, we downweighed the contribution of variants in unphased regions such that all possible mutation motifs represented were counted, in proportion to their probability given an equal chance of each variant being on each haplotype. The approach we take – studying the frequency of ancestral and derived variants in a set of samples of interest, and assessing the consistency of these with different phylogenetic tree topologies – is allied to that taken in recent work investigating the different demographic models of modern human history (Wall, 2017).

We note that relating topologies to demographic histories is complex; for example, given a sufficiently large ancestral population size, each coalescent topology would have an approximately equal probability even if all blocks are Denisovan-introgressed. Nevertheless, studying the *difference* in topology proportions in D1 and D2 to clarify the history of these block sets can be useful.

We categorized the topologies of the blocks based on four heuristic criteria (see inset in Table S4):

I. **Mismatch order.** For a block to be consistent with a given topology in terms of *Mismatch order*, the order of the mismatches between its leaves must be consistent with that topology. For example, given topology (H,(N,(D,X))) and with m_{ij} indicating the mismatch between leaves i and j, the mismatch order is required to be $m_{DX} < m_{DN} \leq m_{XN} < m_{DH} \leq m_{XH} \leq m_{NH}$. For topology ((H,N),(D,X)), there are two mismatch order conditions, $m_{DX} < m_{DN} \leq m_{DH} \leq m_{XN} \leq m_{XH}$ and $m_{HN} < m_{HD} \leq m_{HX} \leq m_{ND} \leq m_{NX}$. The specific cause of inconsistency in the Table S4 inset is $m_{DN} < m_{DX}$.

II. **Branch length order.** The *Mismatch order* requirement above does not consider ancestral or derived status. This makes it robust to multiple hit mutations and incorrect ancestral state inference, but may reduce accuracy if such phenomena are rare. For a block to be consistent with a given topology in terms of *Branch length order*, the order of the average branch lengths, measured in shared derived alleles, between its leaves must be consistent with that topology. For example, given topology (H,(N,(D,X))), and keeping mutation motif notation order [H,N,D,X], the branch length order constraints are $\langle 0001, 0010 \rangle < 0100$ and $\langle 0001 + 0011, 0010 + 0011, 0100 \rangle < 1000$, where e.g., $\langle 0001, 0010 \rangle$ denotes the average of mutation motif counts 0001 and 0010. For topology ((H,N),(D,X)), there are two mismatch order conditions, $\langle 1000, 0100 \rangle < \langle 0010 + 1100, 0001 + 1100 \rangle$ and $\langle 0001, 0010 \rangle < \langle 0100 + 1100, 1000 + 1100 \rangle$. The specific cause of inconsistency in the Table S4 inset is $\langle 0001 + 0011, 0010 + 0011, 0100 \rangle > \langle 1000 \rangle$.

III. **Consistency threshold.** For a block to be consistent with a given topology in terms of *Consistency threshold*, the ratio of the number of topology-inconsistent mutation motifs (ignoring multiple hits and ancestry errors) to the number of topology-consistent mutation motifs should be under some threshold, T_c. For example, given topology (H,(N,(D,X))), and keeping mutation motif notation order [H,N,D,X], $((0101 + 1001 + 0110 + 1010 + 1100 + 1011 + 1101 + 1110)/(1000 + 0100 + 0010 + 0001 + 0011 + 0111)) < T_c$. For topology ((H,N),(D,X)), $((0101 + 1001 + 0110 + 1010 + 1110 + 1101 + 1011 + 0111)/(1000 + 0100 + 0010 + 0001 + 1100 + 0011)) < T_c$. The specific cause of inconsistency in the Table S4 inset is $((0110)/(1000 + 0100 + 0010 + 0001 + 0011 + 0111)) > T_c$.

IV. **Subtree balance threshold.** For a block to be consistent with a given topology in terms of the *Subtree balance threshold*, the absolute log-ratio of two tree branches that are predicted to be equal under that topology should be under some threshold, T_s. For example, given topology (H,(N,(D,X))), and keeping mutation motif notation order [H,N,D,X], we have six conditions $|ln(0001/0010)| < T_s$, $|ln((0001 + 0011)/0100)| < T_s$, $|ln((0010 + 0011)/0100)| < T_s$, $|ln((0001 + 0011 + 0111)/1000)| < T_s$, $|ln((0010 + 0011 + 0111)/1000)| < T_s$, $|ln((0100 + 0111)/1000)| < T_s$. For topology ((H,N),(D,X)) there are six conditions $|ln(1000/0100)| < T_s$, $|ln(0001/0010)| < T_s$, $|ln((1000 + 1100)/(0001 + 0011))| < T_s$, $|ln((0100 + 1100)/(0001 + 0011))| < T_s$, $|ln((1000 + 1100)/(0010 + 0011))| < T_s$, $|ln((0100 + 1100)/(0010 + 0011))| < T_s$. The specific cause of inconsistency in the Table S4 inset is $|ln((0001 + 0011 + 0111)/1000)| > T_s$.

Assessing support for different topologies using each of these constraints independently with $T_c = 0.10$ *and* $T_s = \ln(1.5)$ (Table S4) reveals support for only five topologies – (H,(N,(D,X))), (H,(D,(N,X))), (H,(X,(D,N))), (N,(H,(D,X))) and ((H,N),(D,X)). These topologies reveal a strong signal of human as an outgroup to Neanderthal, Denisovan and the block sequence, and/or the Denisovan and block

sequence forming a clade. Support is substantially greater for the (H,(N,(D,X))) topology, which follows the proposed population tree and suggests that incomplete lineage sorting is not driving the signal of the long blocks we have identified. Importantly, topology (H,(D,(N,X))) is similarly infrequent in both D1 and D2 blocks. This topology is consistent with the introgressing block being placed as most similar to the Altai Neanderthal and is expected to be more common in the D2 block set if the excess divergence were driven by spillover signal from Neanderthal introgression. We further note that we do not observe a D2 peak in all non-African populations, and especially that we do not see this peak in West Eurasians, despite each having considerable Neanderthal introgression – again arguing against this explanation of the D2 mismatch.

Topologies with either the Altai Denisovan or D1/D2 block acting as an outgroup to other genomes – which are consistent with *H. erectus* introgression into blocks or into the Denisovan – are extremely uncommon. While it is helpful to confirm the absence of such topologies, they are not expected given our block identification methodology as they do not allow for excess similarity between blocks and the Denisovan genome. In this context, the ((H,N),(D,X)) topology is interesting. This topology is consistent with, but certainly not unambiguous evidence for, shared *H. erectus* introgression into both an introgressing block and the Altai Denisovan genome. While the topology is common, importantly we do not see clear evidence that the frequency of this topology is substantially different in D1 and D2. This may imply either that the *H. erectus* introgression identified in the Altai Denisovan genome in other studies (see above) occurred earlier than the divergence of D2 from Altai Denisovan or later than the divergence of D1 such that it is Altai Denisovan-specific.

Other frequency differences in topologies are observed and can be informative regarding the demographic drivers of the D1 and D2 block sets. In particular, three topologies show prevalence differences – an increase in the prevalence of (H,(N,(D,X))) in D1 versus D2, and decreases in D1 versus D2 in both (H,(X,(D,N))) and (N,(H,(D,X))) (Table S4, column < D2 > / < D1 >). The increased frequency of (H,(N,(D,X))) in D1 is consistent with D1 originating from a less divergent Denisovan clade, as the D1 blocks join the Altai Denisovan ancestor more recently and hence will be more likely to coalesce with the Altai Denisovan genome before other events. A similar argument applies to the (H,(X,(D,N))) topology – here, proportionally more of the D1 blocks have coalesced with the Altai Denisovan already by the time the Altai Denisovan and Altai Neanderthal share common ancestry, such that (H,(X,(D,N))) should be under-represented in D1 versus D2. Again, this is observed. The increased prevalence of (N,(H,(D,X))) in D2 is not clearly expected and may be associated with detection bias; the greater distance of D2 chunks from the Altai Denisovan render them harder to differentiate from Neanderthal introgression, such that there is a tendency to retrieve topologies in which the Altai Neanderthal is placed deeper in the tree.

The (H,(N,(D,X))) topology is consistent with a series of coalescent events that mirror the proposed population model – with an introgressing population showing greatest affinity to the Altai Denisovan, then the Altai Neanderthal, and then humans. As such, the hypothesis that D1 and D2 represent two divergent populations on the Denisovan clade makes clear predictions about the frequency of different mutation motifs, conditioned on a block showing this topology. Specifically, recalling the mutation motif notation [H,N,D,X], the counts should substantially reflect the branch lengths, as the block- and Altai Denisovan-specific branches are shorter for D1, the motifs 0001 and 0010 are expected to be rarer in D1 than in D2. Given an identical position of the Denisovan/Neanderthal common ancestor for D1 and D2, any shortening of these branches will lead to a corresponding lengthening of the common ancestral branch of D1 and the Altai Denisovan, such that the 0011 motif is expected to be more common in D1. We sought to confirm this pattern. Without conditioning on topologies, the Denisovan-specific motif 0010 was 23% more common in D2 than D1, and the introgressing block-specific motif 0001 was 33% more common. Conditioning on the (H,(N,(D,X))) topology using the *mismatch order* criteria, for example, places these motifs as 28% and 33% more common in D2 than D1, respectively. Providing further evidence of consistency, the Denisovan/block shared motif 0011 is appropriately shortened when conditioning on the (H,(N,(D,X))), such that it is 20% less common in D2. The frequency of this motif is approximately equal when we do not condition on the topology (3% more frequent in D2).

To summarize, the topology proportions in D1 and D2 blocks do not support the idea that D1/D2 mismatch differences are driven by *H. erectus* introgression into the Altai Denisovan, into D1 or D2 blocks independently, or both. The prevalence of the (H,(N,(D,X))) topology, and the topology differences between D1 and D2, are consistent with Denisovan-like introgression in Papuans originating from two populations on the Denisovan clade.

The analysis above is useful in teasing apart the proportions and qualities of coalescent topologies represented in D1 and D2, and can help to rule out specific causes of their mismatch distributions. However, especially given the complexity of block identification, we emphasize that the topologies show consistency with a demographic scenario of interest rather than discounting all other scenarios. The topology differences between D1 and D2 could be consistent with other scenarios, including introgression from a Neanderthal/Denisovan sister-clade or extremely complex bottlenecks on the Denisovan clade.

Having established the likely cause of D1 and D2 mismatches as complexity in archaic hominin introgression, we sought to further explore differences between the two block sets. We proceed by assessing evidence for different introgression dates based on block lengths, and by asking whether a model with introgression from two deeply divergent Denisovan-clade populations is supported by simulations.

h. D1/D2 Denisovan lineages introgressed at different dates

Given the likely demographic origin of the D1 and D2 haplotypes, the question of whether D1 and D2 have different introgression dates is of particular interest. We therefore sought to estimate introgression dates based on haplotype lengths, which are expected to follow an exponential distribution with its decay parameter depending on the introgression date and the amount of introgression

(Equation 1 in Gravel, 2012). The accuracy of this approach depends on the power of our methods to detect haplotypes of different lengths. Two factors are relevant. First, shorter haplotypes are expected to be harder to detect as signals of introgression may be mistaken for noise. Second, haplotypes are expected to be broken up by phasing errors; while the incidence of switch point errors is low in our data (see STAR Methods S4), and while our use of archaic genomes in phasing is expected to substantially reduce errors in introgressed regions, some errors are probable. The haplotypes that we assign to D1 and D2 are extremely long (> 180 Kb), such that the signal of introgression is clear, and the power of our methods is expected to be consistently high. Nevertheless, we caution that date estimates derived from this method may be better considered as relative rather than absolute dates.

We sought to use simulations to profile the potential of date estimation through the distribution of block lengths using a set of long introgressing blocks, and to confirm that fitting dates using longer blocks only does not lead to substantial biases. We first note that deviations from the exponential distribution are known to occur under certain combinations of introgression parameters (especially smaller population sizes and larger admixture proportions; see Figure 3 in Liang and Nielsen (2014)). We therefore assessed the correspondence between simulations and the exponential expectation for our parameter range of interest.

The results of 200 replicates of a Wright-Fisher forward-time simulation of 5 Mb chunks, with recombination rate 1.27×10^{-8} (average rate from the HapMap combined genetic map) and the chromosome discretized into 1 Kb segments for computational simplicity, using an introgression proportion of 0.04, haploid N_e of 8334 (Australian N_e in Malaspinas et al. (2016)), and introgression times from 50 to 2950 generations in steps of 50 generations, show that the exponential fit is close but not exact (Figures S4A and S4B), even when all individuals in the population are sampled. We attempted to fit each simulation both by maximum likelihood (using the scipy.stats.expon.fit function), using either all blocks, those with minimum length 50 Kb, or those with minimum length 180 Kb. We were able to retrieve accurate introgression dates (Figure S4C), although there is a tendency to underestimate the introgression date for more ancient introgression times. In the regime of interest (introgression times < 1800 generations), the deviation is at most 10%–15%. These fittings confirm that it is possible to fit dates using longer block lengths only.

Additional challenges in inferring introgression dates arise from errors in blocks length estimation. We profiled these using the forward-time simulations and fittings as above, but now modified the introgressing block lengths to $B_{error} = B + Laplace(\mu, b)$ on sampling, where B is the error-free simulated block length and the Laplace distribution location parameter $\mu = 0$, while scale parameter $b = 20000$. Choosing the Laplace distribution as our error model assumes equal probability to over and under-estimate block length with a constant probability of error per base pair. If $B_{error} < 0$, the block was discarded, capturing the difficulty in correctly identifying short blocks. The Laplace(0,20000) distribution has a cumulative density function at 2.5% and 97.5% of −59915 and 59915 bp, respectively, capturing very substantial errors in block sizes. Under these models, we are still able to achieve accurate fitting of dates (Figures S4B and S4D), although bigger biases arise when including smaller blocks in the fitting. Again, there is a slight tendency to underestimate introgression dates by 10%–15% when using longer blocks.

Introgression may well have occurred over many generations rather than as a single event, and we considered it probable that fitting using block lengths would emphasize the most recent introgression time. For example, if very weak introgression were (hypothetically) to occur up to the present and even a small number of very long introgressing blocks were sampled, this could lead to a very recent inferred introgression date, likely depending on the fitting procedure. We therefore repeated the forward-time simulations, this time simulating introgression over 520 generations (15080 years with a generation time of 29 years) at a rate $0.04/520 = 7.69 \times 10^{-5}$. Note that the effective introgression rate is only marginally reduced compared to the single-event introgression model due to replacement of haplotypes that are already partially introgressed under this model, and the expected correction when there is relatively low total introgression (as in our case) is minimal. Measuring the simulated introgression date as the mid-point in the introgression process (e.g., weak introgression from 1090 to 1610 generations ago corresponds to a mid-point of 1350 generations), there is again a slight bias to infer more recent introgression dates (Figure S4E). For the introgression times of interest, this bias is again no more than 10%–15%.

Finally, we fitted the output of coalescent simulations generated in STAR Methods S10i, which builds on the Malaspinas et al. (2016) model with Denisovan introgression at 1353 generations ago. A slight bias toward inferring more recent introgression dates was observed, of approximately 5%. Adding errors to the sampled block lengths as above did not change the inference when using long blocks > 180 Kb.

The simulations above suggest that introgression date fitting based on block lengths is effective given our demographic parameters and our use of larger block lengths, even under a strong block length estimation error model or introgression occurring over many generations rather than as a single event. Nevertheless, in each case there is a slight bias toward recent dates, that is greatest when introgression is more ancient. The downward bias in date estimation is limited to 10%–15% for the times most likely corresponding to archaic introgression in humans, and is likely closer to 5%. Based on these simulations, we consider the dates we report to be probable lower bounds on introgression dates, with true dates up to 15% more ancient than our fitting suggest.

We proceeded to perform exponential fittings on the lengths of blocks in the D1 and D2 sets (Figures S4F and S4G) using the Python package statsmodels v.0.8.0 (Seabold and Perktold, 2010) and maximum likelihood fitting, assuming either a constant recombination rate or the combined HapMap genetic map (Frazer et al., 2007). We confirmed 95% CIs through a block-bootstrap procedure, whereby the genome was divided into 2 Mb chunks, consecutive chunks were combined if blocks spanned boundaries, and artificial samples were generated by sampling the same chunks over all individuals with probability proportional to chunk length (usually 2 Mb, but sometimes 4 Mb or more) until the total observed number of blocks corresponded to that expected from the data. When calculating the date of introgression, we assumed an introgression proportion of 2% for each of D1 and D2, such that half of a

proposed total of 4% Denisovan introgression ([Malaspinas et al., 2016](#)) entered from each ancestry into Papuans, and a generation time of 29 years.

The results of the block length fittings are consistent with relatively recent introgression times. Under a constant recombination rate, we estimate dates of D1 introgression as 17.9 kya (95%CI 8.7–29.4) and D2 as 32.9 kya (95%CI 22.9–44.2). While there is no Papuan recombination map, we also sought to incorporate local recombination rates into the fitting by scaling block lengths by the average combined HapMap genetic map recombination rate over all blocks in the D1 or D2 sets, respectively. This maintains the approximately exponential distribution of block lengths. Under this model, we retrieved date estimates of D1 introgression at 29.8 (95%CI 14.4–50.4) and D2 at 45.7 (95%CI 31.9–60.7). The weight of probability supports younger dates within this range (Main Text [Figures 4](#)B and [5](#)E). On average, D2 introgression is relatively older than D1 introgression, by 1.84 and 1.53 times for the two recombination models above, respectively.

To assess the robustness of this finding, we repeated the fitting after removing replicates of haplotypes observed in multiple individuals. In this way, we are seeking to observe recombination histories that are independent, and to limit the impact of haplotypes at higher frequency due to selection. Under a constant recombination rate and using unique haplotypes ([Figures S4](#)F and S4G), we estimate dates of D1 introgression as 20.2 kya (95%CI 10.4–33.5) and D2 as 29.5 kya (95%CI 23.2–36.1); under the HapMap scaled recombination rate, we estimate dates of D1 introgression as 33.7 kya (95%CI 16.8–57.7) and D2 as 44.3 kya (95%CI 34.4–55.4). The D2 average introgression date is now estimated as 1.46 or 1.31 times as ancient as D1, depending on the recombination model. The various block length fittings all suggest that D1 introgression was relatively more recent than D2 introgression.

Several other lines of evidence are consistent with D1 having a more recent introgression date. First, the variance in the frequencies of non-overlapping D1 blocks is less than that observed for D2 blocks (Fligner's test for equal variance = 7.1, p = 0.008). After a pulse of introgression, we expect the variance in haplotype frequencies to increase as haplotypes drift away from their initial frequency. Second, there is structure in the geographic distribution of D1 and D2 introgression (Main Text [Figures 5](#)A and 5B). The amount of identified sequence in the D1 block set (including blocks with $m_D < 0.1$) is significantly lower in Baining samples as compared to mainland Papuans (1.33 Mb per phased haploid genome versus 1.82 Mb on Papua; Welch's t test T = −3.9, p = 4×10^{-4}), while there is no evidence of a different amount of D2 (including blocks with $m_D > 0.23$) sequence (1.28 Mb versus 1.37 Mb, T = −0.8, p = 0.41). To account for sampling differences between New Guinea (N = 52) and Baining (N = 16) and to estimate CIs around the observed mean, we resampled one million times (with replacement) 16 samples from each of two islands. While the average amounts of D2 per individual in both populations overlap (NG: 2.75, 95%CI 2.36–3.12; Baining 2.37, 95%CI 1.96–2.79), Baining has significantly fewer D1 chunks (NG: 3.64, 95%CI 3.10–4.19; Baining 2.60, 95%CI 2.19–2.99). To additionally assess whether the ratio of D1 between mainland Papuans and Baining is greater than the ratio of D2 between mainland Papuans and Baining, we resampled sets of mainland Papuan (N = 52) and Baining (N = 16) individuals with replacement one million times, recording whether the median pairwise D1 ratio was greater than the median pairwise D2 ratio. D1[Papua$_{resample}$]/D1[Baining$_{resample}$] was greater than D2[Papua$_{resample}$]/D2[Baining$_{resample}$] in 95.7% of resampling iterations.

Together, these geographical patterns raise the intriguing possibility that the D1 component is more typical of mainland Papua, and introgression may even have been ongoing in the time-frame of the split between Baining and Papuan populations. Similarly, there is a tendency for populations outside ISEA to show a Denisovan signal more consistent with D2 (Main Text [Figure 3](#)C), although the limited amount of Denisovan introgression means that the blocks contributing to the mismatches are shorter, and hence there is less resolution in the mismatch distributions. While it is possible that the reduced D1 signal in Baining samples is caused by weak Asian admixture (given the lack of evidence for the D1 signal in mainland Asia), this would additionally be expected to reduce the Baining D2 signal compared to mainland Papuans (not observed, see above) and generate an excess signal of Asian ancestry in the Baining as compared to mainland Papuans (not apparent in LOTER results, Main Text [Figure 1](#)A and [Table S2](#); or in the PCA, Main Text [Figure 1](#)B, where the Baining cluster toward Australians rather than with the Asian-admixed Bougainville samples). We additionally note the detailed demographic analyses in [Hudjashov et al. (2017)](#), which strongly place the Baining as a recently separated Papuan population that does not harbor additional admixture signals from a wide range of other regional populations.

i. Assessing the multiple-ancestry hypothesis

Three lines of evidence support the probability that D1 and D2 represent introgression from two different archaic populations, likely both on the Denisovan clade. First, our approach to identifying D1 and D2 blocks, and the coalescent topologies that they represent, are consistent with both sets of blocks showing clear affinity to the Altai Denisovan over the Altai Neanderthal genomes, and clear divergence from most modern humans. Second, there is spatial variation in the prevalence of D1 in populations with some Denisovan introgression (e.g., mismatches consistent with D1 are underrepresented in Baining versus mainland Papua, Main Text [Figures 5](#)A and 5B, and may also be rarer in East ISEA, West ISEA and mainland Asia compared to D2, Main Text [Figure 3](#)C, although resolution is limited, Figure S2). This supports the likelihood of D1 and D2 arising from different source populations rather than a single population of composite ancestry. Third, and supporting the same conclusion, there is some evidence that the introgression dates of D1 and D2 blocks are different ([STAR Methods](#) S10h) and that there is spatial heterogeneity in the frequency of D1 chunks within Near Oceania. We therefore sought to determine whether a model with two pulses of introgression from archaic populations on the Denisovan clade could generate the mismatch distribution observed in modern Papuans using coalescent modeling.

We used the msprime v.0.6.1 program ([Kelleher et al., 2013](#)) to simulate a modified version of the highest-likelihood demographic model inferred by the [Malaspinas et al. (2016)](#) study, using Australians as a proxy for our Papuans. We first translated the original fastsimcoal2 model (provided by the authors) into msprime. We then modified the model as shown in [Figures S4](#)A and S4B, allowing

two pulses of introgression from populations on the Denisovan clade. We did not incorporate reported inbreeding in the Altai Neanderthal. Apart from this modification, the structure of the model remains unchanged. As in that model, sampling times of the Altai Denisovan and Altai Neanderthal are 2058 and 2612 generations respectively. Parameters of the model are also unchanged and are given in Table S5 and Figures S5A and S5B, except:

1. The single time of divergence between the Altai Denisovan and the introgressing Denisovan is replaced by two times, *t1* and *t2* indicating the divergence between the Altai Denisovan and branch D1, and the divergence between the Altai Denisovan/D1 common ancestor and D2
2. The population size of all internal Denisovan-clade branches (Altai Denisovan/D1 common ancestor and Altai Denisovan/D1/D2 common ancestor) is set to $N_{DeniAnc}$.
3. Instead of a single Denisovan introgression into Australians 1353 generations ago of 4%, there are two introgressions 1353 generations ago into Papuans, one from D1 and one from D2. These are in proportion $p_1 \times 0.04$ and $(1.0 - p_1) \times 0.04$.

To determine whether our modified model can return the two observed peaks, and to propose demographic parameters, we simulated genetic data using the modified model and studied the mismatch distribution. Specifically, we simulated 5 Mb of sequence data for a sample of 144 Papuan haplotypes, two Altai Denisovan haplotypes and two Altai Neanderthal haplotypes. As in the Malaspinas et al. (2016) study, the mutation rate was set to 1.4×10^{-8} per base pair per generation. The recombination rate was constant and set to 1×10^{-8} per base pair per year. To mimic our own data, we masked all sites that were heterozygote in either the two Altai Denisovan haplotypes or the two Altai Neanderthal haplotypes. We extracted introgressed blocks from each Papuan haplotype in the simulation (using custom scripts and the detailed migration tables recorded by msprime) and recorded the mismatch between these blocks and the Altai Denisovan. The process was repeated 240 times for each parameter set, yielding a total of 1200 Mb simulated data.

The simulated data output by msprime is 'perfect' – there is no SNP calling process that might miss variation, and no missing data that would be masked by QC filters. As we want to avoid consequent biases in model inference, we sought to express the mismatch between introgressed blocks (simulated and real) and the Altai Denisovan genome as a proportion of the average mismatch to the Altai Denisovan observed in a population lacking introgression. We therefore converted the observed mismatch against Denisovan for each block in the real data into a fraction of the genome-wide average mismatch of our 75 West Eurasian samples. For the simulated data, we generated 1200 Mb of data for 150 West Eurasian chromosomes sampled with two chromosomes from the Altai Denisovan and Altai Neanderthal, using the unmodified model from the Malaspinas et al. (2016) study. As before, we masked archaic heterozygote sites, but this time calculated the mismatch over the entire dataset to obtain a population-average mismatch between simulated humans and Denisovan. When fitting the model, we expressed the mismatch distribution in introgressing Denisovan blocks found in simulated Papuans as a fraction of this simulated West Eurasian genome-wide average.

We first explored the parameters on a coarse grid with $t_1 \in [7000, 8000, 9000, 10000, 11000]$, $t_2 \in [10000, 11000, 12000, 13000, 14000]$, $N_{DeniAnc} \in [100, 200, 500, 1000, 2000, 3000, 4000]$ and $p_1 \in [0.4, 0.5, 0.6]$. For each parameter set, we retrieved the mismatch distribution based on the 2000 longest introgressing blocks in the real and simulated data and calculated the sum of squared difference. Based on the output of this coarse fitting, we were able to localize the region of the parameter space showing a close fit to the data, and fitted a finer grid in this region with $t_1 \in [8750, 9000, 9250, 9500, 9750, 10000, 10250, 10500]$, $t_2 \in [11500, 11750, 12000, 12250, 12500, 12750, 13000, 13250, 13500]$, $N_{DeniAnc} \in [50, 100, 150, 200, 250, 300, 350, 400]$ and $p_1 \in [0.45, 0.50, 0.55, 0.60, 0.65, 0.70]$. Assessing the mismatch fit using sum of squared differences yielded our final parameter values of $t_1 = 9750$, $t_2 = 12500$, $N_{DeniAnc} = 100$ and $p_1 = 0.55$.

To cross-validate our methodology, we simulated 5 Mb of sequence data 24000 times using our final parameter set. We resampled 400 of these 5 Mb simulations (representing the introgression ideally observed from 2000 Mb of total data) from this pool, with replacement, 100 times. We then repeated our fitting procedure using the previously defined parameter space grid, yielding time estimates of *t1* [9000–10250], *t2* [11500–13000], N < 350, p_1 = [0.45–0.7]. The distribution of cross-validation mismatches is shown in Figure S5C.

Our simulations support the probability that the D1 and D2 mismatch peaks reflect archaic ancestry in modern Papuans that derives from two populations on the Denisovan clade. Both of these populations were very distantly related to the Altai Denisovan, and more divergent that than the East Asian- (and Siberian-, in our data; Main Text Figure 3C) specific Denisovan introgression (D0 in Main Text Figure 4B). Based on a mutation rate of 1.4×10^{-8} and a generation time of 29 years, simulations suggests that the population contributing D1 chunks split from the Altai Denisovan approximately 261–297 kya, while the population contributing D2 chunks split from the Altai Denisovan approximately 334–377 kya. These dates are population split times, measured in years before present. In order to fit the sharp peaks we observed in the data, a small population size of the ancestral Denisovan population (< 350) is required. The model we explore is extremely simple, and we do not consider our results as proving that an ancestral Denisovan population of this size necessarily persisted for > 100 ky; a low population size or population bottlenecks, however, are strongly implied.

Our results suggest that Denisovans were highly structured when modern humans encountered them, consisting of multiple, highly diverged populations that remained sufficiently separate for hundreds of thousands of years to show distinct signatures when their genes are identified in modern humans. This raises the intriguing possibility that biogeographical barriers, and possibly islands, played an important role in maintaining Denisovan population structure. While the absence of the D1 signal in East ISEA and elsewhere may reflect a lack of resolution (Figure S2), the different amounts of D1 in our mainland Papua and Baining samples

(Main Text Figures 5A and 5B) hints at geographic variation, potentially indicating different introgression histories in these populations (Main Text Figure 5E). We therefore sought to modify our simulation protocol to directly assess the probability of drift and sampling error generating the difference in D1 observed between mainland Papuans and Baining.

j. Less D1 signal in New Britain than New Guinea

We further modified the Malaspinas et al. (2016) simulation model with two introgressing Denisovan populations to incorporate a population representing the Baining. We sought to construct this model such that it incorporates an amount of drift between the Baining and Papuan population on the high end of realistic values, in order to generate a very conservative estimate of the model distribution of ratios of D1 signal between the two groups. Our model follows the demographic analyses presented above, which indicate that the Baining have no excess Asian admixture compared to mainland Papuans (LOTER; Figure 1A; Table S2) and are closely related to Papuans (PCA; Figure 1B), and additional analyses in Hudjashov et al. (2017), which show that the Baining cluster with Papuans and have no additional admixture signals when analyzed together with an even broader set of regional populations. The structure of the model involves the Baining budding from the Papuan population at a time t_B, after Denisovan introgression into their common ancestor. The haploid population size of the ancestral Papuan/Baining population before the split is 8834 (see Figure S5B). After budding, the Baining have a population size of $N_{Baining}$ and the mainland Papuans have a population size of N_{Papua}; these are either constant or functions of time (see discussion below). The two populations are modeled as entirely isolated after budding, to maximize drift and ensure that the model is conservative. Based on the extremely similar levels of Asian ancestry in Baining and Papuans (LOTER, Main Text Figure 1A; Table S2) and the similar placement of Baining and Papuans by PCA (Figure 1B), the migration rate between Baining and Asians was set to the same rate as between Papuans and Asians. The Baining and Papuan populations have the same introgression history in the simulations, such that both D1 and D2 introgress at 1353 generations ago into the Papuan/Baining ancestral population. The sample sizes of the Baining and Papuans were set to 32 and 104 haploid chromosomes, respectively, corresponding to the 16 and 52 individuals in our Baining and mainland Papuan samples.

To determine the split time between the mainland Papuan and Baining population, we used the SMC++ v1.9.3 *split* option, which analyses pairs of populations simultaneously to infer genetic divergence times jointly with population size histories (Terhorst et al., 2017). These split times are effective split times, based on a hard split model without migration after populations diverge. These estimates do not depend on phasing. We used unphased data with the 99% call-rate filter applied, which yielded a split time between mainland Papuan and Baining populations at 15680 years BP with split time diploid N_e = 4620 (Main Text Figure 5C). Using genomic data without the call-rate filter resulted in a very similar estimate (split time = 16280 years BP, N_e = 4940). The mutation rate was fixed to 1.45×10^{-8} (Narasimhan et al., 2017) and generation time to 29 years; chromosome 6, which contains the hypervariable *HLA* region, was excluded from the analysis.

We used these SMC++ results to implement Model 1, with t_B = 540 generations ago and the population sizes for Baining and mainland Papuans after t_B as inferred by SMC++ (incorporating a recent population bottleneck among the Baining and recent population growth for mainland Papuans). We simulated 40 Gb of data using the model as 8000 independent 5 Mb simulations using msprime, recording the total amount of D1 and D2 introgression observed in the mainland Papuan and Baining samples using the migration tables in msprime. We used this information to construct a simulated null distribution of the ratio of D1 (and D2) sequence in mainland Papuans relative to the Baining. We performed 5000 resampling iterations whereby we drew 5 Mb simulations from the set of 8000 simulations until the average total amount of introgressing D1 and D2 sequence in a simulated individual was equal to or just greater than the average amount observed in our Papuan and Baining samples (3.05 Mb). On average, this led to us using just eighteen 5 Mb simulations totaling 90 Mb of simulated data per resampling iteration. The observed median D1[Papua]/D1[Baining] pairwise ratio (1.36) is placed on the 98.5[th] percentile of the simulated distribution (Main Text Figure 5D), indicating that the excess D1 found in mainland Papuans compared to Baining is highly unlikely to be explained by drift alone. In contrast, the observed median D2[Papua]/D2[Baining] pairwise ratio (1.06) is placed on the 65.3[th] percentile of the simulated D2 ratio distribution, indicating that drift alone is sufficient to explain the excess D2 in mainland Papuans.

Given that we use population sizes inferred based on two different methods (SMC++ for recent times and the joint site frequency spectrum for times before t_B and non-Papuan/Baining populations), we sought to confirm that the model correctly captures the drift observed in mainland Papuans and the Baining, and the average divergence of these populations. The observed average heterozygosity of the Papuan and Baining samples was 6.43×10^{-4} and 6.00×10^{-4} respectively, and the weighted F_{ST} (Equation 10 in Weir and Cockerham, 1984) calculated using all sites that were variable between the samples was 0.0934. We used the simulation model described above to generate null distributions of these values by performing the same calculations on 5000 resampling iterations of four hundred 5 Mb simulations (totaling 2 Gb simulated data per iteration). The observed heterozygosity of the mainland Papuans was at the 0.2[th] percentile of the simulated distribution and the heterozygosity of the Baining was 98th percentile of the distribution, while the observed F_{ST} was well over the range generated by the simulations (Figure S6A). This suggests that the simulated Papuans have insufficient drift and that the two populations are insufficiently diverged, such that the SMC++ informed model may simulate Papuan and Baining samples that are more similar in their D1 ratios than would be expected based on observed drift and divergence.

We therefore supplemented this model with two additional, more conservative models, to check the robustness of the result that the difference in D1 between mainland Papua and the Baining is unlikely to be generated by drift. We first assumed that the relatively low population divergence in simulations was caused by incorrect recent population sizes, and tried to identify a fixed value of $N_{Baining}$ that leads to observed heterozygosity and weighted F_{ST} values, fixing N_{Papua} = 8834 as in our implementation of the Malaspinas et al. (2016) model above. We assessed the fit of constant values of $N_{Baining} \in [2000, 2500, 3000, 3500, 4000, 4500, 5000]$ by, as before,

simulating 40 Gb of data using the model as 8000 independent 5 Mb simulations and generating heterozygosity and weighted F_{ST} null distributions by resampling. We found that the new fixed value of N_{Papua} fitted the Papuan heterozygosity extremely well. $N_{Baining} = 3500$ yielded a good fit between simulated and observed F_{ST} (39th percentile) and Papuan heterozygosity (43rd percentile); the observed Baining heterozygosity was marginally greater than the simulated Baining heterozygosity (99th percentile), indicating that the revised model is conservative with respect to incorporating more drift than is observed (Figure S6B). Thus, our Model 2 used parameters $t_B = 540$ and $N_{Baining} = 3500$.

We second asked how an older population split time between mainland Papuans and the Baining might impact results. There is early archaeological evidence of early human occupation on New Britain from 35.5 kya (Pavlides and Gosden, 1994), although importantly genetic divergence is often expected to be more recent due to migration between two populations after separation, which can affect SMC++ split time estimates (Terhorst et al., 2017). Transportation of obsidian tools occurs within the Bismarck Archipelago during the Pleistocene and externally to mainland Papua by the mid-Holocene (Swadling and Hide, 2005). Evidence for post-settlement contact can also be found in the translocation of plant and animal species (Swadling and Hide, 2005), though these appear to have occurred considerably after initial occupation (O'Connor, 2010), suggesting limited contact over long periods. To assess the implications of an earlier split date, we re-implemented the model setting $t_B = 800$ (23.3 ky). This is more ancient than the inferred split times between mainland Papuan populations (10–20 kya; Bergström et al. (2017)) and is of a similar order to the Papuan/aboriginal Australian split (11–27 kya; Mallick et al. (2016)).

We re-estimated $N_{Baining}$ using the same procedure as above, exploring parameter values $N_{Baining} \in [3000, 3500, 4000, 4500, 5000, 5500, 6000]$. No parameter value could fit both heterozygosity and weighted F_{ST}. We therefore conservatively chose to explore $N_{Baining} = 4500$, which yields F_{ST} values considerably higher than observed F_{ST} (observed 0.0934, 95% CI of simulated F_{ST} 0.112–0.115) and places the observed Baining heterozygosity in the 98.9th percentile of the simulated distribution (Figure S6C), such that our Model 3 used parameters $t_B = 800$ and $N_{Baining} = 4500$. As with Model 2, these parameter values are expected to generate simulated data with more drift in the Baining than is observed in our dataset. Model 3 also simulates substantially greater divergence between Papuans and the Baining than the observed F_{ST}, such that the model will tend to generate more variable D1 ratios and is extremely conservative.

The results from these two additional models are shown in Main Text Figure 5D. As before, the observed D2 excess in mainland Papua is not outside the distribution expected due to drift. Similarly, in both cases the observed D1 excess in mainland Papua is unexpected given a model whereby the difference is introgression followed by drift and sampling – for Model 1 the observed D1 ratio is in the 97.8th percentile of the simulated distribution and for Model 2 the D1 ratio is in the 95.4th percentile of the simulated distribution. Together, these simulations suggest that the reduced frequency of D1 blocks among the Baining is unlikely to result from drift, and instead is more likely to reflect a different Denisovan introgression history among Baining compared to mainland Papua.

S11 - Frequency distribution of archaic blocks
The frequency of archaic introgressed blocks are shown in Table S6.
a. High frequency Denisovan blocks
We sought to assess evidence of adaptive introgression from the two Denisovan ancestries, in our high confidence set of Denisovan introgressing blocks, by calculating the frequency of Denisovan ancestry over the genome. While archaic blocks may drift to high frequency, they are more likely than low-frequency blocks to have been subject to natural selection – either adaptive introgression during the initial introgression process or subsequent selection on introgressed variation. We first retrieved all introgressing blocks > 20 Kb from our data, and filtered out the blocks having more mismatch with Denisovan compared to mismatch with Neanderthal. We then used the bedtools v.2.27.0 'multiinter' command to obtain intersected Denisovan-introgressed regions and frequencies among all Papuan individuals. We assigned genes from the Ensembl 91 (GRCh37) database to each intersected block, and report the top 1% frequency regions and the frequency of all introgressed regions in Table S6A. We repeated this procedure for East ISEA individuals (Table S6B).

A genome-wide map of Denisovan introgression in the Papuan and East ISEA samples (Main Text Figure 6), based on Tables S6A and S6B, reveals several sharp peaks at known (e.g., *WARS2*, Racimo et al. (2017); *TNFAIP3*, Gittelman et al. (2016); and *FAM178B*, Sankararaman et al. (2016) and Ilardo et al. (2018)) and unreported (e.g., *WDFY2*, the *TMPO/IKBIP/APAF1* gene cluster) loci. The replication of several loci that have previously been proposed to be subject to adaptive introgression strongly supports our approach to detecting Denisovan introgression and potentially adaptively introgressed regions. Some of our higher frequency blocks overlap previously identified deserts of introgression (Vernot et al., 2016), but this is not unexpected given the large size of the proposed deserts and the small number of Papuans samples they were identified from (N = 35). Specifically, we see high frequency introgressing Denisovan blocks at the *ROBO2* gene in Papuans (chr3:76572330-76634485, 39.6% frequency) overlapping a proposed 14 Mb desert (chr3:76500000-90500000). Lower frequency Denisovan blocks (maximum 16%) also occur in a proposed 10.9 Mb desert (chr8:54500000-65400000).

b. Overlap with modern selection signals
High frequency Denisovan introgressed blocks could arise due to two different selective processes – either directly and immediately on the introgressing haplotypes, leading to longer high frequency haplotypes, or on introgressed diversity some time after the introgression event. We can approximately predict that the former relate primarily to biological differences between humans and the archaic species, while the latter relate to interactions between humans and their environment (e.g., disease, diet, etc.). In the latter

model, introgression provides a source of genetic variation that is non-random in the sense that it has already been subject to evolutionary forces in the archaic population. This genetic variation may provide novel opportunities for adaptive selection in human groups with archaic introgression, even many thousands of years after the introgression ended.

To detect signals of recent positive selection in genetic regions with high Denisovan introgression, we calculated nSL (Ferrer-Admetlla et al., 2014) on all SNPs with ancestral information for the Baining of New Britain, mainland Papuan population of New Guinea and East ISEA continental group. We divided the genome into non-overlapping 200 Kb windows and defined the nSL statistic score of a window as the proportion of SNPs with |nSL| > 2.0. We discarded windows with fewer than 10 SNPs. We then assessed overlap between top 5% nSL window scores and top 1% frequency introgressed Denisovan blocks (see above), comparing introgression signals in Papuans to nSL for the Baining and mainland New Guinea groups, and introgression signals in East ISEA to nSL for the East ISEA group.

We found that only 3/34 Denisovan introgressed haplotypes that were high frequency in Papua were in nSL top 5% windows in the Baining group and these were not significant. For completeness, these genes were *TNFAIP3* (nSL percentile 3.6%), *WDFY2* (2.2%) and *SUMF1* (4.5%).

In mainland Papuans, 2/34 high-frequency Denisovan introgressed haplotypes were top 5% nSL hits – *GLT8D2* (1.1%) and *ZNF280D* (2.9%). In East ISEA, just 1/39 top 1% high-frequency Denisovan introgressed haplotypes was a top 5% nSL hit – *TMEM131* (nSL percentile 1.7%).

Given the suggested role of *WDFY2* in lipid metabolism adaptation, we assessed the mainland Papuan and Baining nSL top 1% gene lists for enrichment of fat metabolism pathways (method described below). We did not observe enrichment, but did note the presence of genes important in lipid metabolism and synthesis – most notably windows including *FASN* in Baining, New Guinea and East ISEA, and *FADS1* and *FADS2* in Baining only. We also note the presence of the important carbohydrate metabolism gene *AGL* in our top 1% nSL gene list in both the Baining and mainland New Guinea. Further work is required to determine the precise role of adaptation and the detailed evolutionary history of these genes in Oceanian populations.

c. Gene ontology enrichment

We tested whether specific sets of genes have significantly elevated frequencies of Denisovan ancestry using the Ontologies tab of the Enrichr web interface (Kuleshov et al., 2016). Specifically, we retrieved all genes identified as introgressed at high frequency (top 1%, using Tables S6A and S6b) and searched for enrichment in the Gene Ontology lists 'GO Cellular Component 2018', 'GO Biological Process 2018' and 'GO Molecular Function 2018', as well as the two phenotype lists 'MGI Mammalian Phenotype 2017' and 'Human Phenotype Ontology' and one tissue expression list 'Jensen TISSUES'. We performed this analysis for both combined Papuan and East ISEA groups; results that survive multiple hypothesis test corrections and are not driven by clusters of co-located genes are reported in the Main Text, and include enrichment associated with expression in adipose and uterine tissue and fetus development. Full results, including categories that either i) had uncorrected p values < 0.005 (the corrected p values using Benjamini-Hochberg method are also reported) and/or ii) were driven by multiple co-located genes are given in Table S6C. Enrichment was observed in categories related to smooth muscle cell proliferation, immunity and adipogenesis in both Papuans and East ISEA, e.g., '*negative regulation of smooth muscle proliferation*' involving *TNFAIP3/PPARG* genes (NG: p value = 0.001, corrected p value = 0.1; EISEA: p = 0.0005, corr-p = 0.049); '*negative regulation of inflammatory response*' involving *TNFAIP3/SAMSN1* genes in Papuans (p = 0.0005, corr-p = 0.09) and *TNFAIP3/PPARG* genes in East ISEA (p = 0.003, corr-p = 0.07); and '*positive regulation of fat cell differentiation*' involving *PPARG* and *WDFY2* genes (NG: p = 0.002, corr-p = 0.1; EISEA: p = 0.0009, corr-p = 0.05).

d. High frequency long and D1/D2 blocks

As longer high-frequency introgressing blocks are expected when a Denisovan haplotype rises to high frequency early in the introgression process, we repeated our introgressing block frequency analysis for blocks > 180 Kb that we were able to assign to one of the two Denisovan ancestries, D1 (Table S6D) and D2 (Table S6E). Analyzing blocks assigned to D1 introgression revealed two regions at high frequency (> 20% in Papua), containing *FAM178B/FAHD2B/ANKRD36*, *ZNF280D* and *FBXL20/MED1/CDK12*. Analyzing blocks assigned to D2 introgression revealed five regions at high frequency, containing *ANKRD28*, *NFAT5/NQO1*, *COG7/GGA2/EARS2/UBFD1/NDUFAB1* and *ARID4A/TOMM20L/TIMM9/KIAA0586*. A gene-free region 15 Kb downstream of *CENPW* was also highly introgressed based on D2 blocks. We observed an extreme nSL signal (nSL percentile 0.2%) in the window containing *CENPW* in the Baining group, and note that the window containing *ZNF280D* (D1) also had a high nSL signal (see above).

As we are only able to assign D1 and D2 ancestry to large blocks > 180 Kb, we additionally explored a concept whereby confident D1 or D2 blocks might be used as local 'flags' for their respective ancestries. In this way, we can adopt an assumption – that short, < 180 Kb, introgressing Denisovan blocks overlapping a > 180 Kb D1 (or D2) chunk are also from the D1 (or D2) population – to leverage off our high confidence Denisovan ancestry dataset. We performed a bootstrapping analysis whereby we repeatedly sampled two Papuan individuals from our dataset and, using their > 20 Kb high confidence introgressing Denisovan blocks, identified the overlap between them. We divided the genome into 40 Kb non-overlapping windows and, for each window, recorded whether the pair had overlapping introgression. We performed this resampling 100000 times, counting the number of observations in each 40 Kb genomic window. Then, for each > 180 Kb D1 and D2 block, we identified the most commonly observed 40 Kb window, and ranked D1 and D2 blocks according to this frequency (Tables S6D and S6E, column 'BOOTSTRAP_RANK_20KB'). While the frequency of D1 and D2 blocks themselves and their ranks according to the above analysis are highly correlated, some rare low-frequency introgressed blocks assigned to D1 and D2 cover regions that are highly introgressed based on smaller blocks. This may reflect occasional

misclassification (STAR Methods S10d), such as when a small number of D2 blocks are erroneously identified as D1 leading to an apparent low-frequency D1 introgression event, or adaptive introgression of primarily smaller Denisovan blocks.

e. High frequency residual S* windows

We additionally determined the frequency of uncommon residual S* windows (see STAR Methods S12, below) found in Papua (Table S6F) and East ISEA (Table S6G). Residual S* is a signal that would be expected given non-Neanderthal, non-Denisovan archaic introgression (e.g., it would be consistent with introgression from *H. erectus*), but could equally be caused by other processes including balancing selection or local properties of molecular evolution (e.g., an accelerated mutation rate in non-African populations). In our combined Papuan sample, top 1% residual S* frequency blocks include a cluster of genes around *VN1R1* (Vomeronasal 1 Receptor 1), as well as *PDE1C* (Phosphodiesterase 1C), *DPH6* (Diphthamine Biosynthesis 6) and *PRKCH* (Protein Kinase C Eta). In our East ISEA sample, top 1% residual S* frequency blocks include a cluster of genes around *HLA-A* (Major Histocompatibility Complex, Class I, A), and *PDE1C* and *PRKCH*. There is considerable correlation between the frequency of residual S* blocks in Papua and East ISEA, such that the *HLA-A* region is also found at high frequency in Papuan residual S* data and the *VN1R1* region is at high frequency in East ISEA residual S*. While these two genes are especially intriguing – *VN1R1* may be involved in the species-specific pheromone system in other species (Rodriguez and Mombaerts, 2002) and sociosexual behavior in humans (Henningsson et al., 2017), and the hypervariable *HLA-A* gene plays a critical role in immunity – further study is required to determine the evolutionary history detected by the residual S* signal in each case. In particular, archaic introgression (Abi-Rached et al., 2011) and balancing selection masquerading as archaic introgression (Yasukochi and Ohashi, 2017) have both been proposed for the HLA region, and may likewise play a role in the signal around *VN1R1*.

S12 - Residual S* signal

The S* method is designed to identify archaic introgression without requiring the introgression to be derived from a population with similarity to a known, sequenced archaic hominin. As such, studying this signal may reveal otherwise cryptic evidence of introgression from hominins outside the Neanderthal and Denisovan clades. Additionally, the signal that S* identifies – non-African variation in high linkage disequilibrium – would be expected to occur due to structure in the Out of African migration(s). Given the known presence of *Homo floresiensis* in our study area (Brown et al., 2004; Sutikna et al., 2016), the possibility that late *Homo erectus* was contemporary with the earliest anatomically modern humans in ISEA (Yokoyama et al., 2008), and that a proposed early Out of Africa model may be required to explain genetic diversity patterns in Papuans (Pagani et al., 2016), we sought to further profile the S* signal (Main Text Figure 7).

a. No more than 1% unexplained archaic introgression

The output of the S* analysis consists of non-overlapping 50 Kb windows reported for each genome (rather than each chromosome copy). Global patterns of S* (> 99% confidence, i.e., higher confidence signal, see STAR Methods S7c) show a sharp peak in Papuans (Table S3A; Figure S7A). Calculating pairwise sharing of these S* windows (Figure S7B) indicates that the signal is quite broadly shared, with Papuans again unusual in sharing a lot of signal between each other and with East ISEA. These patterns are consistent with known patterns of Denisovan introgression, but could also be caused by other demographic or introgression processes. We first sought to assess to what extent this signal might be driven by Denisovan introgression. We used bedtools to remove S* > 99% confidence windows that were inferred to be caused by Neanderthal introgression, based on > 5% coverage of the merged set of HMM and CP Neanderthal introgressed blocks over both chromosome copies. We refer to this trimmed dataset as S^*_{NoNean} (Figure S7A, right pane). We observe that S^*_{NoNean} retains its sharp peak in Papua, while causing a reduction in the overall introgression signal of 75%–80% in all populations when compared to S*. Repeating this process but instead removing S* windows inferred to be caused by Denisovan introgression leads to a slight dip in S^*_{NoDeni} signal in Papua (Figure S7A, right pane), consistent with Denisovan introgression explaining the majority of the excess S* Papuan introgression signal. While the overall introgression signal drops by 84% in Papua compared to S*, there is still a fall of 54% in West Eurasia.

This analysis raises two interesting points. First, it is possible to detect the distinctive introgression signal in Papua using S*. With only a Neanderthal genome available, we would further be able to classify the source of introgression as non-Neanderthal using S^*_{NoNean}. Alternatively, with only a Denisovan genome available, we would be able to use S^*_{NoDeni} to identify the primary driver of this signal as 'Denisovan' introgression, as opposed to early out-of-Africa (OOA) processes involving modern humans, or additional introgression from an unknown archaic source. This suggests that S* is also well-suited to discovering introgression from unknown hominins, by studying signal behavior when masking introgression from known hominins.

Second, studying the West Eurasian signal is particularly informative as West Eurasians carry minimal known Denisovan introgression. Two statistical patterns are important. Removing Denisovan introgression blocks from West Eurasian S* might be expected to cause a minimal reduction in introgression signal. Instead, there is a substantial 54% reduction in introgression signal relative to S* when studying S^*_{NoDeni}, confirming that our CP and HMM Denisovan block sets contain considerable spillover from outside the Denisovan clade. This spillover is likely due to Neanderthal introgression (as explored in STAR Methods S9a and S9b), but as we do not study this ambiguous signal in depth, we cannot rule out introgression from Neanderthal/Denisovan sister clades. Conversely, removing Neanderthal introgression blocks from West Eurasian S* might be expected to remove virtually all the introgression signal. Instead, a considerable 27% of the introgression signal remains. This could be due to false positives in the S* signal; or limited power of other methods to detect Neanderthal introgression; or a result of hitherto unknown introgression processes detected by S* but not CP or the HMM. The overlap in the S* signal that is removed when trimming Neanderthal or Denisovan introgression confirms our

observation in Table S3B – that a great deal of introgressing blocks are ambiguous, showing greater similarity to both the Neanderthal and Denisovan genomes than human variation, likely due to the more recent common ancestry of the archaic hominins.

Because the excess Papuan S* signal is so completely eliminated by filtering out Denisovan introgression (Figure S7A, right pane), a very simple calculation puts a tentative upper bound on the amount of introgression into humans from outside the human/Neanderthal/Denisovan clade. Papuans have 97.2 Mb S* signal compared to the 40.8 Mb observed in Europeans. Assuming the 56.4 Mb excess corresponds to 4% Denisovan introgression, we might expect S* to detect 28.2 Mb from 2% Neanderthal introgression – given that the power of S* to detect introgression from Neanderthals and Denisovans in humans is expected to be similar following their similar genetic distance from humans and introgression times. This leaves 12.6 Mb of S* signal unaccounted for in West Eurasians and Papuans – a combination of false positives, limited power of the CP and HMM, and, potentially, unknown introgression signals – suggesting a maximum of ~1% introgression from outside the human/Neanderthal/Denisovan clade. As such introgression would be expected to be easier to detect, given a similar introgression date, than Neanderthal or Denisovan introgression due to greater divergence from humans, this is only intended as an approximate upper bound. The bound is on average additional introgression in West Eurasia and Papua, but the absence of obvious excess signal in other regions suggests it applies more broadly. Nevertheless, individual populations within continents or isolated groups not captured by our sampling may have greater amounts of highly divergent introgression.

b. Profiling the residual S* signal

While the calculation above suggests that if introgression from outside the (Human, Denisovan, Neanderthal) clade occurred, it was limited; it remains interesting to attempt to identify possible regional peaks in S* that are consistent with such introgression. We therefore attempted to remove introgression signals from the (Neanderthal, Denisovan) clade by filtering out both Neanderthal and Denisovan introgressing blocks, as inferred by CP and the HMM. Starting with the S* > 99% confidence output, we now used bedtools to remove any S* windows with more than 5% cumulative overlap from the union of CP and HMM Neanderthal and Denisovan blocks (see Figure S7C schematic). We are interested in the remainder, which we call residual S* (RS*).

On average, individuals had 172 residual S* windows. We observed that sharing of residual S* between continental groups is common. To quantitatively profile this pattern while taking sample size into account, we randomly down sampled each population to 20 individuals 1000 times and counted the number of residual S* windows that were observed in all continental groups ('global'), 4 to 8 continental groups ('widespread'), or 1–3 continental groups ('uncommon'). The southeast Asian group was excluded due to its small sample size, such that the analysis incorporated Papua, East ISEA, West ISEA, South Asia, East Asia, Siberia, America and West Eurasia. Table S3G shows the average amount of residual S* sequence per individual in each category (also see Figure S7D).

Papua has the lowest signal of residual S* (151 blocks/individual covering 8.8 Mb, 10.4% of the original 1265 S* blocks/individual), while South Asia has the highest residual S* signal (185 blocks/individual covering 10.6 Mb, 23.1% of the original 710 S* blocks/individual). The differences between groups are small (Figure S7A, right pane), and approximately 15%–20% of residual S* windows are found globally (Figure S7D), and over half are widespread. This broad distribution may reflect limitations of our African sample in capturing African variation, demographic events such as pre-OOA genetic structure or shared drift during the OOA bottleneck, evolutionary forces such as purifying selection within Africa, or unusual genomically local patterns of molecular evolution that are not captured by the simulation model. Interestingly, Papua, West Eurasia and South Asia show the highest proportion of uncommon residual S* signal (Table S3G; Figure S7D). While this may partly reflect an Asian ancestry bias in our definitions of continental groups, the pattern is consistent with local demographic processes specifically impacting these populations.

A potential cause of excess uncommon residual S* is region-specific introgressive sequences that coalesce earlier than the (H,N,D) group of known hominins. This is consistent with the placement of *Homo erectus* on the hominin species tree (but also many other causes; see below). Such sequence could be caused by direct introgression from *H. erectus*; or introgression from Denisovans if the introgressing Denisovan population had, like the Altai Denisovan (Meyer et al., 2012), mixed with *H. erectus.* It could also be caused by incomplete lineage sorting within the Neanderthal or Denisovan populations that are known to have mixed with modern humans; by balancing selection; and by increases in local mutation rate in non-Africans. The topologies of interest are (X,(H,(D,N))), (X,(D,(H,N))) and (X,(N,(D,H))). While we cannot accurately calculate topologies (see STAR Methods S10 g) on genomic windows, which cover both chromosome copies and will frequently be chimeras of different coalescent histories, we can make simple predictions about the frequency of certain mutation motifs given *H. erectus* introgression – following the [H,N,D,X] notation, a substantial increase in the frequency of 0001 and an increase in 1110 that is dependent on the split time of *H. erectus* and modern humans. To assess evidence for *H. erectus* introgression, we therefore retrieved all global and uncommon residual S* blocks in each continental group, and divided the sum of the 0001 and 1110 mutation motifs observed in these blocks by their total sequence length.

While our initial calculations identified a clear excess in average 1110 and especially 0001 mutation motifs/bp in East ISEA and Papua, further investigation revealed that this was largely driven by high-frequency introgressed windows around the *HLA-A* gene. HLA regions have been discussed in the context of archaic introgression (Abi-Rached et al., 2011), and balancing selection masquerading as archaic introgression (Yasukochi and Ohashi, 2017). Given the possible role of balancing selection or locally accelerated evolution in the HLA region, we profiled the frequency of 0001 and 1110 motifs when excluding chromosome 6 from the analysis (Figure S7E). There is a tendency toward higher 0001 and 1110 in East ISEA and Papua, centered on the islands of Flores and Lembata. Uncommon residual S* windows in West Eurasia tend to have relatively high rates of the 1110 motif.

These mutation motif patterns suggest a slight excess of unique variation that is not shared with humans, the Altai Denisovan or the Altai Neanderthal in East ISEA and Papua. However, the signal is not strong, and the difference in total RS* between populations is

small, suggesting at most little introgression from outside the Human/Neanderthal/Denisovan lineage in these populations. Still, the question remains as to the cause of this mutation motif pattern. *Homo erectus* introgression has been suggested among Andaman populations (Mondal et al., 2016), but debate is ongoing (Skoglund et al., 2018). The broader region is known to have harbored both *H. floresiensis* and *H. erectus* in a time frame potentially overlapping occupation by modern humans. However, Papua especially is the global center of gravity of Denisovan introgression among modern human populations. The Altai Denisovan is thought to have some *H. erectus* ancestry (Lipson and Reich, 2017; Mallick et al., 2016; McColl et al., 2018; Prüfer et al., 2014; Skoglund et al., 2016), though it is not yet clear whether this is also true for introgressing Denisovan populations. Alternatively, region-specific introgression from either Neanderthals or Denisovans could introduce haplotypes coalescing outside the (H,N,D) tree due to incomplete lineage sorting. Further analysis of other statistics, or the specific haplotypes driving the residual S* signal, coupled with complex simulations, would be required to fully clarify this question, and are beyond the scope of this work.

S13 – Rampasasa is not an introgression outlier

Our dataset includes 19 samples from Rampasasa, Flores, a village that is home to some individuals of unusually short stature and close to the cave where *Homo floresiensis* (Brown et al., 2004) bones were found. The dataset also includes two other villages on Flores (Cibol and Bena) and samples representing many other islands in East ISEA. This offers the opportunity to test for anomalous signals of unusual archaic introgression into Rampasasa, as recently also assessed by Tucci et al. (2018), with the benefit of being able to include samples from nearby and regional populations. Compared to surrounding regions, we did not detect any unusual signs of Neanderthal or Denisovan introgression in the village – the total amount of the genome with evidence for Neanderthal introgression only (62.9 Mb) was similar to neighboring villages (e.g., Cibol 64.4 Mb) and at the lower end of the East ISEA range (62.9–67.2 Mb). Denisovan introgression is similarly low (23.6 Mb; Cibol 23.8 Mb; region 23.6–42.9 Mb). The levels of Denisovan and Neanderthal introgression are exactly as expected based on the proportion of Papuan ancestry in Rampasasa (Main Text Figure 7).

As with all other populations, the S* statistic detected a substantial archaic signal in Rampasasa that could not be assigned by CP or the HMM to either Denisovan or Neanderthals. We also studied residual S*: S* windows that explicitly exclude Neanderthal or Denisovan introgression and so may be enriched for introgression signal contributed by genetically uncharacterized hominins, such as *H. erectus* introgression if it occurred. Although the residual S* signal in Rampasasa is high, there was no clear evidence of excess residual S* signal compared to regional or global populations (per individual, 20 Mb in Rampasasa; Cibol 19.4 Mb; region 18.7–20 Mb; also see Main Text Figure 7). An analysis of the composition of the residual S* signal (STAR Methods S12) indicates that Rampasasa, and East ISEA and Papua more broadly, are relatively more consistent with limited *H. erectus* introgression (Figure S7E), but we emphasize again that the signal is not conclusive and that various other explanations exist (see STAR Methods S12 above). Our findings are consistent with those of Tucci et al. (2018), in that while they cannot rule out additional archaic introgression into Rampasasa, they suggest that any such introgression must have been extremely limited. By including highly local populations in our analysis we are able to provide additional regional context, further emphasizing that Rampasasa is not an outlier compared to nearby villages and islands.

DATA AND SOFTWARE AVAILABILITY

FASTQ files for each individual are available in the European Genome-phenome Archive (EGA) with accession number EGAS00001003054 (https://www.ebi.ac.uk/ega/home). Variant files are available from the Estonian Biocenter data archive (http://evolbio.ut.ee).

New code has been uploaded to GitHub:

The new HMM model: https://github.com/guysjacobs/archHMM
Topology counting code: https://github.com/guysjacobs/archTopoCount
Code to combine BED-format introgressed windows: https://github.com/guysjacobs/archBedCombine
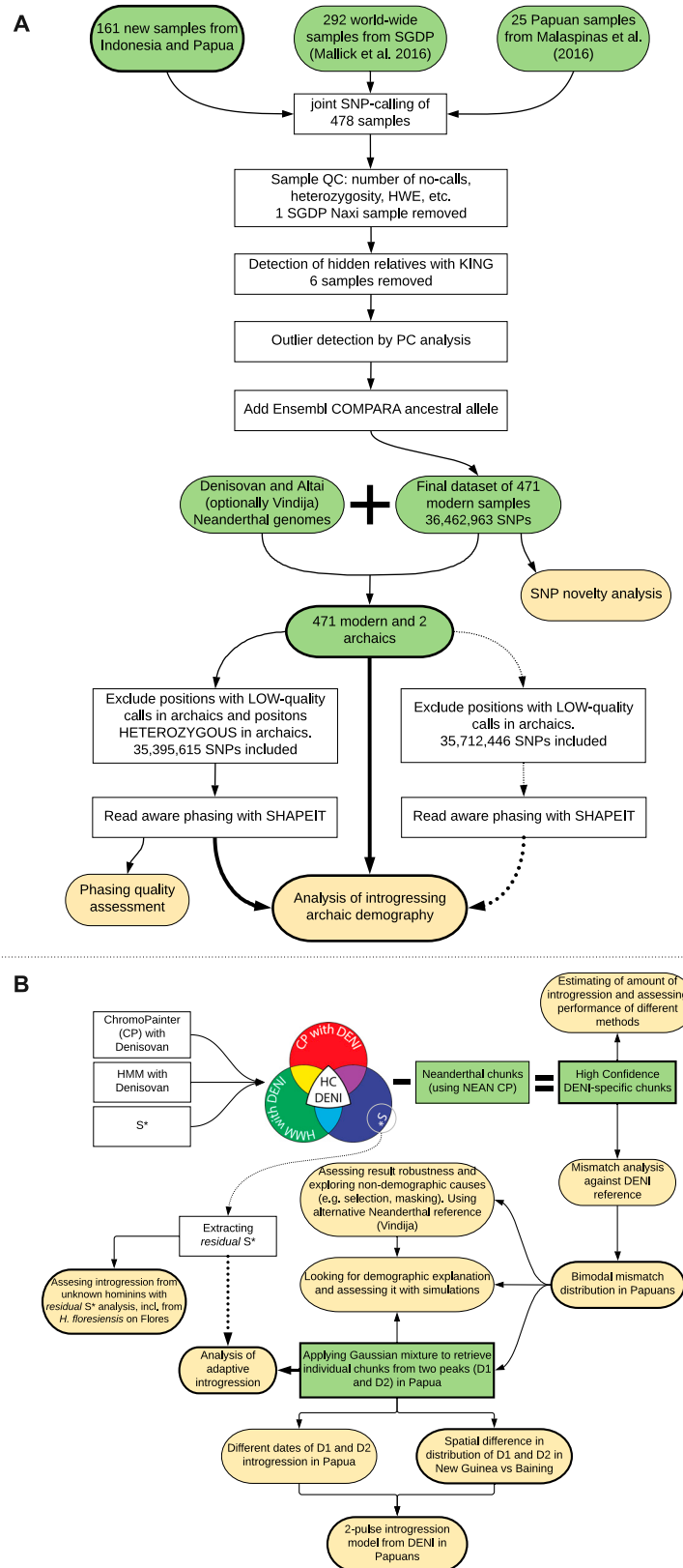
Supplemental Figures

Cell

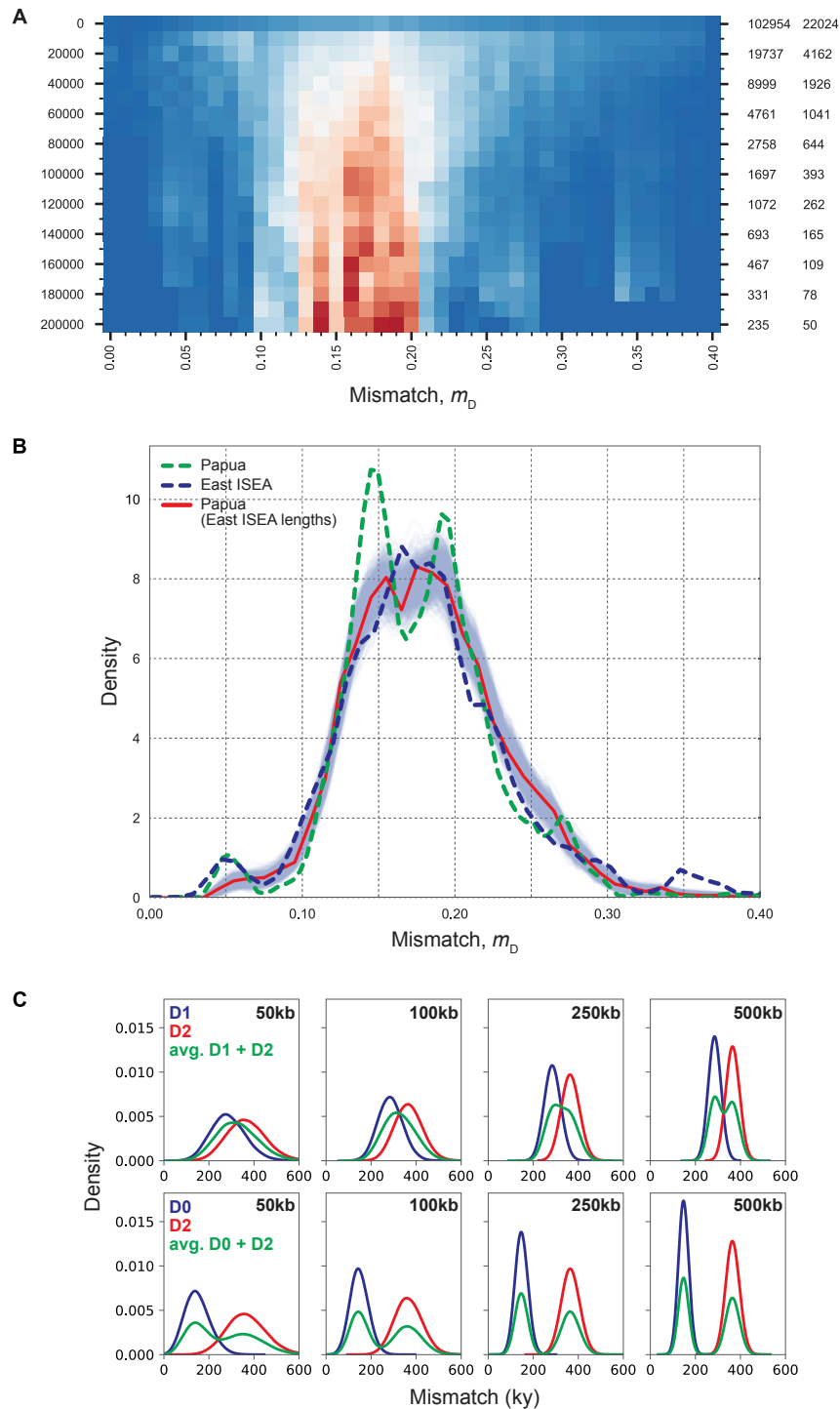Figure S1. Flowcharts of Analyses, Related to STAR Methods

Figure S2. Assessing the Mismatch Distribution in East ISEA and Resolution to Distinguish Mismatch Peaks Using Different Block Lengths, Related to Figure 3 and STAR Methods

(A) Mismatch of East ISEA high-confidence Denisovan blocks against the Altai Denisovan. The two peaks observed in the Papuan data do not clearly resolve due to low sample size. (B) Resampling Papuan high-confidence Denisovan blocks to the East ISEA chunk length distribution and re-calculating the mismatch indicates that the resolution to detect the dual peak signal is low given the East ISEA block lengths. The light blue lines indicate individual resampling iterations and the red line the average of resampled sets. The mismatch of the 2000-longest blocks in Papuans (dashed, green) and East ISEA (dashed, blue) are shown for comparison. (C) Simple theoretical model showing the impact of block length on the expected mismatch distribution, given a Denisovan introgression scenario

representing Papuans (top) and East Asians (bottom). The expected mismatch is scaled, using the simulated mutation rate, to thousands of years. Left to right are the simulated mismatch distribution based on 50 Kb, 100 Kb, 250 Kb and 500 Kb blocks. The blue line corresponds to introgression from the Denisovan clade diverging from the Altai Denisovan at t_1, while the red line corresponds to introgression from Denisovan clade diverging at t_2. The green line is the mixture of the two, assuming each introgression has a 50% weighting.
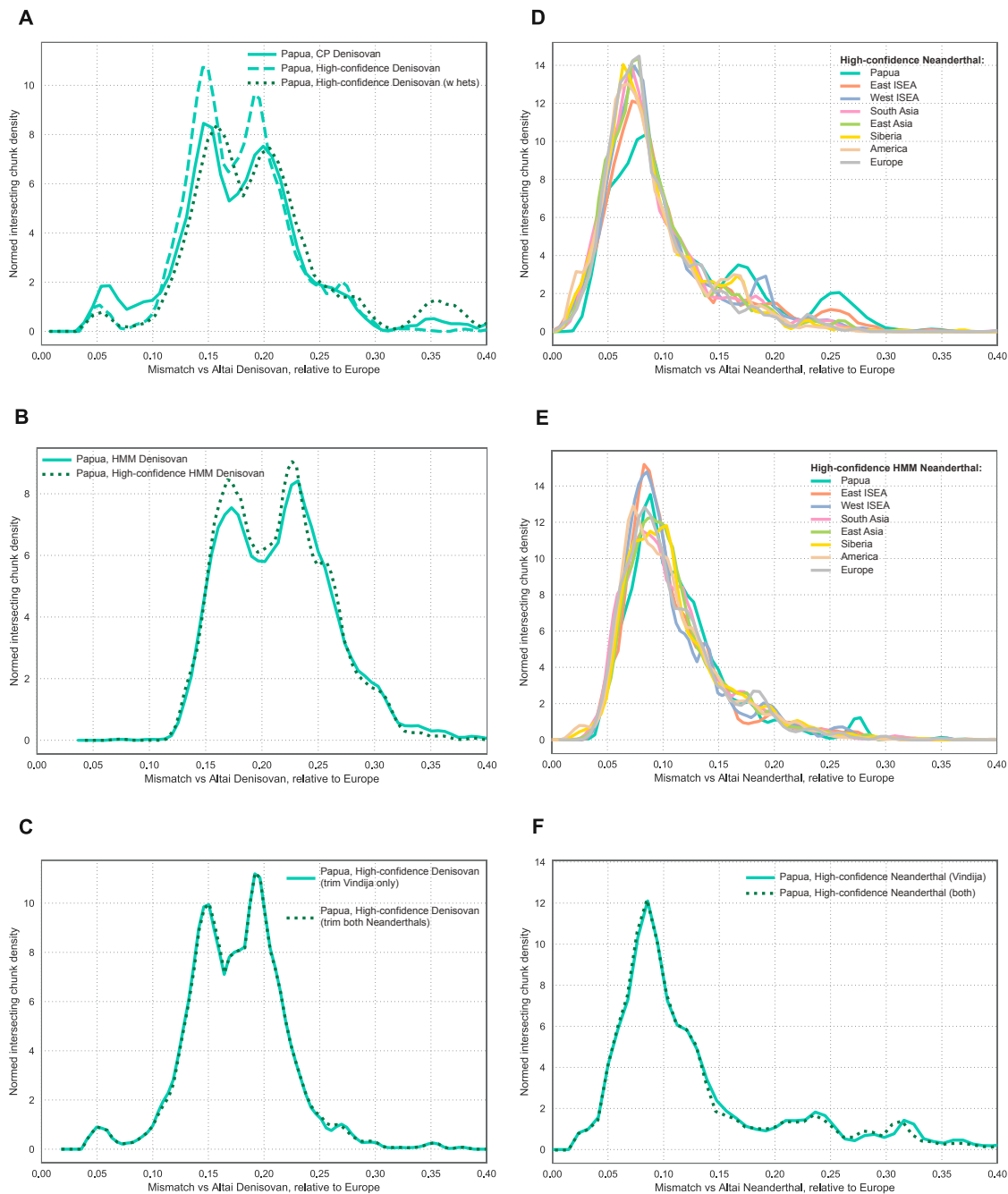
Figure S3. Mismatch Distributions Using Different Block Sets, Related to Figure 3 and STAR Methods

(A to C) show mismatches of Denisovan introgressed blocks against the Altai Denisovan, while panels D to F show mismatches of Neanderthal introgressed blocks against the Altai Neanderthal. (A) CP-derived block sets, showing raw CP Denisovan output, the high-confidence Denisovan block set, and the high-confidence Denisovan block set when keeping archaic heterozygotes for phasing (see STAR Methods S3). (B) HMM-derived block sets, showing raw HMM Denisovan output and a filtered high-confidence HMM Denisovan block set with HMM Neanderthal signal removed. (C) High-confidence Denisovan block set, this time removing the Neanderthal signal by dropping blocks overlapping the CP Vindija Neanderthal output, or a CP with the Neanderthal population defined as both the Altai and Vindija Neanderthal genomes. (D) Regional mismatch of 2000-longest blocks of high-confidence Neanderthal introgressing sequence, based on trimming the CP Neanderthal (Altai) block set. (E) Regional mismatch of 2000-longest blocks of high-confidence Neanderthal introgressing sequence, this time based on trimming the HMM Altai Neanderthal block set. (F) As (D), but using raw CP Neanderthal sequence extracted using either the Vindija Neanderthal or both Altai and Vindija Neanderthal genomes.
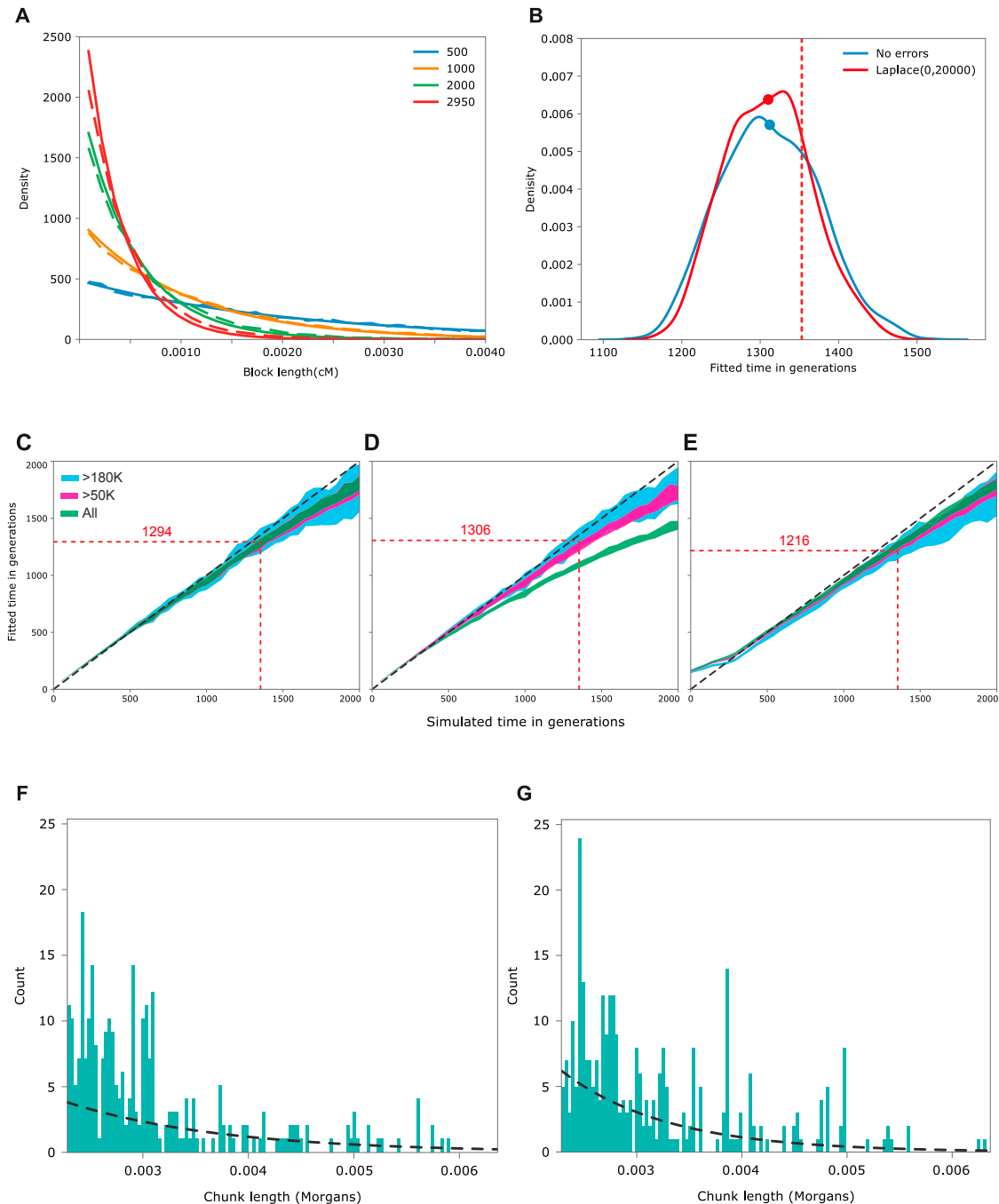
Figure S4. Using Simulations to Assess the Accuracy of Introgression Time Inference Based on Exponential Fitting of Block Length Distributions, and Example Fits, Related to Figures 4 and 5 and STAR Methods

(A) Close correspondence between theoretical (dashed) and simulated (solid) block length distributions 500, 1000, 2000 and 2500 generations after a pulse introgression event replacing 4% of a population of size 8334. (B) Fitting the introgression date using data coalescent simulated for demographic model fitting. The dates are accurately inferred, with only a slight downward bias, even when errors are added. (C) Accuracy of introgression date inference based on forward-time Wright-Fisher simulations and a single pulse of 4% introgression. (D) As in (C), but with block length errors added to the output. (E) As in (C), but with introgression occurring more gradually over 540 generations instead of a single pulse. (F) Exponential fitting of unique > 180 Kb D1 blocks, assuming a genome-wide average recombination rate of 1.27×10^{-8}. (G) As in (F), but for D2 blocks. The relatively flatter distribution of D1 blocks may reflect more recent introgression of that ancestral component.
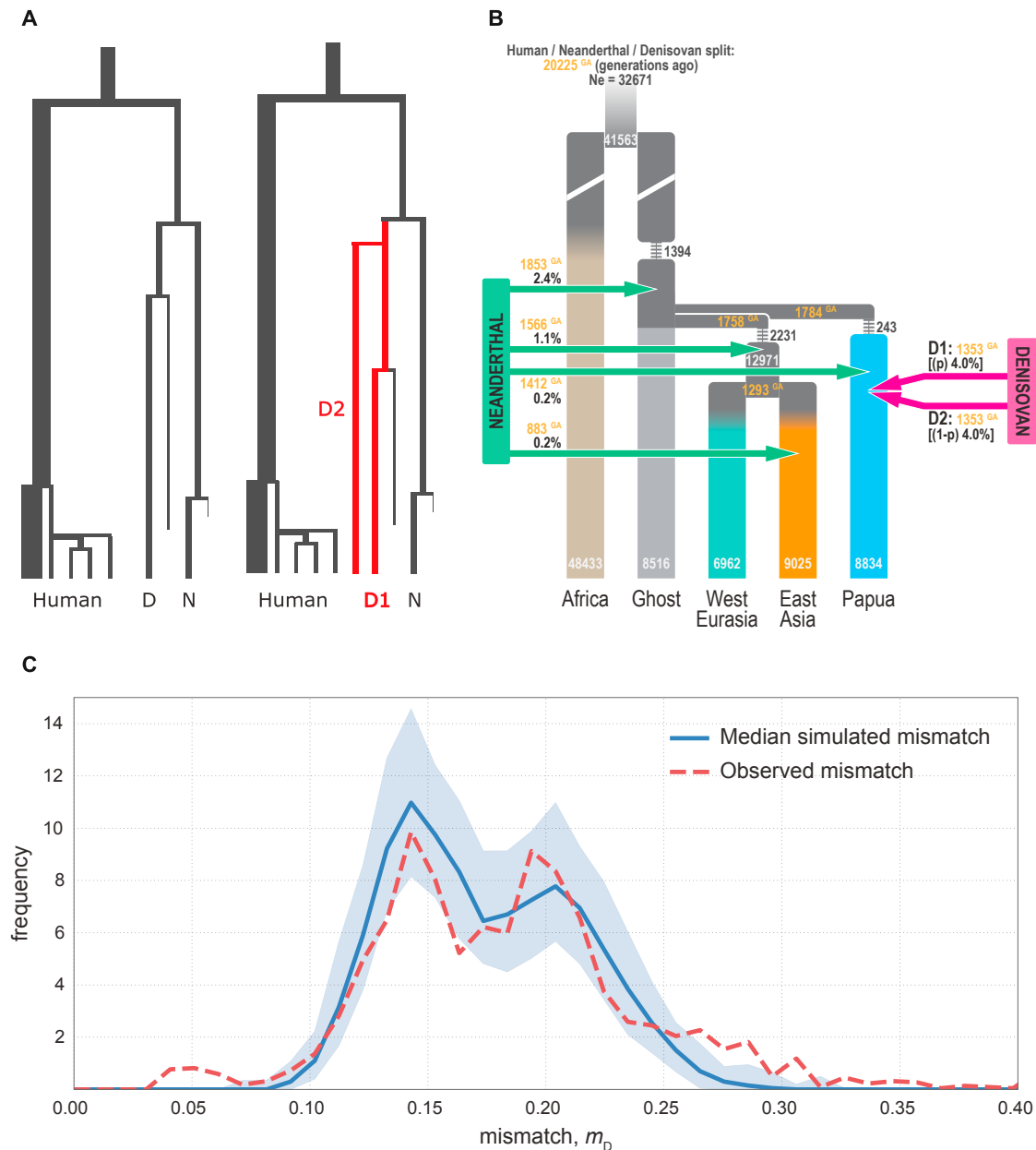
Figure S5. Simulation Model Schematic and Mismatch Results, Related to Figure 4 and STAR Methods

(A) Schematic of the Malaspinas et al. (2016) model, showing (left) traditional relationships between humans and archaic hominins (Denisovans, D; Neanderthals, N) and (right) our modified model allowing for two Denisovan-related branches, D1 and D2, both of which introgress into Papuans. Branch lengths are drawn to scale, and branch widths represent population sizes. (B) Detail of the modified Malaspinas et al. (2016) model, which incorporates four introgression events from the Neanderthal branch, one to Asia (883 generations ago, 0.2%), one to Australia/Papua (1412 generations ago, 0.5%), one to Eurasia (1566 generations ago, 1.1%) and one to the common ancestor of Australians/Papuans and Eurasians (1853 generations ago, 2.4%). While the original model incorporated a single Denisovan introgression into Australians/Papuans (1353 generations ago, 4.0%), here we include two introgression events, one from each of D1 and D2 (1353 generations ago, total 4.0% between both introgressions). Migration occurs between 'neighboring' human populations, and post-split bottlenecks are also included, see Table S5A and Malaspinas et al. (2016). (C) Cross validation (blue) of best-fitting parameter values to the mismatch of high confidence Denisovan-specific blocks (red). The shaded blue region indicates the 95% interval of mismatch distributions generated.
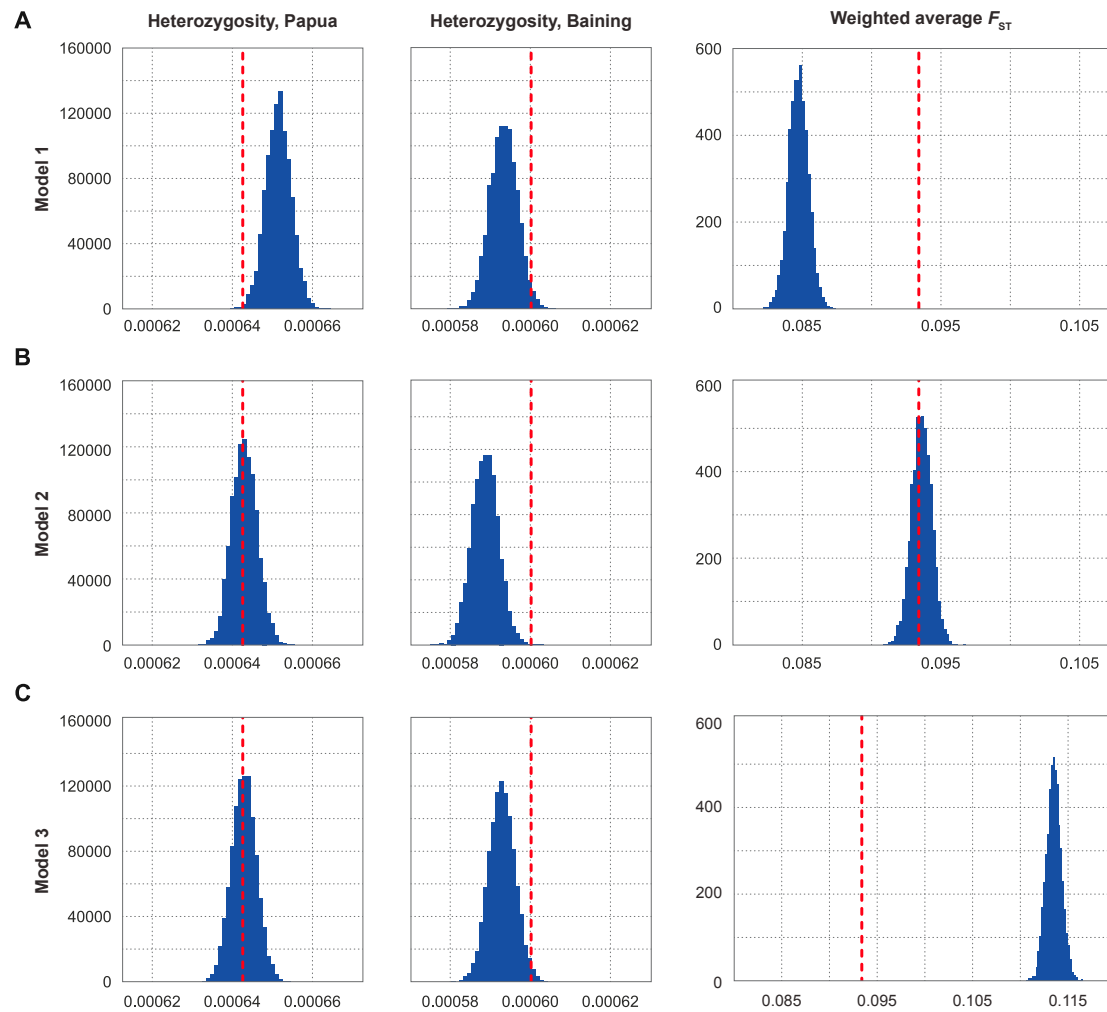
Figure S6. Using Heterozygosity and Fst to Inform Models of Mainland Papuan/Baining Drift, Related to Figure 5 and STAR Methods

Observed (red vertical line) and simulated (blue histogram) heterozygosity and weighted average F_{ST} for our mainland Papuan and Baining sample, with (A) Model 1, t_B = 540 generations ago and mainland Papuan and Baining population sizes from the present to 540 generations ago set as inferred by SMC++ (see Main Text Figure 5C), (B) Model 2, t_B = 540 generations ago and Baining population $N_{Baining}$ = 3500, and (C) Model 3, t_B = 800 and Baining population size $N_{Baining}$ = 4500. Note that the scale of the F_{ST} plot of model 3 differs from the other two models.
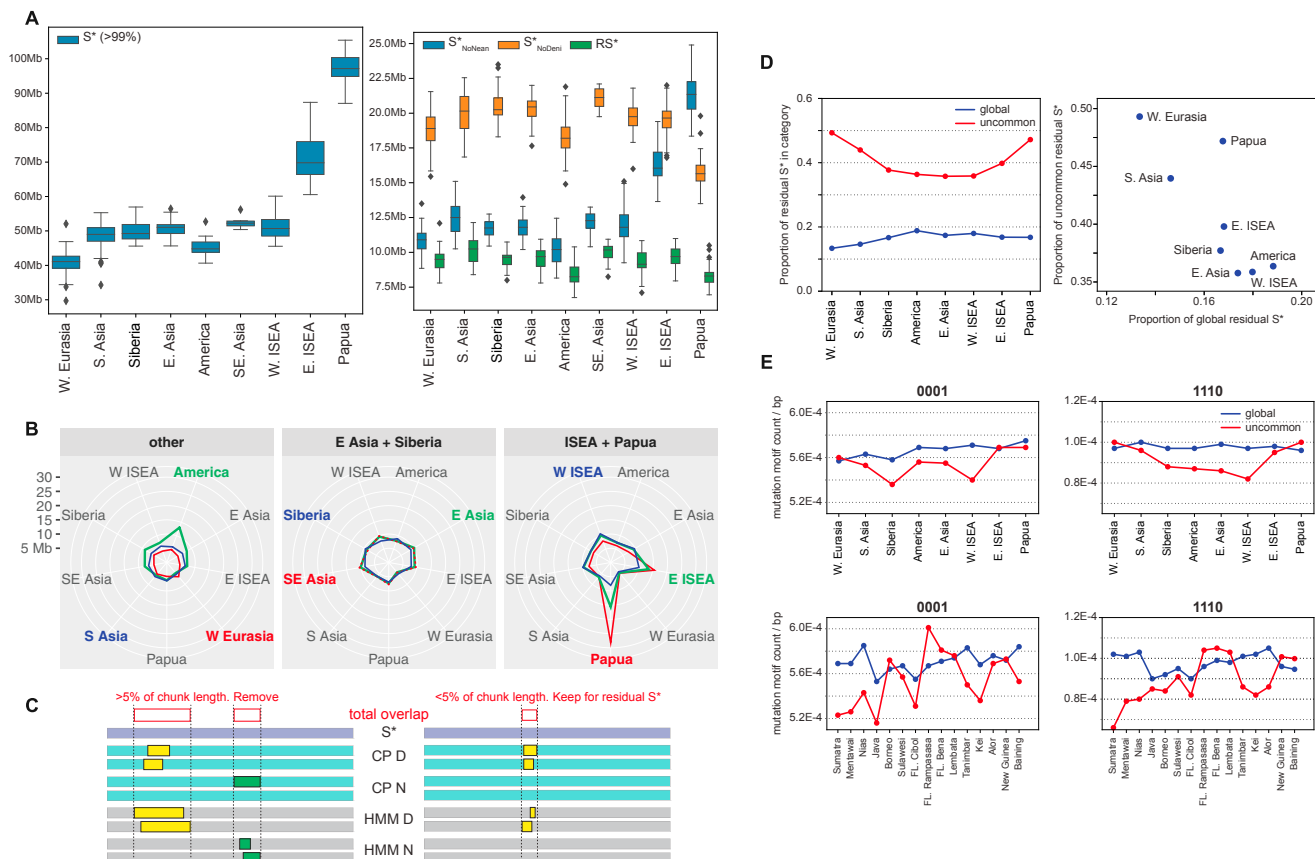
Figure S7. Regional Distribution of S* and Residual S*, and Mutation Motif Characteristics of Residual S* Windows, Related to Figure 7 and STAR Methods

(A) Continental distribution of S* (left), S* after excluding Neanderthal (S*NoNean) or Denisovan (S*NoDeni) blocks, and residual S* (RS*) after excluding both archaic blocks (right). (B) Average sharing of total S* signal between all possible pairwise comparisons of samples from different regional groups, reported in Mb. Populations are split into three groups for ease of visualization; individual population estimates are colored according to population label colors. (C) Schematic of residual S* filtering procedure, whereby a 50 Kb S* window (top, purple; only one prediction is made that covers both chromosome copies) may be removed (left) or kept (right) depending on whether it is over 5% covered – in total – by introgression block predictions from CP (turquoise, middle) or the HMM (gray, bottom) from either Neanderthal (green) [S*$_{NoNean}$], Denisovan (yellow) [S*$_{NoDeni}$] or both [RS*]. (D) Continental pattern of the relative proportions of global and uncommon residual S*. (E) Local variation in the 0001 and 1110 motifs across continental groups and within ISEA and Papua, with chromosome 6 excluded to discount the impact of residual S* windows in the hypervariable HLA region.